AN ABSTRACT OF THE THESIS OF

Edwin J. C. Sobey for the degree of Doctor of Philosophy

in Oceanography presented on 15 February 1977

Title: THE RESPONSE OF OREGON SHELF WATERS TO WIND FLUCTUATIONS: DIFFERENCES AND THE TRANSITION BETWEEN WINTER AND SUMMER

Abstract approved: Redacted for privacy

Robert L. Smith

The physical characteristics of continental shelf waters off Oregon during late winter and spring of 1975 are described and compared with observations taken previously during summer. The currents in winter are barotropic in the monthly means while in summer the currents are baroclinic. Alongshore current fluctuations on the time scale of a few days are depth dependent in winter but become depth independent in summer. The current shear changes sign on the several day time scale in winter while in summer the deeper currents are always northward with respect to the near surface currents.

Alongshore coherences of sea level and currents indicate that winter fluctuations generally propagate southward rather than northward as previously observed in summer. These winter fluctuations in alongshore currents also have onshore/offshore phase speeds that are comparable in magnitude to their alongshore phase speeds. There is no

evidence for free continental shelf wave activity in winter although forced waves (travelling predominately southward, as do the meteorological disturbances) may exist. The Gill and Schumann (1974) model, which predicts sea level from a knowledge of the alongshore components of winds along the coastline, is tested for winter and summer in 1975 and found to have some predictive ability for fluctuations on the time scale of several days.

The transition from winter to summer is initiated in a dramatic barotropic event and continues as a longer period baroclinic adjustment. The former is marked by a sudden reversal of currents and a lowering of sea level while the latter is marked by a slow rising of the pycnocline and with it the layer of maximum vertical shear. Both the barotropic changes at the transition event and the adjustment of the density field, which occurs after the transition event, are directly forced by the local wind.

The Response of Oregon Shelf Waters to Wind Fluctuations: Differences and the Transition between Winter and Summer

by

Edwin J. C. Sobey

A THESIS

submitted to

Oregon State University

in partial fulfillment of
the requirements for the
degree of

Doctor of Philosophy

Completed February 1977

Commencement June 1977

APPROVED:

Redacted for privacy

Professor of Oceanography
in charge of major

Redacted for privacy

Dean of School of Oceanography

Redacted for privacy

Dean of Graduate School

Date thesis is presented February 15, 1977

Typed by Mary Jo Stratton for Edwin J. C. Sobey

ACKNOWLEDGEMENTS

My grateful acknowledgements are extended to the following:

To Prof. Robert L. Smith, for his financial support of my research and me, for his guidance throughout my career as a Ph.D. candidate and for his laborious assistance in the redrafting of this manuscript;

To Profs. A. Huyer, J.F. Lahey, P.P. Niiler and J. Allen for their freely given time and suggestions;

To Dr. P. Kundu for his ideas and for the use of his computer programs;

To Profs. F. Ramsey, S. Neshyba, H. Crew, V.T. Neal and S.E. Wilson for serving on my committee throughout the period of my course selection until my final examination;

To Mssrs. J. Bottero and W. Gilbert for quickly responding to my many requests for data or computer assistance;

To Mrs. L. Hardenburger and to Ms. Rebecca Rakish for their typing of the drafts;

To Mrs. B.L. Sobey for her assistance both financial and moral;

And to the Yacht Enterprise which offered me a safe and occasionally stable platform while I completed the first draft.

TABLE OF CONTENTS

LIST OF TABLES

LIST OF FIGURES

THE RESPONSE OF OREGON SHELF WATERS TO WIND FLUCTUATIONS: DIFFERENCES AND THE TRANSITION BETWEEN WINTER AND SUMMER

INTRODUCTION

Variations in the physical behavior of the ocean over the continental shelf zone off Oregon have a strong seasonal signal: the mean northward flow and the relatively unstratified water during the winter change into a mean southward flow and increased shear and a stratification which increases with the coastal upwelling of spring and summer. The WISP (winter-spring) experiment, of which this study was part, was designed to examine this transition from winter oceanographic conditions to those of summer.

The particular emphasis of this study is to describe winter oceanic conditions on the Oregon continental shelf and to compare them to conditions during summer, and to describe the changes in physical parameters that are associated with the change in seasons. Although summer oceanic conditions have been extensively studied (e.g., Huyer, 1974; Smith, 1974; Kundu et al., 1975; Kundu and Allen, 1976), winter conditions have not been. It is also intended to investigate some possible mechanisms through which the transition is achieved, and to develop a conceptual model of the seasonal shelf dynamics.

In this chapter a brief description of the dominant seasonal characteristics will be given, previous research that motivated the present study will be summarized, some questions will be posed, and the experiment will be described.

Background: The Annual Cycle

In Figure 1 are time series plots of currents and sea level on the Oregon continental shelf from December, 1972 to May, 1974 (Smith et al., 1975). During the months of November to March, the mean currents are northward and are quasi-barotropic.[1] At this time, sea level is above its yearly mean but from April through September or October, the sea level is below its mean. The mean currents from April to October are southward near the surface but as summer progresses the deeper currents become more northward. Eventually this northward flow spreads upward so that by November the mean flow at all depths is northward. Drift bottle experiments (Wyatt et al., 1972) give results which are consistent with the near surface current meter observations in both winter and summer.

---

[1] A barotropic field is one in which the current velocity is constant with depth. (Fofonoff (1962) defines it as having the magnitude of the current at the bottom. Lighthill (1971) says that the barotropic current is equal to the depth average of the currents.) The term quasi-barotropic will be used to describe a field that has considerable depth dependence, but which does not experience a change of sign of velocity. Barotropic and quasi-barotropic fields differ from baroclinic fields: in the latter, the current changes sign at least once in the water column.

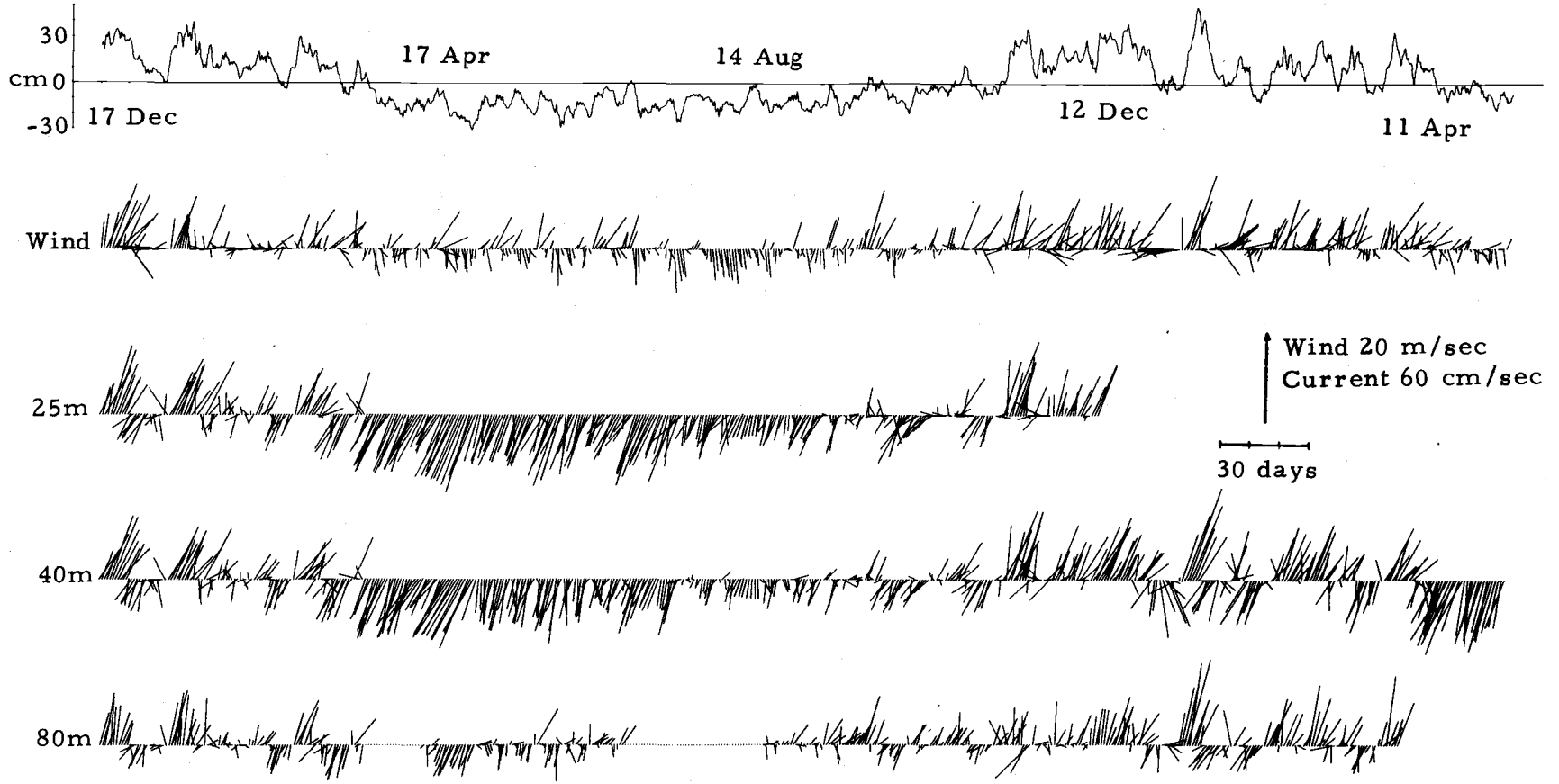

Figure 1. Newport sea level and winds, and Poinsettia currents, 17 December 1972 to 11 May 1974. The units are: cm for sea level; m sec^{-1} for wind; and cm sec^{-1} for currents.

During the winter season, Pacific Ocean storms stagnate over Vancouver Island and in the Gulf of Alaska battering the coasts of British Columbia, Washington, Oregon and northern California with a barrage of eastward winds. The southern boundary of these storm systems lies of Cape Mendocino, California (Bryson and Hare, 1974).

Whereas in winter the meteorological conditions are dominated by low pressure systems, the summer season is dominated by a high pressure system centered on average at 43^{o} N, and 1500 km off the coast (Bryson and Hare, 1974). Thus the local coastal winds are predominately from the northwest. Northward winds occur only about 20% of the time. Although southward winds in winter have about the same velocity as they do in summer, the northward winds in summer are much weaker than those in winter (Bakun, 1975). In general the variance of the wind field is greatly reduced in summer.

Bryson and Hare (1974) point out that in spring the winter cyclones of the Pacific begin to weaken. Their statistical position moves northward so that, by June or July, Oregon and California are almost storm free. The reverse transition in autumn is marked by the reappearance of storms along the coast. The time of the spring atmospheric transition is late March according to Bryson and Lahey (1955). This agrees with Bakun's (1973) observations that the local winds become upwelling favorable in April.

Figure 2 shows the seasonal changes in the offshore Ekman transport. Ekman transport is computed from the wind stress, and gives the net transport of water in response to the wind; the direction of the transport is perpendicular to the wind's direction (to the right in the Northern Hemisphere). At a coast the removal of water under the influence of southward winds can cause deeper waters to rise and the phenomena of upwelling can occur. Along the North American coast the offshore Ekman transport has a maximum at 33^{o} N and extends as far north as 53^{o} N. At the latitude of this study (45^{o} N) the upwelling season (the season of offshore Ekman transport) extends from April to September. During the rest of the year, the mean Ekman transport has an onshore component.

The seasonal changes observed in the variables shown in Figure 1 can be used to make phenomenological definitions of the seasons on the Oregon continental shelf based on the behavior of sea level, currents and wind. Winter is the period when the currents are barotropic and northward in the mean; sea level is high; and the winds generally are not favorable for upwelling. The baroclinic current with southward flow at the surface and northward flow at depth, lowered sea level, and offshore Ekman transport define summer. The four defining characteristics mentioned above do not all change at the same time: wind and sea level have already exhibited summer characteristics early in the spring season, while

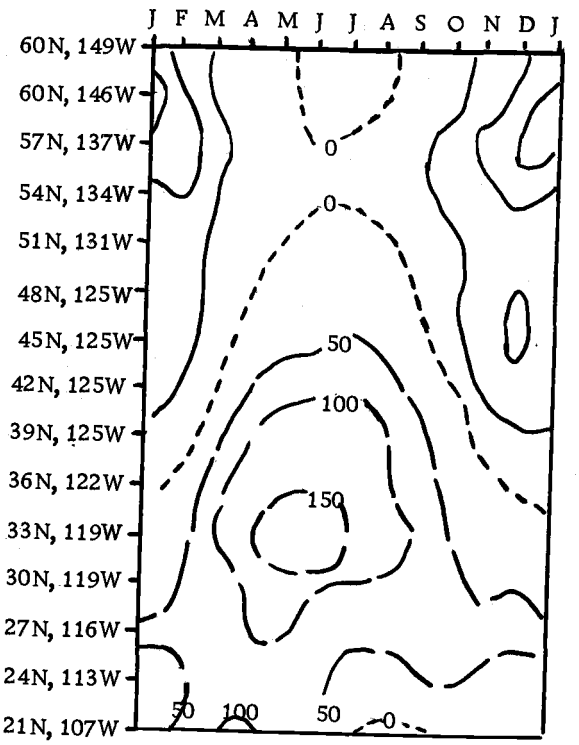

Figure 2. Offshore Ekman transport (from Bakun, 1975). Monthly averages are formed from six hourly wind observations. The units of transport are cubic meters per second per hundred meters of coastline. Contours are drawn every 50 (m^3/sec/100 m). Short dashed lines represent values of zero; long dashed lines represent positive values; and solid lines are used for negative values.

currents at all depths may still be southward in the mean although a large vertical shear is present (i.e. quasi-barotropic conditions).

Motivating Questions

1. What are the differences between winter and summer in the ocean off Oregon?

The study of winter conditions off the Oregon coast has not received the attention that summer conditions (largely supported by the Coastal Upwelling Experiment) have. The most complete set of winter data up to the time of the WISP experiment was that shown in Figure 1. In order to make a full comparison to the already described summer data, a more extensive set of winter data is required.

How do the fundamental statistics of the flow field differ?

Are the spatial scales of motion different?

How do the patterns of velocity fluctuations differ?

Several studies have shown that northward traveling, coastal trapped waves play an important part in shelf dynamics in summer (e.g., Cutchin and Smith, 1973; Huyer et al., 1975b). Free continental shelf waves can travel only northward along the North American Pacific coast. Based on tide gauge data from 1933-1934, Mooers and Smith (1968) found evidence for waves traveling both northward and southward in winter. The latter were probably

fluctuations directly forced by southward propagating wind fluctuations. With a more extensive data base, we might hope to answer the following:

Is the behavior of long shelf waves fundamentally different in winter and summer?

It has been suggested that in summer the waves are resonantly forced (Kundu and Allen, 1976) and a simple model has been proposed (Gill and Schumann, 1974). Are winter waves forced? Does the same model work in winter?

How do the observed characteristics of long, coastal trapped waves compare to the expected characteristics?

2. When and how is the transition from winter to summer accomplished?

Do large changes in sea level and currents occur to make a spring transition or was the 1973 transition (seen in Figure 1) an anomaly?

Is the transition locally generated or advected as an upwelling event? It has been suggested that upwelling events propagate northward (Gill and Clarke, 1974).

What changes occur in the density stratification in going from a non-upwelling season to an upwelling season?

Are changes in sea level at the time of the transition consistent with wind changes and the density field redistribution on the shelf?

What is the cause of the transition?

Huyer (1976) in a discussion of hydrography, lists and evaluates several possible factors that might be important in the spring transition. Of these the more plausible are the following.

1. Fresh water runoff, especially from the Columbia River, might influence the shelf stratification (and hence its response to the wind) by forming a low density layer over, or near, the Oregon shelf.
2. Local winds must be important both directly (forcing currents) and indirectly (influencing the position of the fresh water plume). These winds are controlled by the dominant meteorological pressure systems (the North Pacific high or the Aleutian low).
3. The position of the bifurcation of the North Pacific Current (into a northward Alaska Current and a southward California Current) shifts positions seasonally thus affecting the local shelf dynamics.

This last possibility cannot now be evaluated. This study will concentrate on the influence of the alongshore wind on low frequency continental shelf dynamics and on the influence of the seasonal changes in stratification. It is clear that neither the change in the wind field or the stratification can individually cause the seasonal changes in shelf dynamics. Although the wind is of obvious importance, Huyer (1976) notes that the mean annual surface current

is in the opposite direction to the mean annual windstress. Thus both stratification and wind are involved in the overall problem of shelf dynamics.

The Experiment

The experiment was conducted from January through September, 1975 off the coasts of Oregon, Washington and British Columbia. Currents, temperature and conductivity were measured by moored current meters. Additional temperature and conductivity data were collected by hydrographic cruises. Sea level data were obtained from tide gauge stations and wind data were obtained from a coastal meteorological station at Newport, Oregon.

The principal sets of data used in this study were collected as part of the WISP project. This experiment, conducted by the School of Oceanography at Oregon State University, was one part of a three institution study of the winter and spring shelf dynamics. The other two participating institutions were the University of Washington and the Institute of Ocean Sciences, Victoria. Data reports of this research have been prepared for Oregon State University (Gilbert et al., 1976) and for the Institute of Ocean Sciences (Huyer et al., 1976).

The locations and depths of the 11 Oregon State University Aanderaa RCM-4 current meters are shown in Figures 3 and 4. The

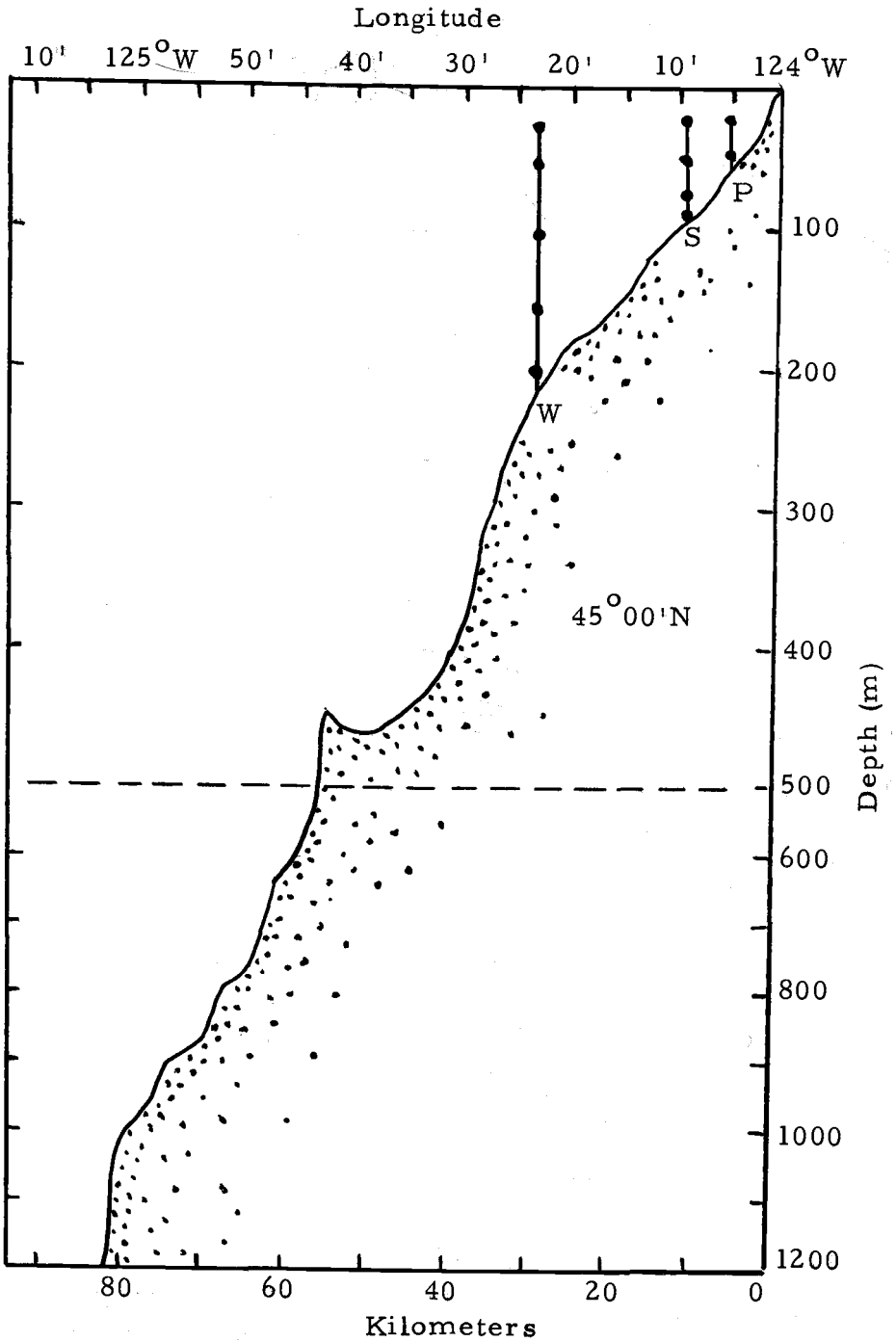

Figure 3. The WISP current meter arrays (Wisteria, Sunflower and Pikake) and the bottom profile along 45°N.

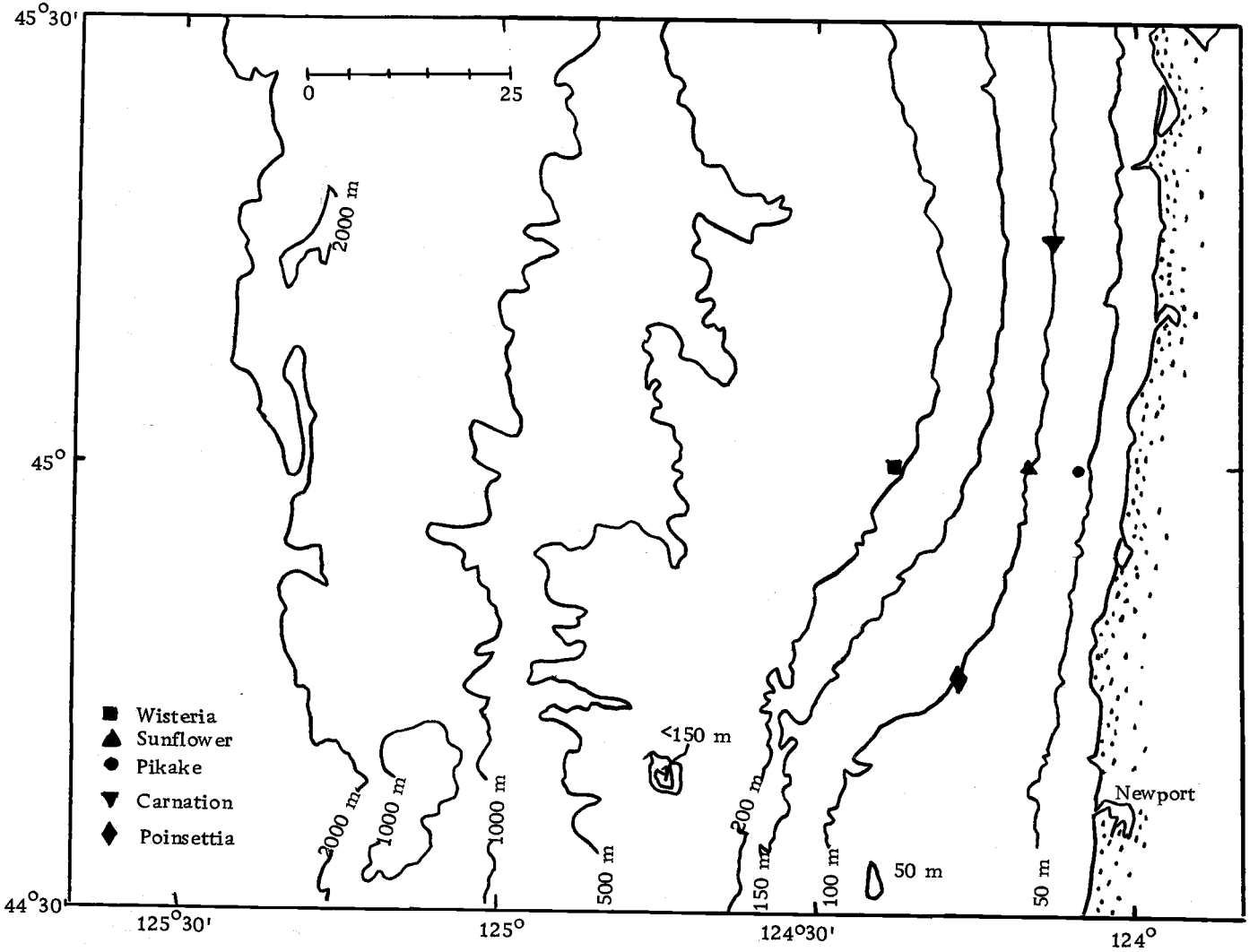

Figure 4. The location of the WISP current meter arrays and of the Carnation and Poinsettia arrays.

current meters were set in three arrays along 45° N latitude.[2] The arrays were moored with subsurface floatation, in the style described by Pillsbury et al. (1969). Flower names were used for a name convention: Pikake, Sunflower, and Wisteria, in order with Pikake closest to the coast. They were installed on 27 and 28 January 1975. Wisteria and Sunflower were recovered on 26 April. At that time Sunflower was replaced by Sunflower B, which was, in turn, replaced by Sunflower C. This last installation was set in late July and recovered in mid-September. The two current meters of Pikake were recovered on 16 May.

All 11 current meters of the original installation recorded current speed and direction, temperature, conductivity (except at Wisteria 50 m), and pressure (except at the two deepest meters at Wisteria) every 20 minutes. With Sunflower B, temperature was recorded at all but the 50 m instrument and conductivity was collected at the 25 m and the 90 m instruments in addition to the current measurements. Sunflower C, operating during the late summer, recorded currents at 25, 75, and 90 m and temperature at 25 and 75 m.

The current meters were calibrated and their data processed in

---

[2] Also shown in Figure 4 are the locations of the Poinsettia and Carnation current meter arrays. Data from Poinsettia were presented in Figure 1 and data from Carnation will be introduced later.

the manner described by Pillsbury et al. (1974a). The 20 minute samples were filtered to yield hourly values and these were further low pass filtered and decimated to give values every six hours. These low-low passed (or LLP) series have a half power point at 0.6 cpd (cycles per day) and a 90% power point at 0 .5 cpd. For most of this study the currents were transformed from North and East orthogonal pairs into alongshore-onshore components based on the local bathymetry. The angles of rotation for this transformation were:

Pikake:	-8.0^{o}
Sunflower:	-13.5^{o}
Wisteria:	-21.0^{o}

Here negative angles denote clockwise rotations. The principal axes system (Fofonoff, 1969) was not very different from that dictated by the local bathymetry.

The conductivity sensors' range/resolution were modified to yield an increased precision (Mesecar and Barstow, 1975) and were used for the first time in this experiment. Both the temperature and conductivity probes were laboratory calibrated before and after their installation. Because a pressure effect on the conductivity cells was found (Huyer, 1975), the conductivity probes were also calibrated in situ using CTD observations. Salinity was calculated from the temperature and conductivity observations by the equations of Perkin and Walker (1972). The precision of the measurements by the

Aanderaa current meters is:

Temperature:	$\pm 0.03^{o}C$
Salinity:	$\pm 0.1^{o}/oo$
Sigma-t:	± 0.1

The temperature, salinity and sigma-t time series were filtered in the same manner as the currents.

Hydrographic data were collected during eight cruises along 45^{o} N, from January to July, 1975. Each one consisted of at least eight to ten stations taken to either 600 m depth or to the bottom. At each station an NIO water sampling bottle with a reversing thermometer was attached to the geodyne CTD in order to provide a calibration point. This calibration was conducted to an accuracy of $\pm 0.02^{o}C$ and ± 0.03 mmhos cm^{2}.

Sea level time series were obtained from tide gauge observations at four locations: Tofino, British Columbia; Toke Point, Washington; and Southbeach and Charleston, Oregon. The effect of atmospheric pressure fluctuations on sea level was accounted for by adding 1 cm of sea level for each millibar of atmospheric pressure. This pressure was obtained from the closest meterological observation station. The sea level series were then low pass filtered and decimated into six hourly samples. Plots of sea level show variations about the sample mean.

Hourly observations of wind were made at Newport, Oregon. The wind time series were low pass filtered in the same manner as the sea level. Wind stress was calculated from the hourly wind series by the equation:

$$\tau = \rho_a C_d \left| \overline{W} \right| \overline{W}$$

where

ρ_a = density of air = 1.25×10^{-3} g/cm^3,

C_d = drag coefficient = 1.5×10^{-3}, and

$\overline{W}$ = wind vector.

The hourly wind stress values were then low pass filtered to give six hourly values. Additional wind data were obtained from Bakun (1976) for every two degrees of latitude from 25° N to 49° N along the coast.

DESCRIPTION OF THE DATA

Currents

Stick diagrams for the 11 current meters of the first installation are given in Figure 5. We note that in the first two-thirds of the records that the currents are quasi-barotropic and that the entire shelf seems to respond homogeneously. It also responds quite rapidly to changes in the wind: in the course of a few hours, the entire current regime can change directions by 180°. The shallowest currents are slightly stronger than the deeper ones, regardless of the direction of the shelf currents.

The mean current for each record is not easy to discern from the stick diagrams. The early part of the record shows alternating northward and southward events, but in the last third of the series (after 25 March) the currents are predominantly southward, especially at the shallow current meters. Means and variances for the 11 current meters are given in Table 1. The data used for this table were divided into two segments because of the obvious lack of stationarity in the records.

Alongshore Means and Variances

The largest mean and variance of the alongshore currents in the first segment occur at Pikake 25 m. In the second segment the

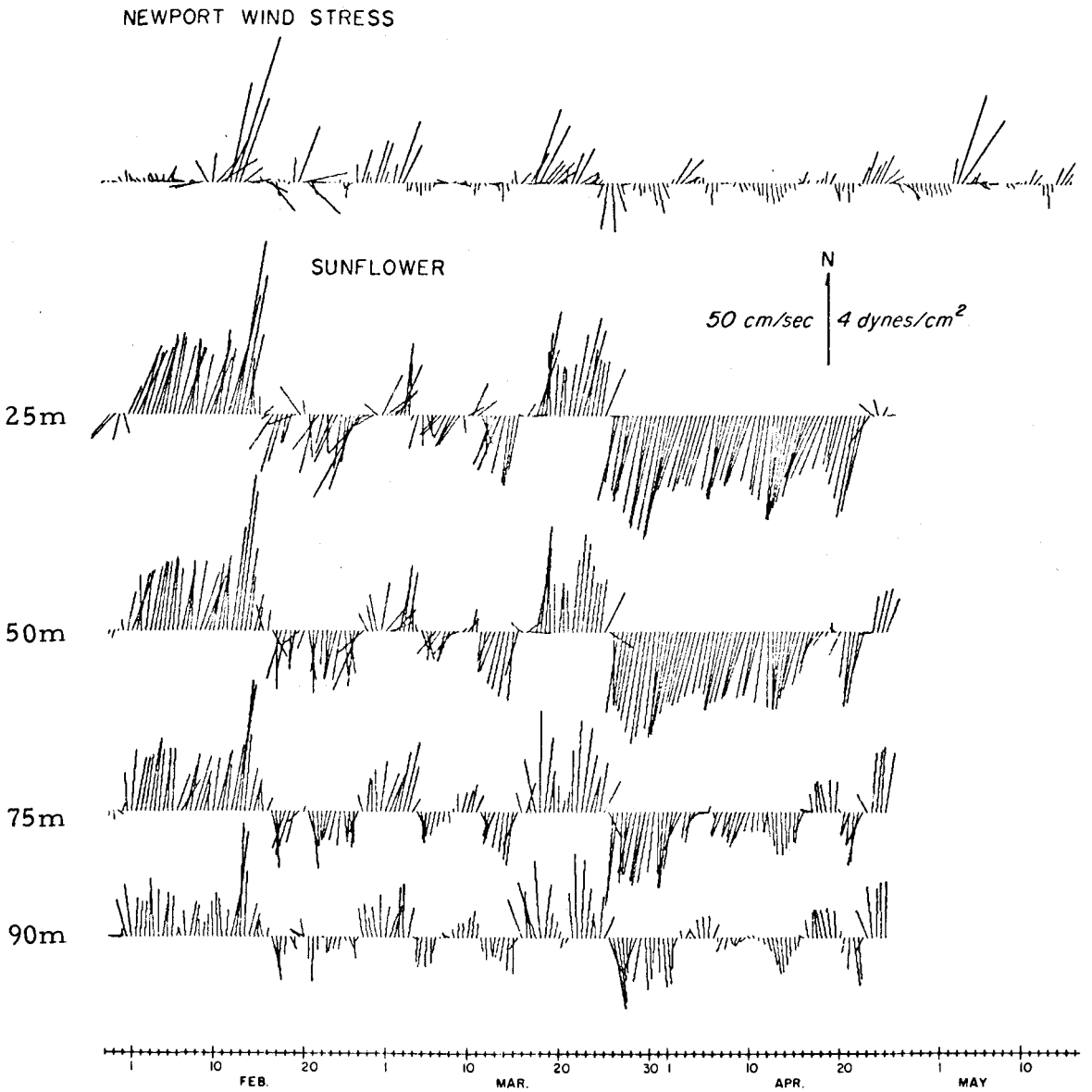

Figure 5. Stick diagrams of the Newport winds and the WISP currents from installation A, 29 January to 18 May 1975. The sticks are drawn every 12 hours.

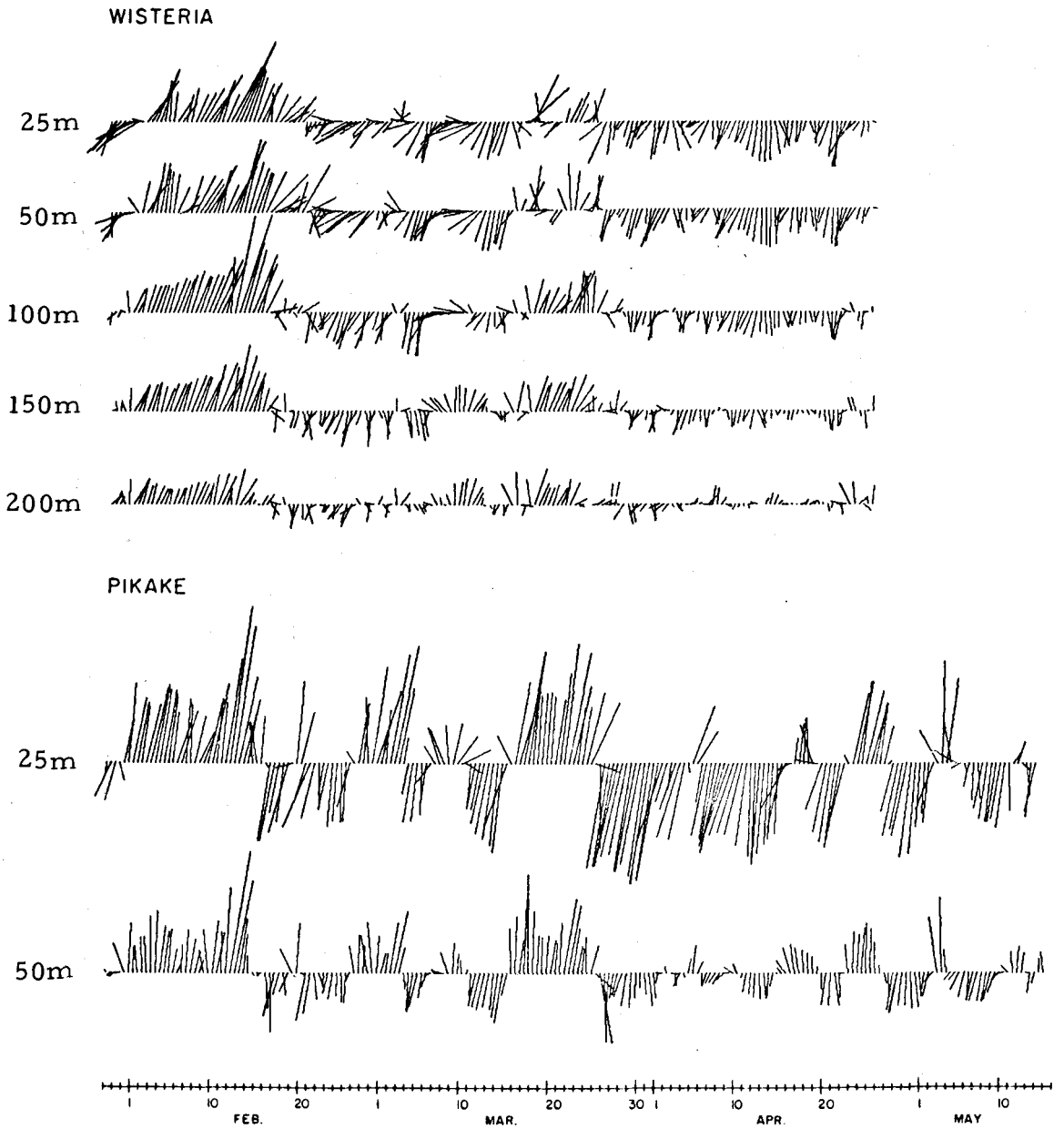

Figure 5. (Continued)

Table 1. Means and variances of the 11 current meter observations. The components u and v were aligned perpendicular to and parallel to the local bathymetry and represent the onshore and alongshore components. The means are given in units of cm/sec and the variances are given in $(cm/sec)^2$.

Depth (m)	29 January-23 March				27 March-				End date
	u		v		u		v		
	mean	variance	mean	variance	mean	variance	mean	variance	
Pikake array									
25	0.10	17.14	14.13	1145.60	-1.21	18.53	-21.19	1001.70	15 May
50	-1.00	6.82	8.20	415.68	-0.64	6.99	- 3.18	177.88	
Sunflower array									
25	-0.89	29.15	9.28	908.07	0.72	18.94	-35.11	314.67	18 May
50	-1.10	25.65	9.70	752.49	1.90	18.66	-24.50	416.61	
75	-0.41	17.10	9.76	500.33	0.59	13.00	- 8.58	325.31	
90	-1.68	19.54	8.57	270.93	0.78	20.97	- 2.46	200.71	
Wisteria array									
25	-2.42	43.75	2.23	306.63	1.68	14.77	-11.85	30.69	24 April
50	-2.42	39.88	2.95	282.02	1.88	9.34	-11.85	29.10	
100	-0.89	23.03	4.95	298.75	1.49	7.19	- 7.39	23.05	
150	0.14	15.47	5.49	177.08	1.00	6.56	- 4.38	24.42	
200	-0.07	8.90	4.04	69.84	0.19	9.11	0.09	23.87	

variance of the shelf currents is even more concentrated at that location. However, the current meter with the largest mean is now Sunflower 25 m. The variances of the alongshore components are smaller in the second than in the first segments. In almost all cases the alongshore means and variances decrease with increasing depth.

The maximum alongshore variance at 25 m depth occurs at Pikake, and at 50 m depth it occurs at Sunflower, for both segments. During the first segment, the variance at Wisteria 100 m is larger than at Sunflower 90 m. Thus the maximum variance for each depth occurs farther offshore for increasing depths. This differs from the summer when the variance of the alongshore components (at 40 m depth) decrease with distance offshore (Kundu and Allen, 1976).

Alongshore Current Shear

The vertical shear of the alongshore currents is shown in Figure 6 as the difference between the alongshore components of the various current meters at Sunflower. During the period of the first segment (29 January-23 March), the shear frequently changes sign and the mean shear is close to zero. The magnitude of the currents is always larger at 25 m than at 90 m, regardless of the direction of the flow. After March 25 the sign is constant: the deeper current is more northward with respect to the shallower one, regardless of the direction of flow.

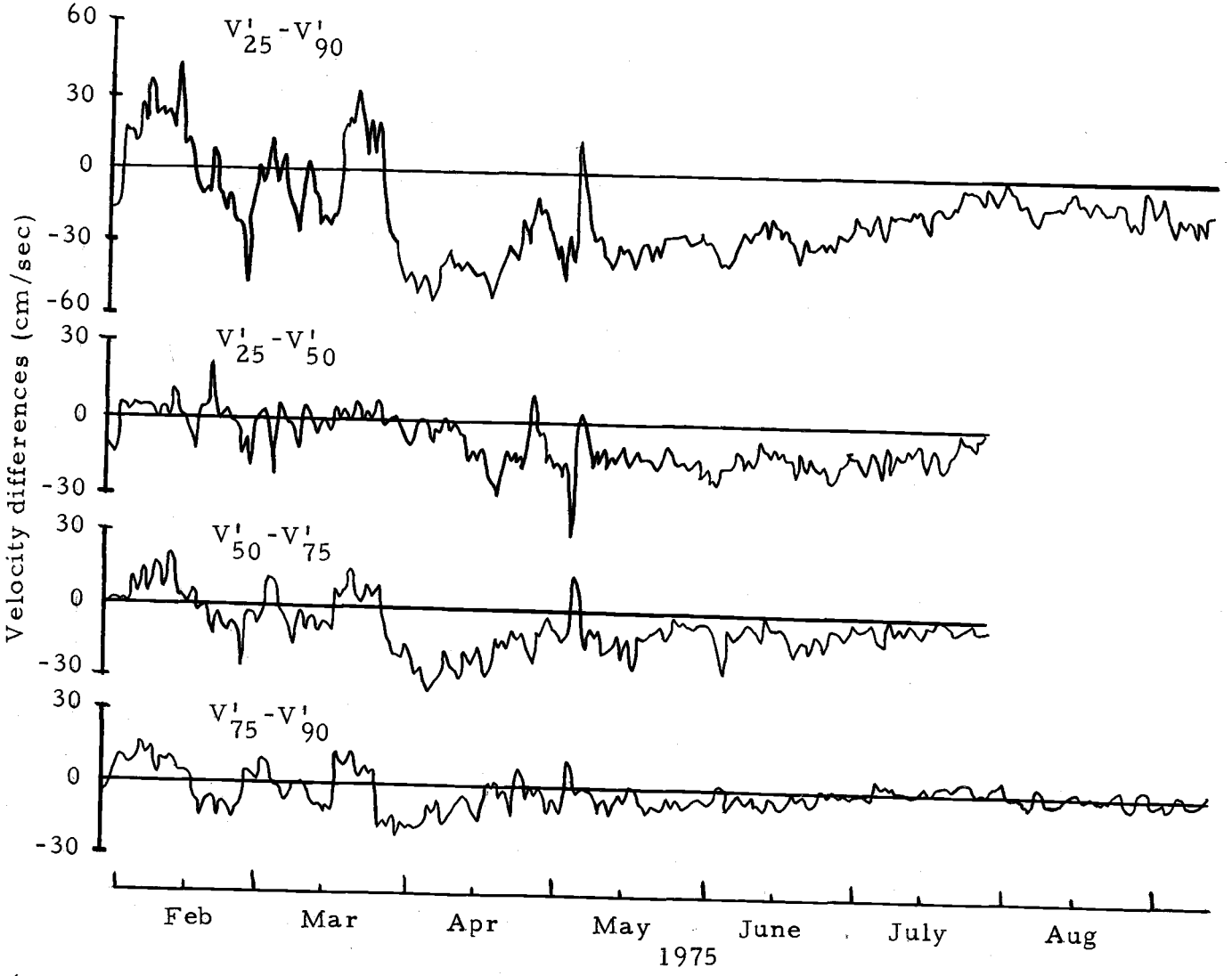

Figure 6. The difference in velocities between various vertical pairs of Sunflower current meters.

Onshore Means and Variances

The mean cross shelf components for the first segment are offshore at all current meters except for Pikake 25 m and Wisteria 150 m. They were all onshore for the second segment except for the two at Pikake.

The onshore component's variance generally decreased with increasing depth. In the first segment, the variance increases with distance offshore. The maximum onshore variance is at Sunflower during the second segment. During summer the onshore variance increases with distance from the coast over the width of the WISP array (Kundu and Allen, 1976).

Later Installations of Arrays at Sunflower

Stick diagrams for the Sunflower B array are shown in Figure 7. The southward velocity at all levels decreases with time. Deeper current meters recorded an event-like nature similar to that seen in the late winter months during the first installation. The tendency toward northward flow gradually permeates the rest of the water column from the bottom up. The mean alongshore currents for Sunflower B are very similar to those for the summer of 1973 (Kundu and Allen, 1976).

Surface velocities during the third installation of Sunflower are event-like at all depths as in the winter (Figure 8). However, the sign

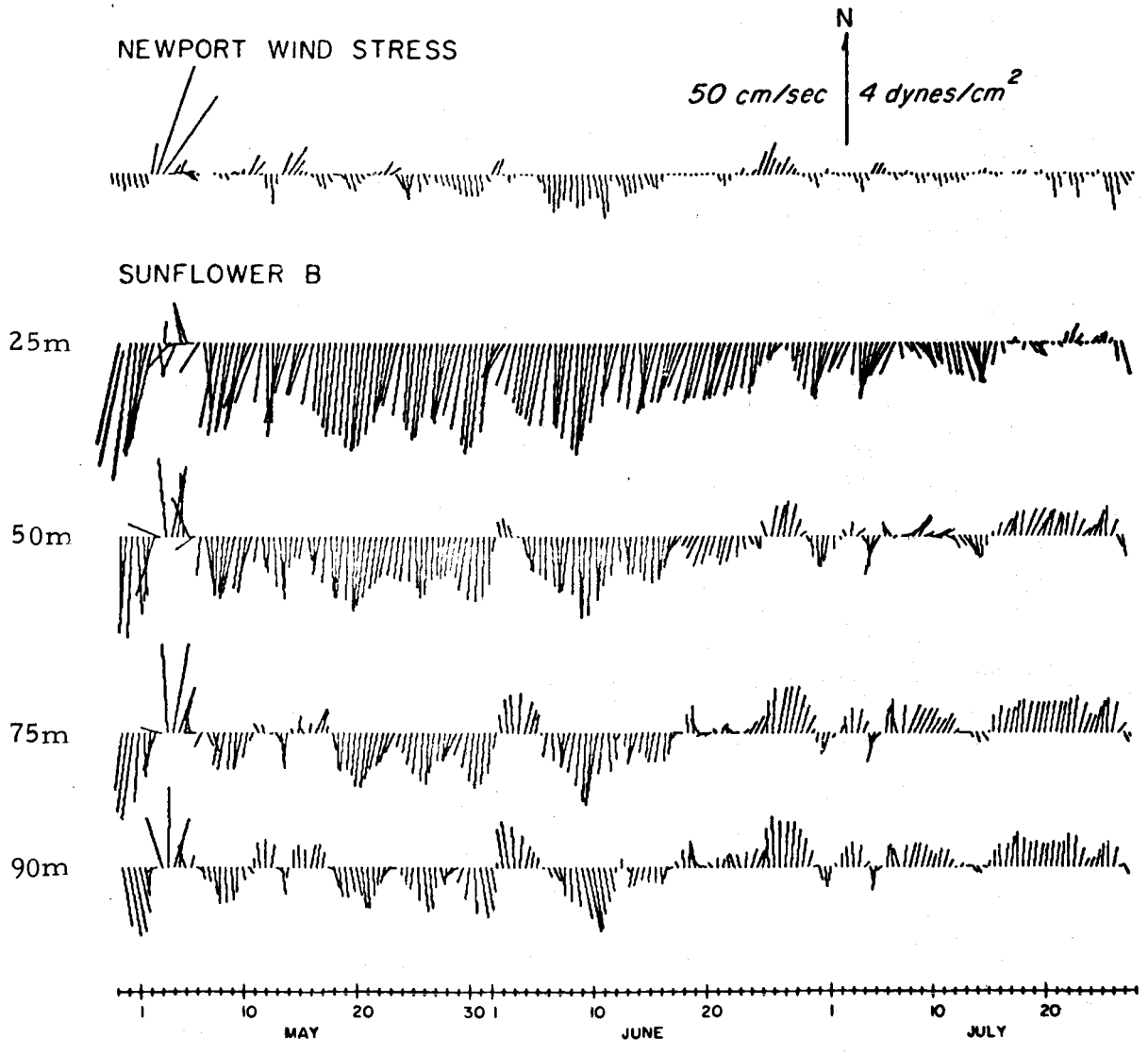

Figure 7. Stick diagrams of Newport winds and Sunflower installation B currents, 27 April to 29 July 1975.

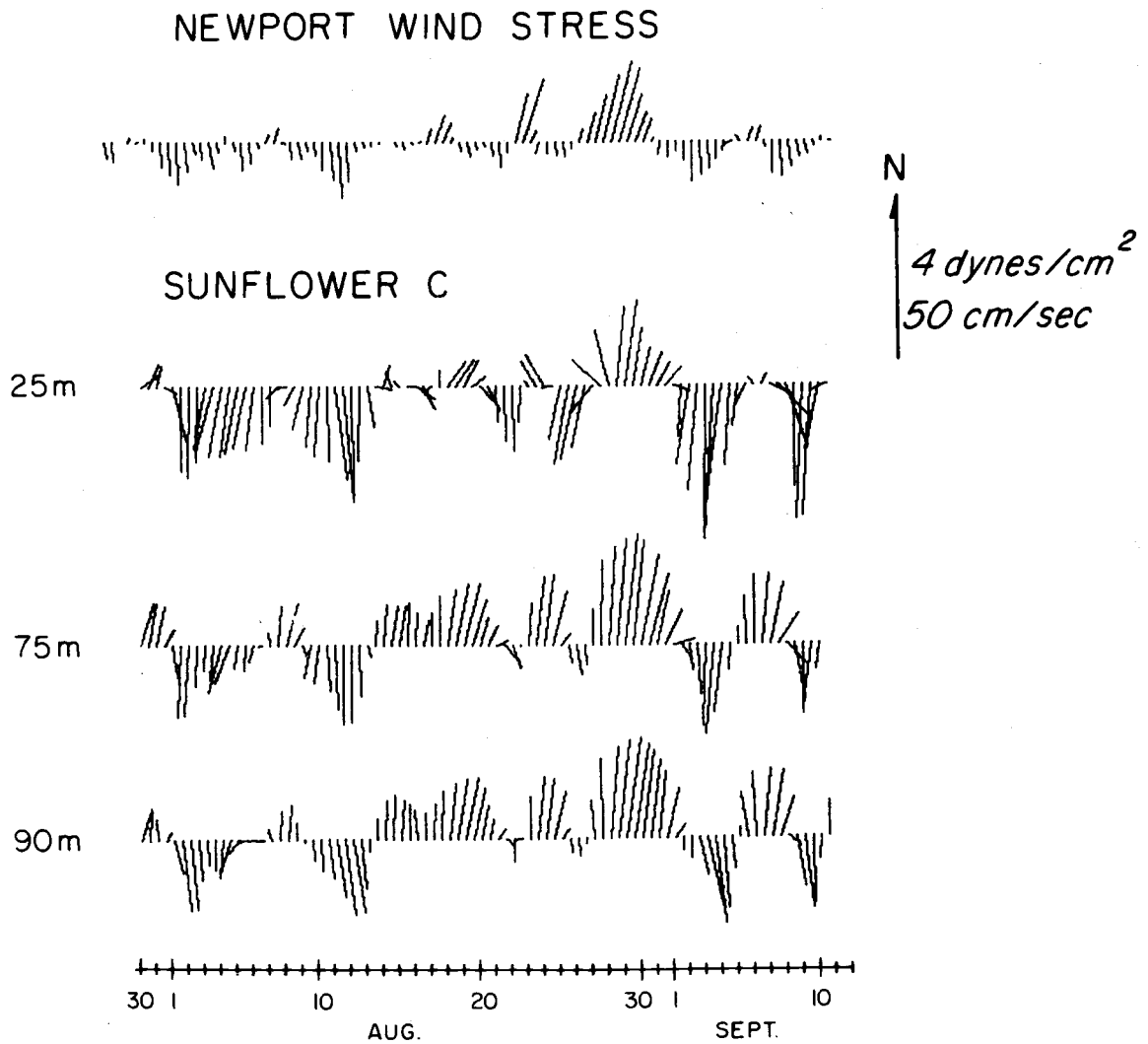

Figure 8. Stick diagrams of Newport winds, and Sunflower installation C currents, 29 July to 12 September 1975.

of the shear is constant: the deeper currents have a stronger northerly component than do the shallow currents.

Temperature, Salinity and Density

Temperature

The temperature records of the 11 current meters in the first installation are shown in Figure 9. The two temperature series at Pikake are initially quite close together and there are periods during which the waters are isothermal. These periods are 6-11 February and 23-25 March. The average temperature for these periods is about 9.2°C. The 50 m temperature drops rapidly on 25 March; thereafter it averages between 8.0 and 8.5°C. At the same time the shallow temperature begins a slow cooling trend. However it is to remain warmer than the deeper layers. Fluctuations of a period of several days occur, especially after 25 March.

A similar behavior can be seen at Sunflower. Isothermal conditions (9.2°C) exist on 10-11 February and on 21-24 March. Then a rapid cooling is seen at 75 m (it cools to 8.5°C) and at 90 m (7.5°C). The shallower records show a more gradual cooling.

The 25 m and 50 m temperature series for Wisteria lie quite close together and show an isothermal layer during the same time periods as do the other arrays. Strong events can be seen throughout

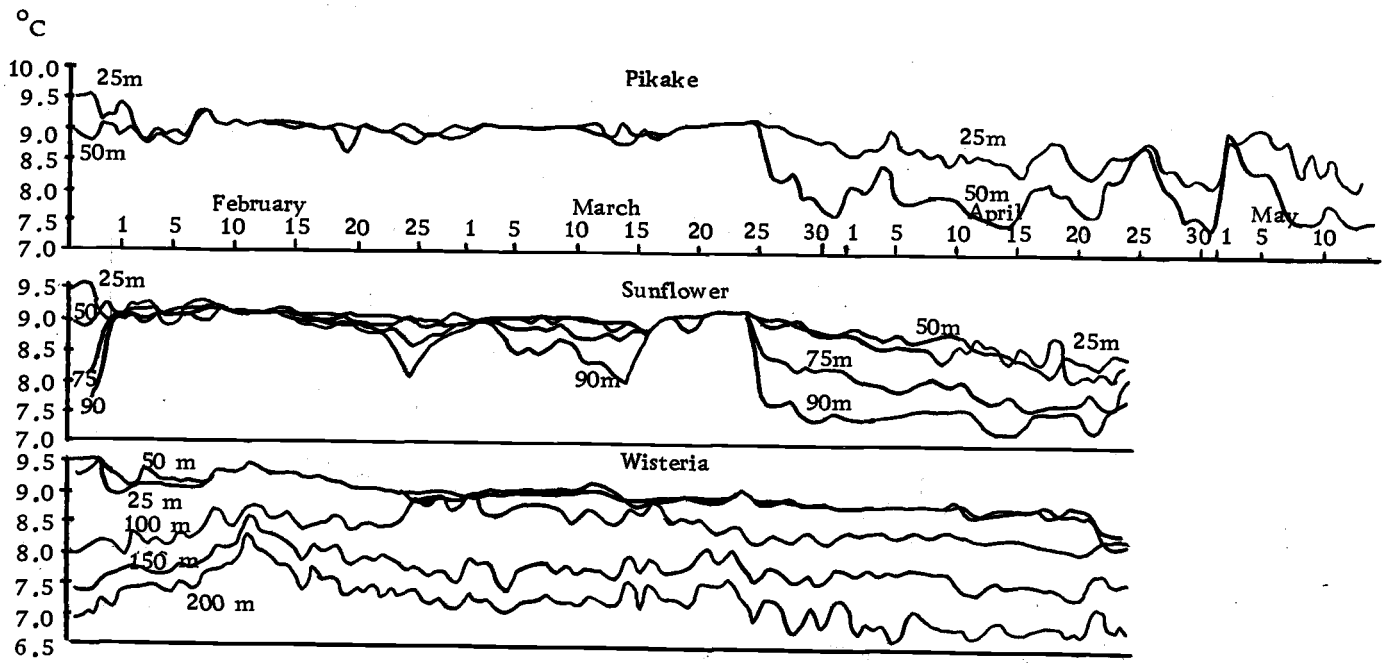

Figure 9. Temperature records from the current meters during the first installation of WISP, 29 January to 18 May 1975.

this record, especially at the deeper locations. One of the largest events occurs on 12 February when a warming at all five instruments takes place. At 200 m this warming is about 0.5°C. Although there is some activity on 25 March, it bears little resemblance to the striking events at the two inshore arrays. Throughout the observation period a general cooling can be seen at all levels.

Salinity

The behavior of the temperature records is mimicked in the records of salinity (Figure 10). In general, increased temperature is accompanied by decreased salinity and vice versa. At Pikake the waters are never isohaline but the vertical salinity gradient is small until 25 March. The relative minimums in salinity gradients occur simultaneously with those in the temperature gradients' minimums.

Two periods of isohaline behavior can be seen at Sunflower (again, coinciding with isothermal conditions). These periods represent a downwelling of low salinity (and warm surface water).[3] The vertical salinity gradient is small and is nearly constant with depth before 25 March. After that date, the 75 m salinity increases and approaches the salinity of the 90 m depth. When these two

---

[3] Since the near surface temperature and salinity remain relatively constant during these periods, mixing is unlikely. Also the winds are strongly favorable for downwelling at these times.

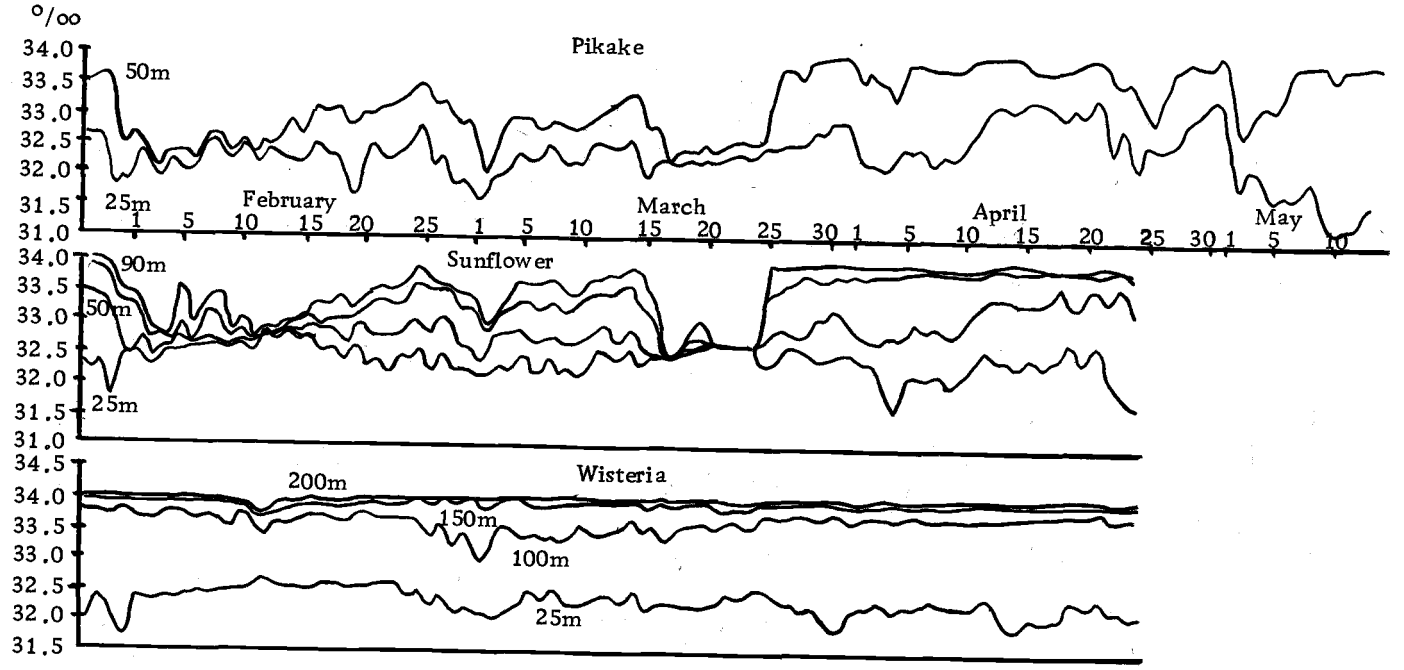

Figure 10. Salinity records from the current meters during the first installation of WISP, 29 January to 18 May, 1975.

layers have almost the same salinity, the next shallower meter (50 m) begins to experience an increase in salinity.

Unfortunately, the 50 m conductivity probe at Wisteria did not operate. The four Wisteria records that are available show constant salinities at their respective depths, occasionally interrupted by small events.

Density

Temperature and salinity variations occurred simultaneously, and occurred so as to modify the density in the same direction. Thus the sigma-t time series (Figure 11) look much like the two previous parameters. At Pikake the vertical density gradient is small before, and larger after 25 March. On two occasions at Sunflower the entire water column becomes isopycnic: 12 February and 21-24 March. Immediately before and after the latter period the density difference between 25 m and 90 m is the same. However, whereas before the density differences were uniformly divided between each current meter at Sunflower, afterwards they definitely were not. The stratification was now more localized into a pycnocline and this pycnocline moved upward with time. On 26 March the largest vertical difference in density was 0.6 sigma-t units which occurred between the 50 m and 75 m current meters. A month later, on 24 April, the largest density difference occurred between the depths of 25 m and 50 m and it was 1.3 sigma-t units.

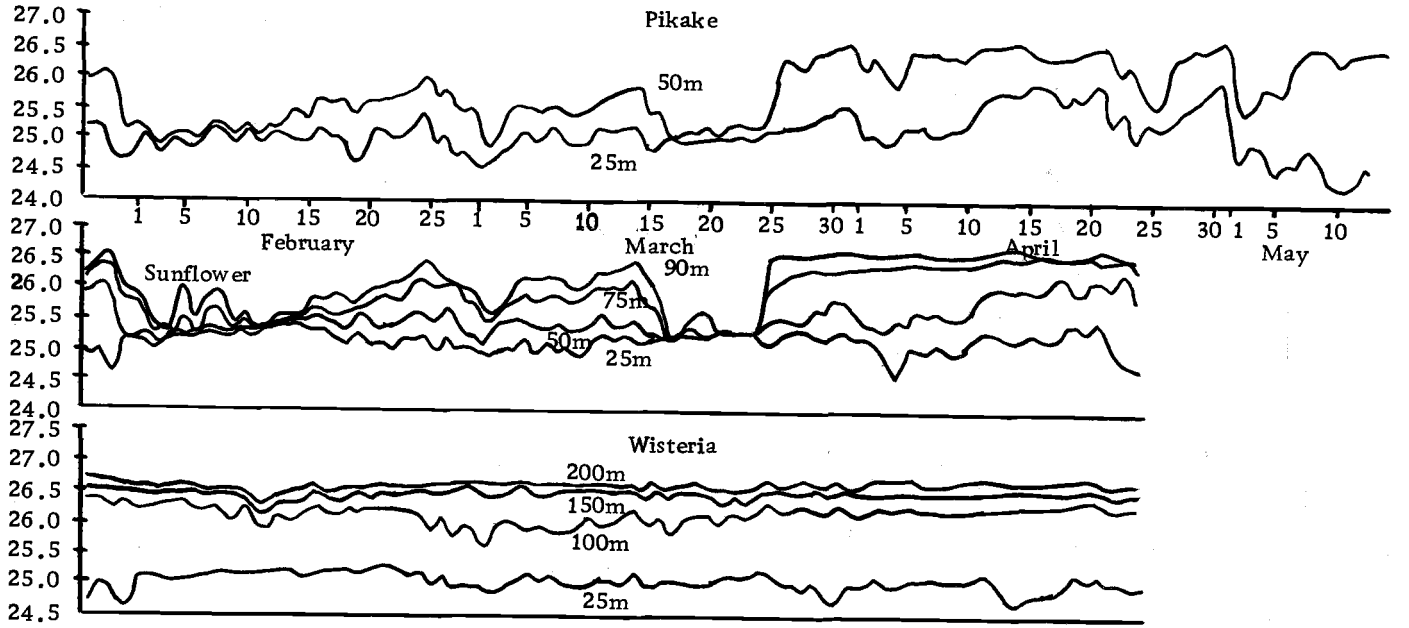

Figure 11. Sigma-t records for the current meters during the first installation of WISP, 29 January to 18 May 1975.

Later Installations of Arrays at Sunflower

During the second installation of the Sunflower array, temperature was successfully recorded at 25, 75 and 90 m, and conductivity was recorded at 25 and 90 m (Figure 12). Both the 25 m and the 75 m records show cooling throughout with the latter merging with the 90 m record by the end of June. The salinity and sigma-t plots show that the deeper layer maintains its characteristics while the shallow layer becomes increasingly saline and dense.

Only temperature was recorded at the third installation (Figure 13). The 75 m temperature is fairly constant and immune to wind force variations except during the first and ninth days of September. The 25 m record is influenced greatly by the wind and is very event-like in nature. The variations occur with a period of five to seven days.

Sea Level

The low passed, adjusted sea level for Newport is given in Figure 14. The observation period is the first nine months of 1975; the mean for this period has been removed. The events correlate well with those of the alongshore current and those of the north component of the wind. The two strongest events occurred on 12 February and on 23 March. Before 25 March the sea level is

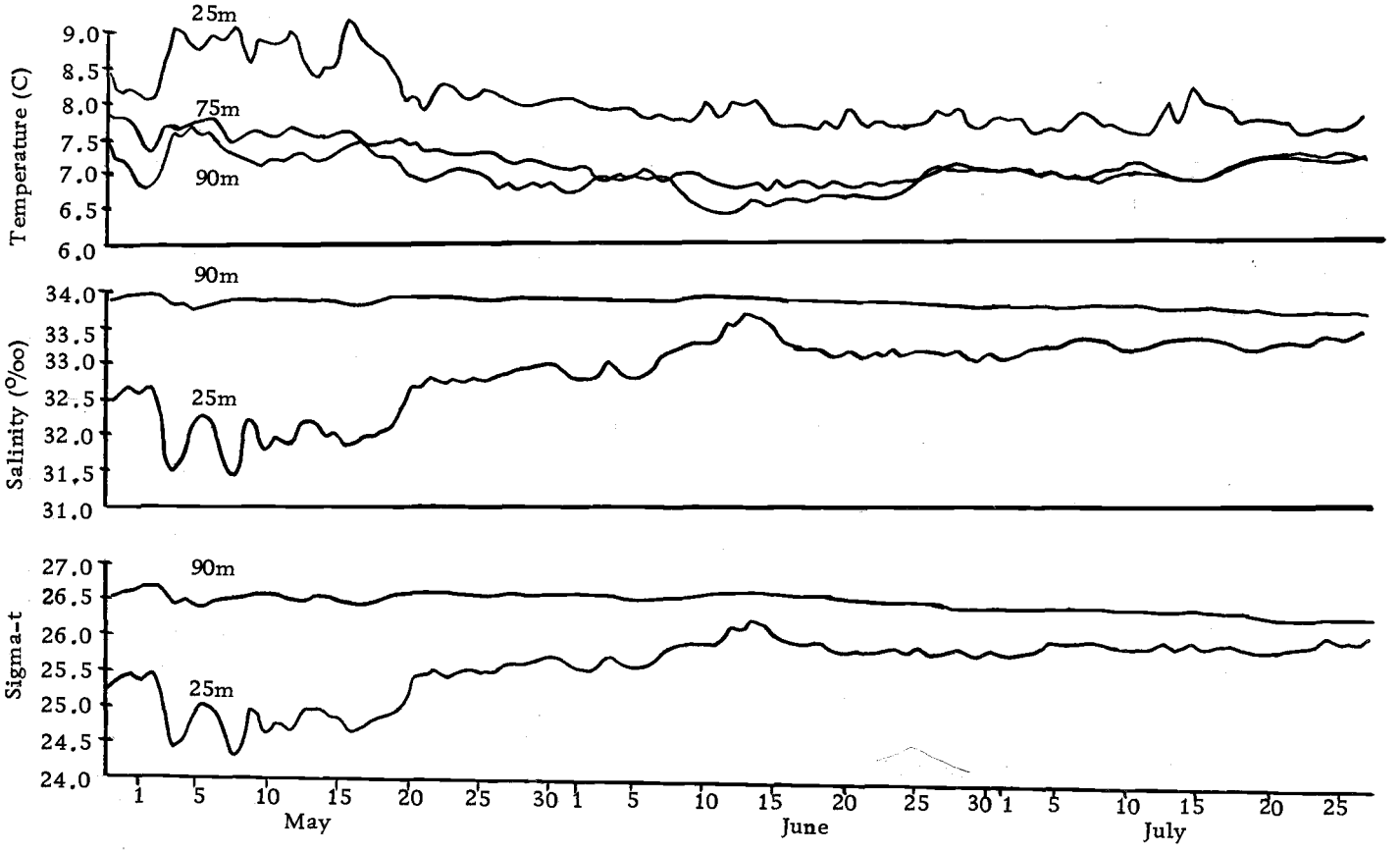

Figure 12. Temperature, salinity and sigma-t records for the Sunflower current meters during the second installation, 27 April to 29 July 1975.

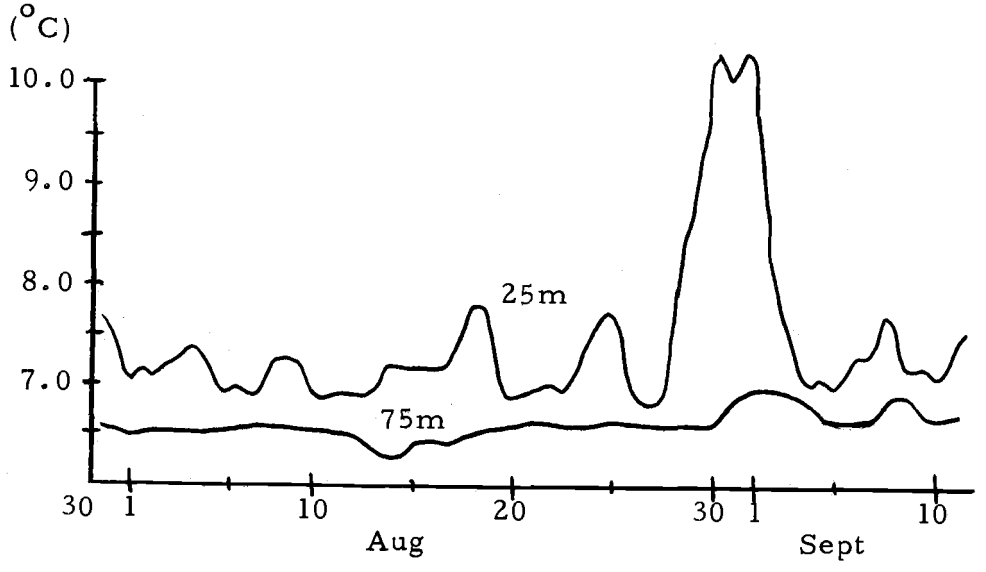

Figure 13. Temperature records from the Sunflower current meters during the third installation, 29 July to 12 September 1975.

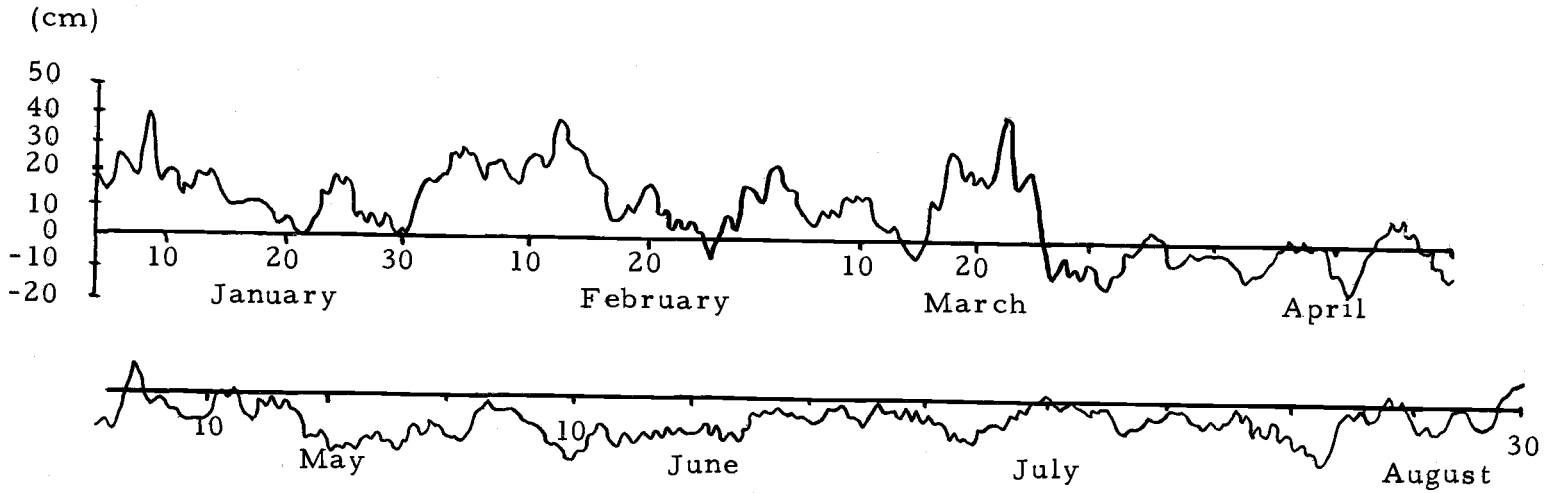

Figure 14. Sea level at South Beach, January through August 1975. The sea level has been adjusted for atmospheric pressure and the mean of the sample has been removed.

above its mean and after that date it is almost entirely below it. Gradually the level rises throughout the summer and by September it is again above its mean. The variations in sea level have a dominant period of about a week.

Winds

The zonal (east-west) component of the Newport Winds is dominated by west winds; the variance of this component decreases with time. The north component has a much larger mean and variance than does the east component. For the first two months the averaged winds are northward. The winds are not steady but blow in a series of events. For the next two months the mean winds are small as the record is composed of a series of northward and southward events. Starting in late May and running through mid-August, the average is southward with only an occasional northward event. At the end of the observation period a northward event occurs which appears as if it might mark the end of the season.

Bakun's Winds

Additional wind data were provided by Bakun (1976). These series were calculated from surface atmospheric pressure charts on a 3^{o} by 3^{o} grid: the geostropic winds were rotated 15^{o} counterclockwise

and reduced in magnitude by 30% to simulate surface frictional effects (Bakun, 1973).

Stick diagrams for three (of the 13 provided) wind time series are given in Figure 15. The series are for latitudes 45°N, 35°N and 25°N for the first five months of 1975. At 45°N the first part of the time series is dominated by strong northward events. These are interrupted by much weaker and shorter duration southward events. The first major southward event occurred on 25 March, closely following a strong northward event. After this date the wind speed decreased, the number of northward events diminished and no strong northward events occurred. The winds then became steadier in strength (about 10 m/sec) and in direction (southward).

The winds were southward more at 35°N than at 45°N. Before 25 March there were only two strong northward events and afterward there were none. The wind velocity increased in magnitude after that date. Its predominant direction was southward with a fairly consistent eastward component.

At 25°N the wind speed was smaller than at the higher latitudes. The wind was southward and contained both eastward and westward components. In the early part of the time series, none of the three wind records bore close resemblance to the others. However, in the later part the 35°N and the 25°N time series were similar. The intermediate latitude wind record shows an orderly transition from

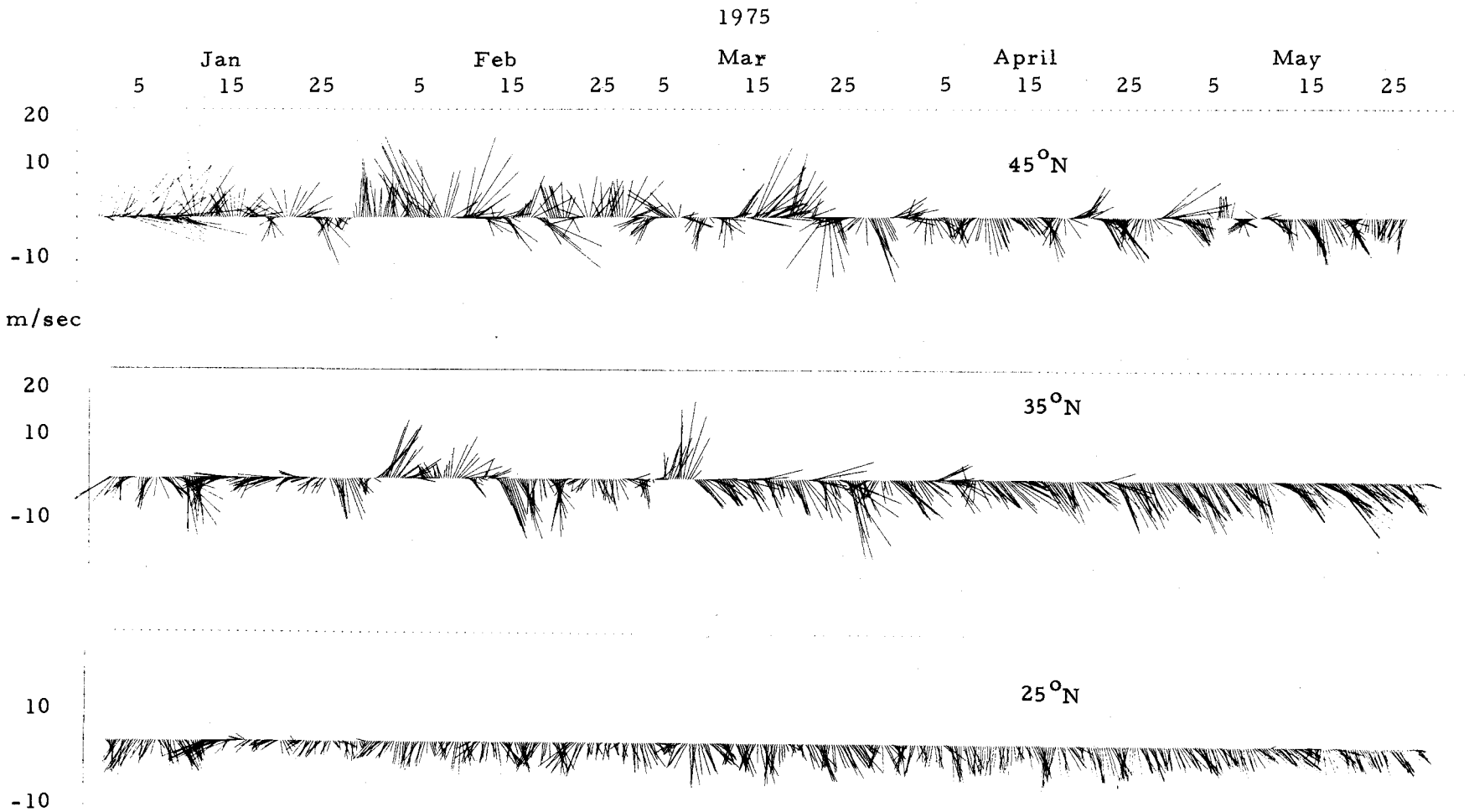

Figure 15. Stick diagrams of Bakun's winds at 45°N, 35°N and 25°N along the coast. Units are m sec^{-1}.

one regime to the next. From this comparison it is apparent that the winter meteorological system dominant at 45°N is different from that ten or more degrees of latitude to the south.

COMPARISON OF SHELF DYNAMICS IN WINTER, SPRING AND SUMMER

In this chapter we will compare various physical parameters to determine which have a seasonal behavior and what that behavior is. One hypothesis of this study is that the transitional event marks the change from winter to spring conditions. Evidence to support this idea are the changes on 25 March 1975 in the data records presented in Chapter II. Using the definitions of the seasons given on page 5, the winter season ends on that date. A distinction between spring and summer is not immediately apparent.

The structure of the alongshore fluctuating flow will be examined in a section perpendicular to the coast for winter and spring data from 1975 and for summer data from 1973. The 1973 data have been analyzed by Kundu et al. (1975) and by Kundu and Allen (1976).

In general the various data series were divided into two sections: before and after the transition event (25 March). We will present statistics of the physical parameters (e.g., means and variances) and will test whether they are significantly different on each side of that date. The periods before and after the transition event were further divided in situations where the data series or the analysis warranted it. A four day gap (23 March-27 March) was left between the segments so that the transition itself would not be included.

Wind

The purpose of this section is to ascertain differences between winter and summer and whether atmospheric disturbances propagate at the same velocity in both seasons. The seasonal changes in the Newport winds can be seen in plots of 30 day averages (Figure 16). In February and March the mean of the north component is northward, while after March the means are southward. The change in the direction of the mean winds closely corresponds to the change in the direction of the mean currents (also in Figure 16).

In the low-low pass filtered time series of Newport wind stress (Figure 5), no sharp seasonal change is immediately apparent. A change is more apparent in the geostrophic winds (Figure 15), which are averages over three degree squares. There is a decrease in the wind velocity and there are fewer northward events in summer.

A statistical testing of the significance of the change in the means and variances of upwelling indices (offshore Ekman transport) for the periods before and after the transition was carried out. The test for differences in mean values was a normality test on the statistic d, where

$$d = (\overline{X}_1 - \overline{X}_2) / \sigma$$

and

$$\sigma^2 = \frac{S_1^2}{N_1} + \frac{S_2^2}{N_2}$$

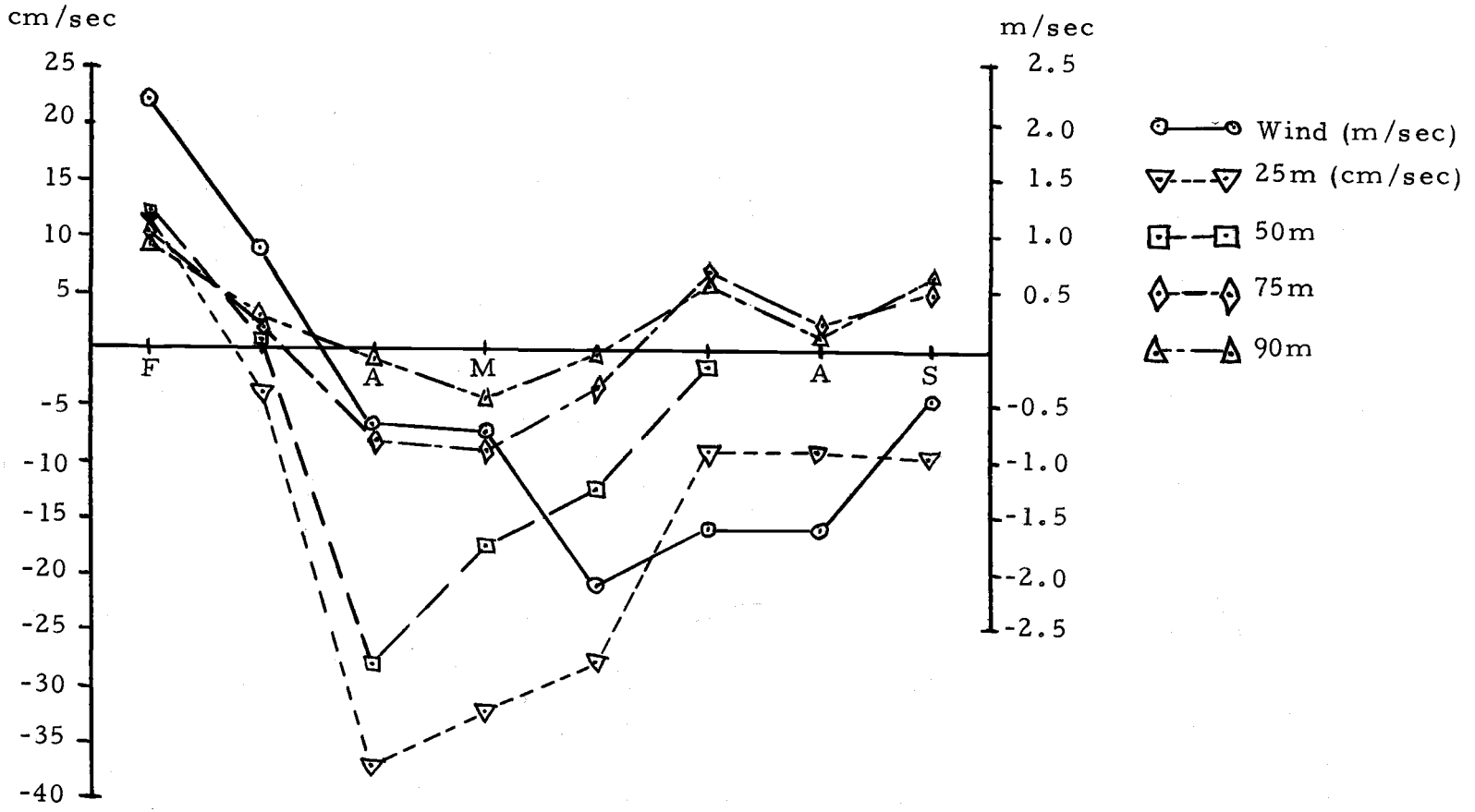

Figure 16. Thirty day means of the northward components of Newport wind (in m/sec) and Sunflower currents (cm/sec).

The statistic d is compared to a Gaussian distribution with a zero mean and variance (σ^2) of one (Petersen, 1973).

For testing the differences in variances, another statistic, z, is computed and compared to a Gaussian distribution. For sample variances from the same population

$$\ell n\left(\frac{S_1^2}{S_2^2}\right) \sim N(0, \sigma^2)$$

$$\sigma^2 = \frac{1}{df_1} + \frac{1}{df_2}$$

Form $$Z = \frac{\ell n\left(S_1^2/S_2^2\right)}{\sigma^2} \sim N(0, 1)$$ (Ramsey, 1976).

For this test, data were taken from the periods 29 January to 23 March and from 27 March to 19 May 1975. This period coincides with the period of the first installation of the Sunflower current meter array, for which a similar statistical testing is done later. For the upwelling indices both the means and variances were significantly different (at the 0.99 level) before and after the transition. Thus it appears that there is a fundamental change or transition in the atmosphere at the same time as in the ocean over the continental shelf.

In Figure 17 are the spectra of the northward components of Bakun's winds at 45°N for winter (1 January to 1 April) and summer (1 June to 30 August) 1975. The winter spectrum is approximately

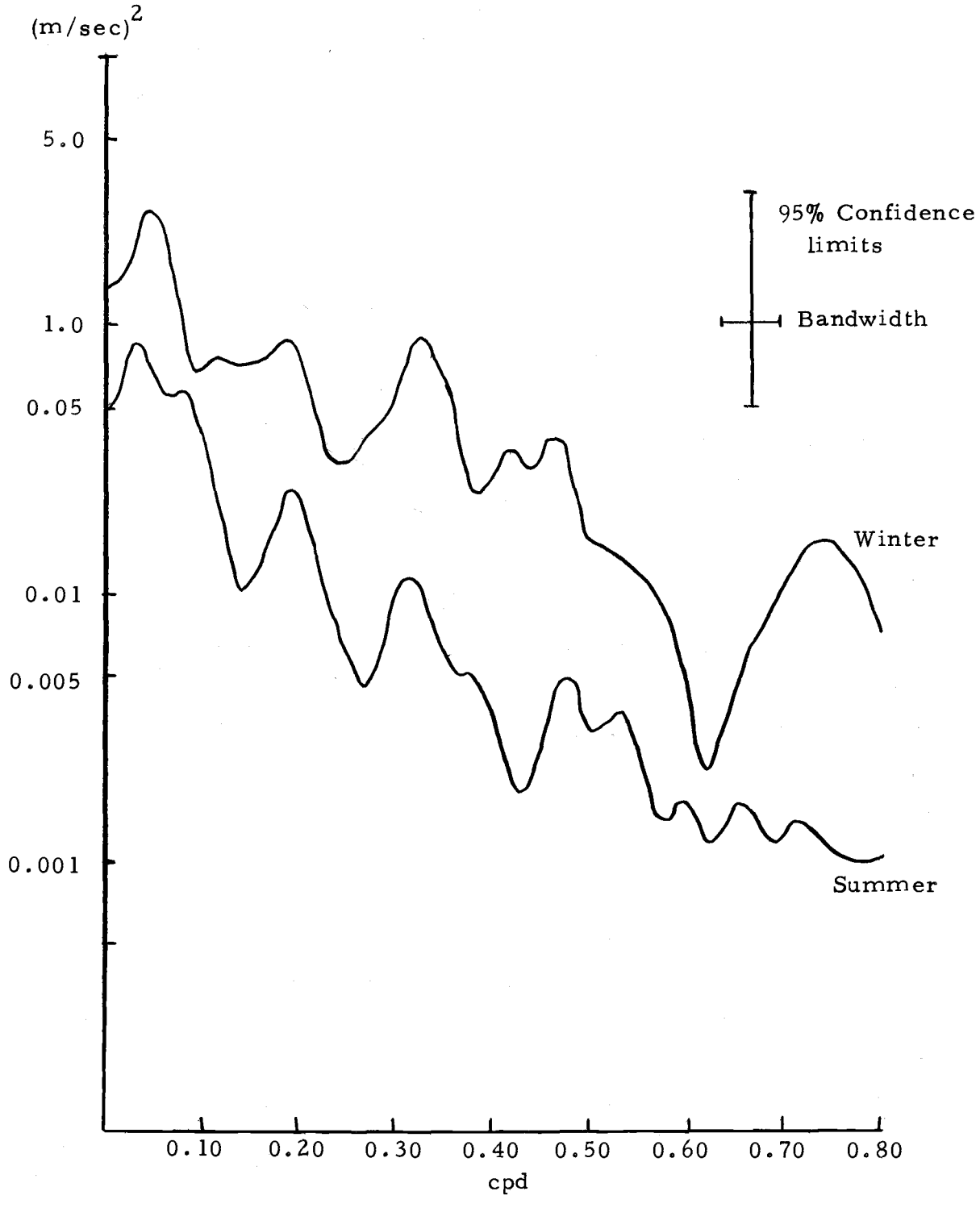

Figure 17. Spectra of the north component of Bakun's winds at 45°N for winter and summer.

a half an order of magnitude larger than the summer spectrum. Peaks occur in nearly the same frequency bands in both spectra. The major contradiction to this last statement is at 0.73 cpd: the winter spectrum has a significant peak there, while such a peak is absent in the summer spectrum.

Cross correlations between the wind at 45°N and at various other latitudes are shown in Figure 18. In the first part of this figure is the correlation for winter, and in the second is that for summer. The correlations with wind at 47°N and 43°N are quite high for both seasons. However the correlation is also high for the winds at 37°N in winter, but not in summer. Thus it appears that in winter the atmospheric systems that influence conditions at 45°N extend farther south than they do in summer. (We note the sawtooth appearance of correlations in summer. This is due to the daily sea breeze effect.)

Coherence squared and phase between the north components of wind at 47°N and at 43°N are shown in Figure 19 for both seasons in 1975. Throughout most of the frequency range, especially from 0.13 to 0.60 cpd, the coherence is higher in winter than in summer. Both seasons have significant coherence almost throughout the frequency range tested. The phases are shown in the bottom half of this figure. Values are not plotted if the corresponding coherence was not significantly greater than zero at the 5% level. For both seasons the

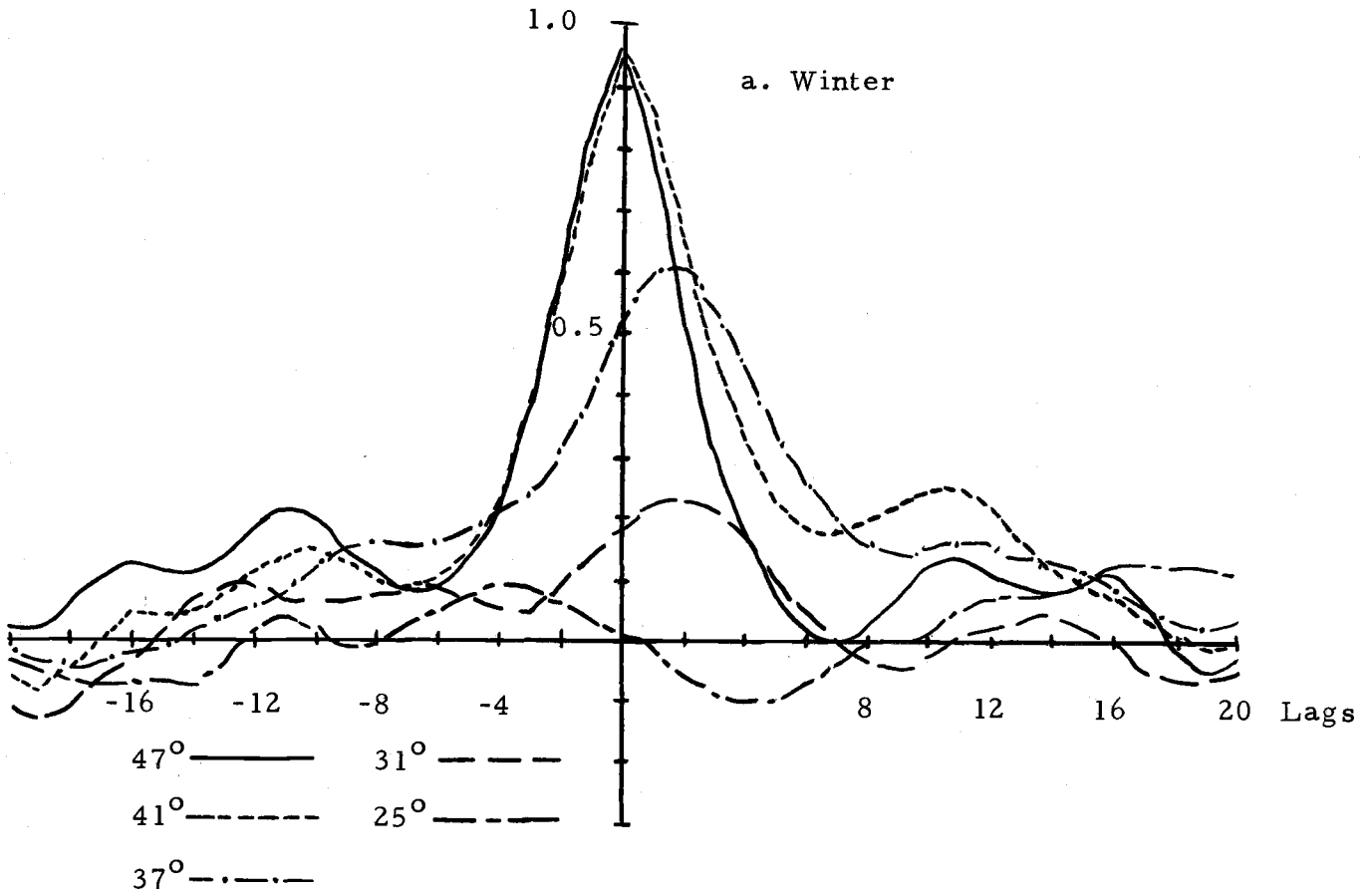

Figure 18. Cross correlations between the north components of Bakun's winds at 45°N and various other latitudes. Each lag corresponds to a time lag of six hours. Positive lags mean that the winds at 45°N lead. a. Winter. b. Summer.

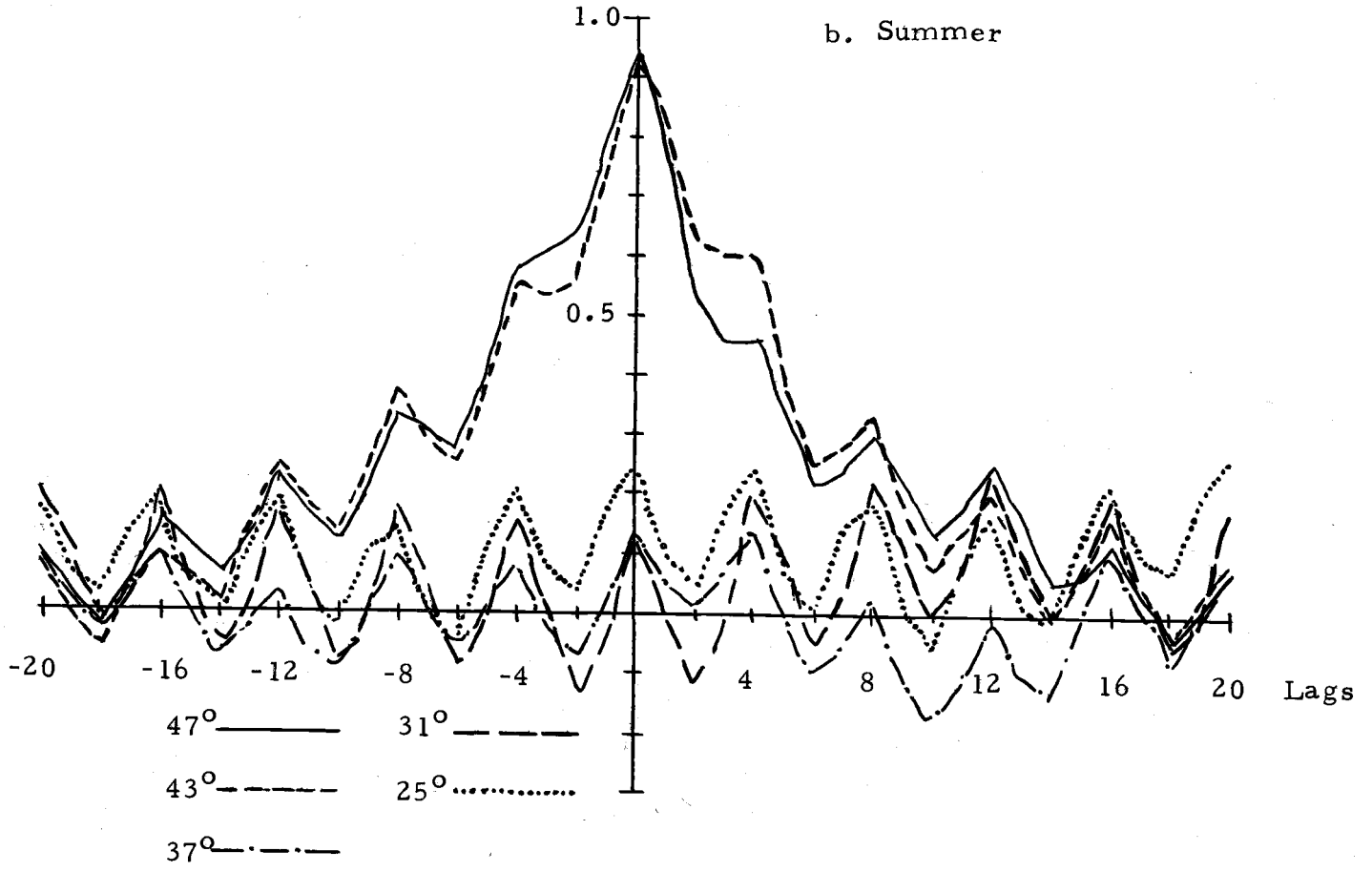

Figure 18. (Continued)

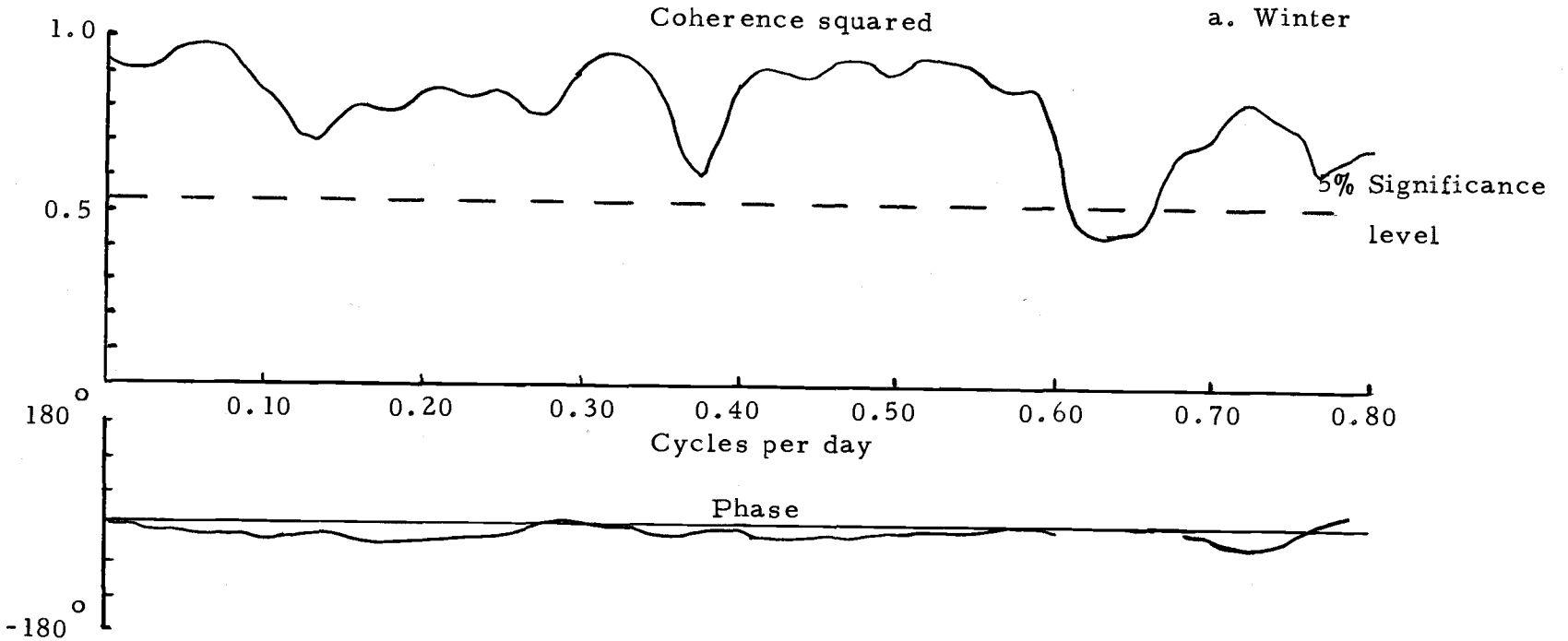

Figure 19. The cross coherence squared and phase between the north components of Bakun's winds at 47°N and 43°N. Phases are plotted only when the coherence squared is significantly greater than zero at the 5% level. Negative phase angles indicate southward propagation. a. Winter. b. Summer.

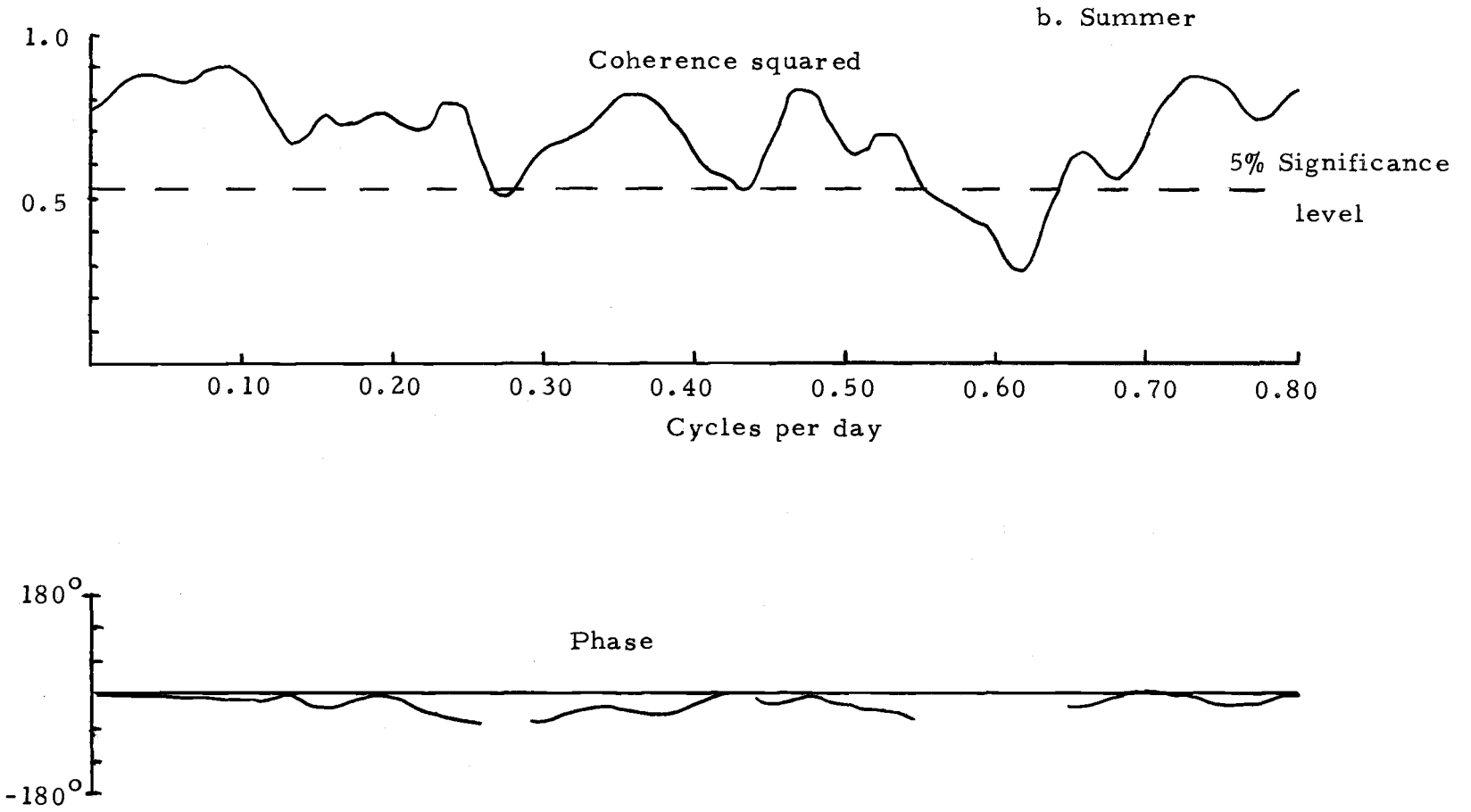

Figure 19. (Continued)

phase angle is small and indicates a southward propagation. Table 2 summarizes the phase relationships at frequencies that were also coherent in the alongshore direction for currents and sea level currents (see Chapter IV). All four frequency bands show a southward propagation both in winter and summer.

The Current Field

Means and Variances

Thirty day means of the north components of Sunflower currents show the seasonal change in flow direction and vertical structure of this component's flow (Figure 16). The large increase in shear and the change from northward to southward currents occurs between March and April. The shear then rises in the water column and the currents become more northward. The undercurrent appears at the deepest current meters and rises upwards. Data taken in 1973 (Huyer et al., 1975a) show the same behavior.

Figure 20 gives another visualization of the seasonality in the alongshore currents. Plotted here are the means and standard deviations (about those means) for the Sunflower array. These data were obtained by joining the data from the three installations at Sunflower. They have been divided into four equal length segments; each has a length of 53.75 days. A four day gap encompassing the

Table 2. Coherence squared and phase of Bakun's winds at 47°N and 43°N for selected frequencies. These bands were chosen because they have peaks in the alongshore coherence of sea level or alongshore current components. Also shown are the computed wavelengths and phase speeds.

Frequency	Season	Coherence squared	Phase (°)	Phase error (°)	Direction	Wavelength (km)	Phase speed (km/day)
0.06	winter	0.98	15	2	southward	5400	320
	summer	0.86	3	7	southward	27000	1600
0.16	winter	0.79	25	15	southward	3200	512
	summer	0.72	13	17	southward	6200	985
0.24-0.26	winter	0.85	10	8	southward	8000	2000
	summer	0.79	48	15	southward	1700	420
0.38-0.42	winter	0.91	18	4	southward	4500	1800
	summer	0.57	0	25			

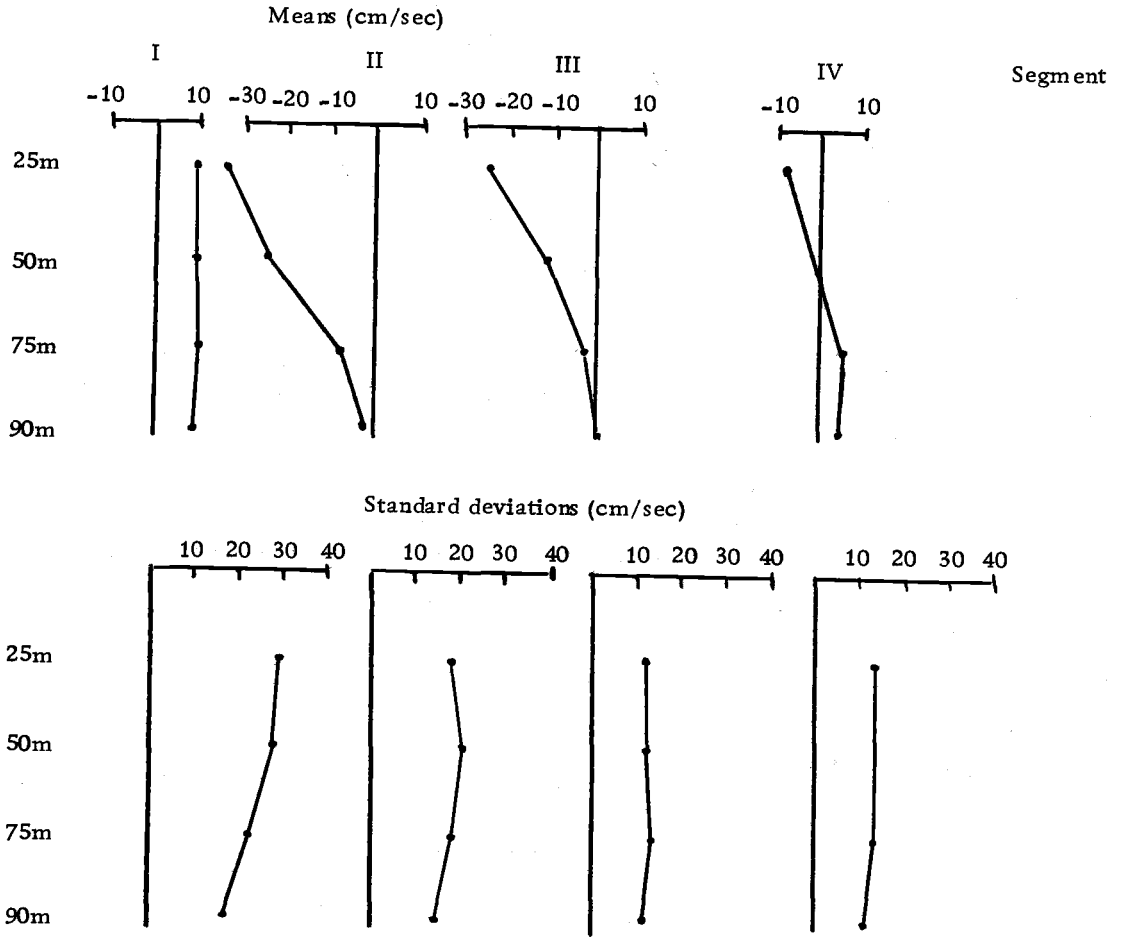

Figure 20. Means and standard deviations of alongshore currents for four segments of the Sunflower installations. The periods of the segments are: 29 January to 23 March; 27 March to 19 May; 19 May to 12 July; and 12 July to 4 September.

the transition was inserted between the first and second segments. In the first frame of Figure 20, the mean currents are northward and essentially barotropic. The time period for this segment is 20 January to 23 March. A strong mean shear is seen in the second frame (27 March to 19 May) with the maximum current at the surface and the current decreasing almost linearly with depth. Now all velocities are southward. The shear, which develops at the time of the transition, persists throughout the rest of the current meter installation. The velocities have decreased in the third segment (19 May to 12 July) and the 90 m mean is almost zero. Finally a northward flow at depth and a reduced southward flow at shallower depths is seen in the last frame (12 July to 4 September). Note that there is no 50 m data from the last segment.

The standard deviations show a decline in magnitude from the first to the third frames. In the last frame a slight increase over the standard deviations in the preceding one is seen. During the first three segments the surface standard deviations have the greatest decrease with time, and by the third segment the standard deviations are almost uniform with depth.

Thus the characteristics of the current regime change at the time of the transition event. Especially at the shallow meters the high variance, low mean, northward winter conditions are replaced by lower variance, high mean, southward currents of the summer

condition. Soon after the transition, the currents show a decline in the strength of their southward flow. By mid-June a northward undercurrent is established. The northward flow gradually erodes the shallower southward flow, eventually making the current uniform in direction. This seasonal description has been reported previously by Huyer et al. (1975a).

The alongshore components experienced a larger decrease in variance than did the onshore components in the succeeding segments of Sunflower. In each of the four segments the ratio of the alongshore variance to the onshore variance decreased from the preceding segment. For Sunflower 25 m these ratios were:

Segment	Ratio
1	31
2	17
3	14
4	11

The largest decrease occurred between the first two segments. Using Table 2 from Kundu and Allen (1976) the same ratio can be calculated for the Coastal Upwelling Experiment-II (CUE-II). This experiment was conducted in July and August, 1973. The Carnation array in that study was near the location of the Sunflower array. For the 20 m Carnation currents, the ratio was approximately 5. Thus the distribution of energy seems to be more equally distributed between

the alongshore and onshore components as summer season is approached.

In order to show that the changes in the flow field at the transtion event were significant, statistical testing of the difference of the means and variances of the current components before and after the transition was carried out. The tests that were used were the same as those used for the wind data.

The 11 time series of each current component were averaged in two segments: 29 January to 23 March, and 27 March until 25 April for Wisteria, 14 May for Pikake, or 19 May for Sunflower. The 11 pairs of mean values are shown in Figure 21. Prior to the transition all flow is northward with the maximum occurring at Pikake 25 m. Post-transition means show a strong southward flow, centered at Sunflower, and near the surface. It decreases towards the bottom.

The before and after transition means were significantly different for both components of all current meter records except for the 200 m Wisteria onshore time series. The variance of the alongshore components had a significant decrease (at the 0.99 level) across the transition except for Pikake 25 m. Only four of the 11 onshore components had a significant change in their variance: Sunflower 25 m, 50 m and 75 m; and Wisteria 200 m. The distribution of

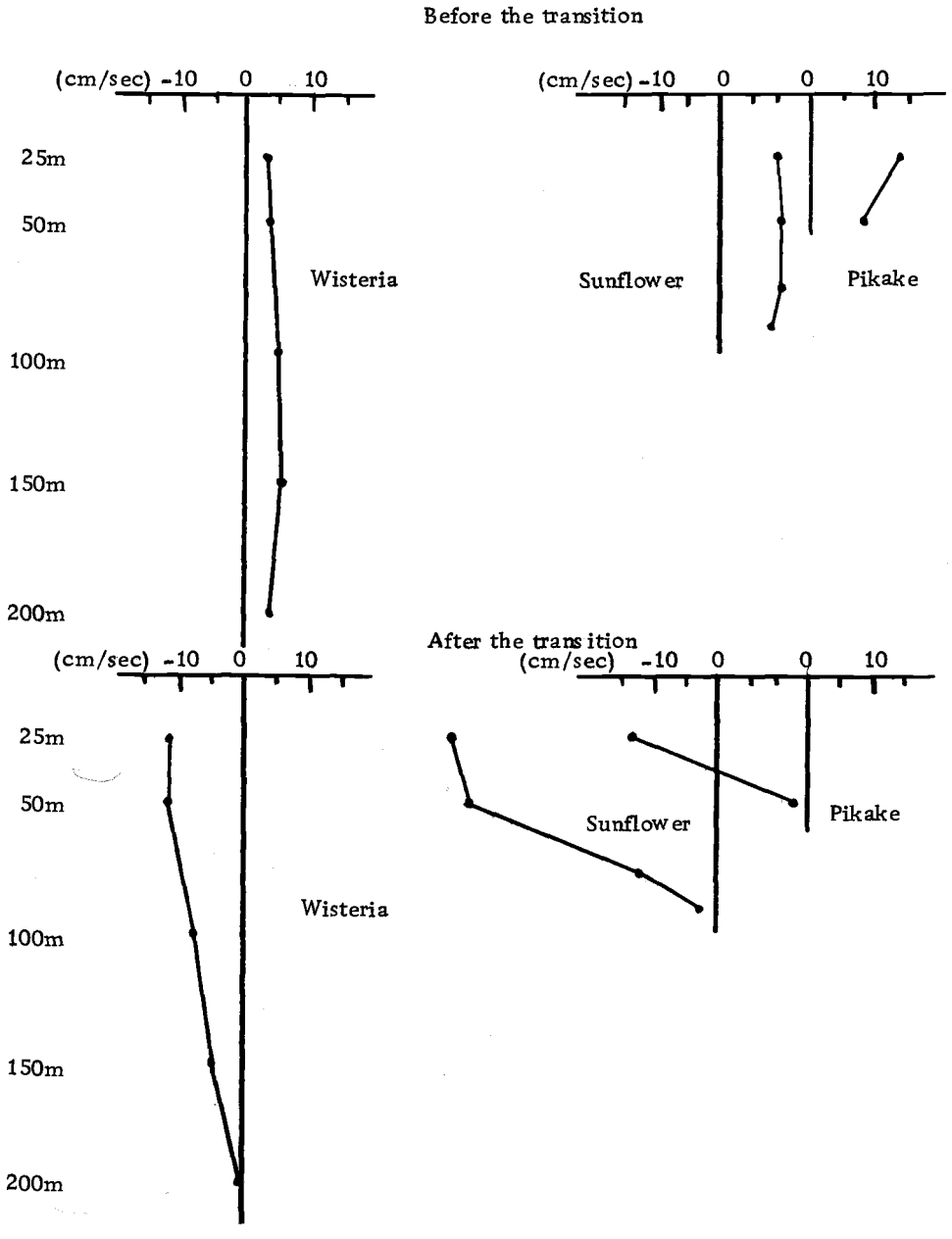

Figure 21. Means of the WISP currents before the transition (29 January to 23 March) and after it (27 March until 25 April for Wisteria, 14 May for Pikake, or 19 May for Sunflower).

variance is strongly asymmetrical with the alongshore components dominating.

Vertical Shear

The mean vertical shear, which was quite small prior to the transition, increased immediately after it. As seen in Figure 6 the shear before the transition changes sign on the event time scale. The shallower currents were larger than the deeper ones regardless of the direction of the current. After the transition the shallower currents were more southward than the deep currents and the sign of the shear was constant. The shear between 75 m and 90 m at Sunflower decreased quickly and, by the middle of April event time scale changes in the sign of the shear were seen. The shear in the other records also showed a decrease in magnitude but, except for one or two occasions, they were constant in their sign.

Before the transition the shear was evenly divided throughout the water column on the shelf. Immediately after the transition, most of the shear was concentrated at depth. Gradually the shear progressed up the water column.

The onshore velocities vary with the position of the maximum vertical shear in the alongshore currents. We refer to this maximum in shear, which slopes upward toward the coast, as a shear front. The maximum shear at Sunflower immediately after the transition is

located between 75 m and 90 m. After April first, it is located between 50 m and 75 m. By the end of April, it is between 25 m and 50 m. Immediately after the transition all of the cross shelf current components are directed westward, except at 90 m where there are fluctuations of both signs. By the first day of April, the westward component at 75 m has become an oscillating flow. This change occurs by mid-April at 50 m. At 25 m occasional eastward events are seen in late April, but not until early July does the flow show event time scale sign changes.

The same upward progression is seen in the density stratification (see Figure 11) as was seen in the current shear. Thus on the bases of this casual analysis, we find westward flow at depths that are above the maximum shear and the pycnocline. These surfaces are inclined and they move offshore as they move upward. The presence of these surfaces at the sea surface indicates upwelling. Below or inshore of these surfaces, the flow oscillates eastward and westward, probably in response to local wind forcing.

Empirical Orthogonal Analysis of Currents

To further examine the distribution of the horizontal velocity in the section perpendicular to the coast (at 45°N) we perform a modal analysis. Empirical orthogonal techniques have two advantages. They allow for the objective analysis of the structure of the fluctuating

components of the time series. They also offer the ability to simplify data analysis of large data sets by generating new time series which concentrate most of the variance into a few time series which can be used for subsequent analysis instead of the more numerous original time series. Thus significant features of the original data are represented in only one or two series. A description of the techniques is given by Kundu et al. (1975).

Technique

In empirical orthogonal decomposition a set of intercorrelated data is represented by a new set of time series. These new time series are uncorrelated (at the zero lag). The advantage of this technique is that with a judicious choice of expanding functions, only a few of the new time series are needed to account for a high percentage (e.g., 90%) of the original series's variances. Thus instead of dealing with a fairly large number of data series, we would be able to use a much smaller number of the new series in analysis and still be able to include almost all of the variance in the original series.

The generating functions for the new series are the eigenvectors of the correlation matrix of the original data series. The first eigenvector accounts for more of the data variance than could be taken into account with any other eigenvector. The second eigenvector similarly can account for the largest amount of variance once the variance

associated with the first eigenvector has been removed. Associated with each eigenvector is an eigenvalue that describes the amount of variance that is accounted for by that eigenvector.

Each of the components of an eigenvector is associated with a particular data series. Thus for data series collected at different locations, the components of each eigenvector constitute a characteristic pattern of those data. This pattern is called an empirical mode.

In empirical orthogonal decomposition, a correlation matrix is calculated by taking the correlations of each associated scalar series (e.g., onshore currents are correlated only with other onshore currents). This matrix is solved for its eigenvectors and eigenvalues. The former determine the characteristic pattern of the variance of the field, and the latter represents the energy content of each particular pattern. A time series for each mode is generated by taking the inner product of the eigenvector and the several time series at each time step in the data. The units for this new time series are the same units as for the original data series.

Data will be analyzed by the method of empirical orthogonal decomposition in both one and two dimensions. In one dimensional analysis the several time series at an array of current meters are combined to yield a vertical description of the fluctuations there. By analyzing all of the WISP current meter data a two dimensional

(vertical and cross shelf) picture of the fluctuating time series can be obtained.

Analysis Including the Transition Event

For the one dimensional analysis at Pikake, the alongshore dominant mode was quasi-barotropic and contained 96% of the energy that was in the alongshore components. At Sunflower 94% of the energy was in the first mode and 5% was in the second. For Wisteria, the dominant mode was quasi-barotropic (84%) and the second mode was similar to the first dynamic baroclinic mode (12%). This relatively high percentage of energy in Wisteria's higher modes is probably due to the fact that the pycnocline was typically deeper than the bottom current meters at the other two arrays. Thus in the water column at Wisteria there was probably more current shear (associated with the pycnocline) than at the inshore arrays. In an analysis of the north components of summer shelf currents, Kundu et al. (1975) found 91% of the energy in the first mode (barotropic in nature) and 7% in the second (which was the first dynamic baroclinic mode).

A time series for each array's modes was generated. As expected, the first modes at each array were very similar to the current meter time series there. These first mode series were also similar to one another.

A comparison between the first and second modes of the Sunflower alongshore currents was conducted to see if a linear relationship might exist between them. Their cross correlation yielded a small but significant relative maximum value at a lag of 3.75 days. The first mode lead. A high cross coherence between the two was also found. At low frequencies the second mode led and at high frequencies the reverse was true. (This calculation was repeated for the onshore components, but only four small frequency bands had even barely significant coherence. Their phases were large in magnitude and were variable.) It thus appears that there is a leakage of energy between the two modes over a wide range of frequencies.

The empirical orthogonal modes of the alongshore velocity at Sunflower were correlated with both the temperature and the sigma-t records at 50 m at Sunflower. The first mode had a correlation of 0.40 (-0.50) with the temperature (sigma-t) record and the second mode had a correlation of -0.69 (0.50) for the same variables. Kundu et al. (1975) found the same correlation (-0.67) between the second mode and the temperature in summer for a current meter in approximately the same location and depth. This seems to indicate that as current shear strengthens (the second mode's energy is increased) colder temperatures are encountered. Current shear is

increased during upwelling favorable wind events and colder temperatures would be expected.

In Figure 22 are the time series computed for the first three modes of the two dimensional analysis of the WISP alongshore data. The relative amounts of energy contained in these are:

Mode	Percent of total energy
1	85
2	6
3	4

The characteristic patterns for these modes are shown in Figure 23. Of special interest here is the behavior of the various modes at the time of the transition. A large change is seen in the first mode and little or no change can be seen in the other modes. Since the first mode is quasi-barotropic, and since the transition is manifested only in the first mode, the transition must be quasi-barotropic.

Principal Axis System

As mentioned in Chapter II, the current meter data were rotated to be in alignment with the local bathymetry. In the initial analysis of the modal structure, it appeared that the much weaker onshore flow was being washed out by a small component of the alongshore flow. To eliminate this, all of the current data used in the remainder of this section have been rotated into their individual principal axis

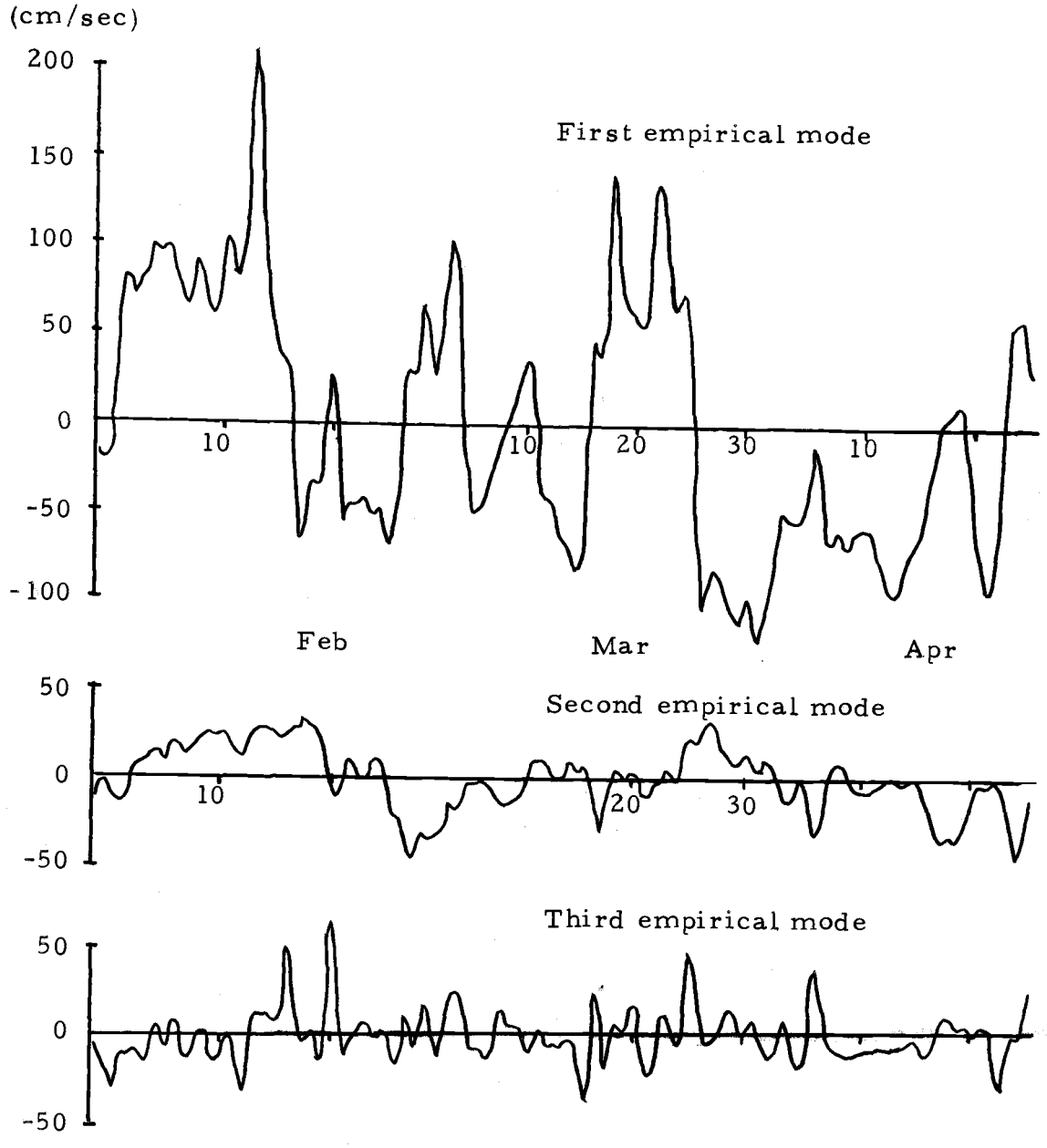

Figure 22. Time series for the first three modes of the two dimensional empirical orthogonal decomposition of the WISP alongshore currents. The time period is late January to late April, 1975.

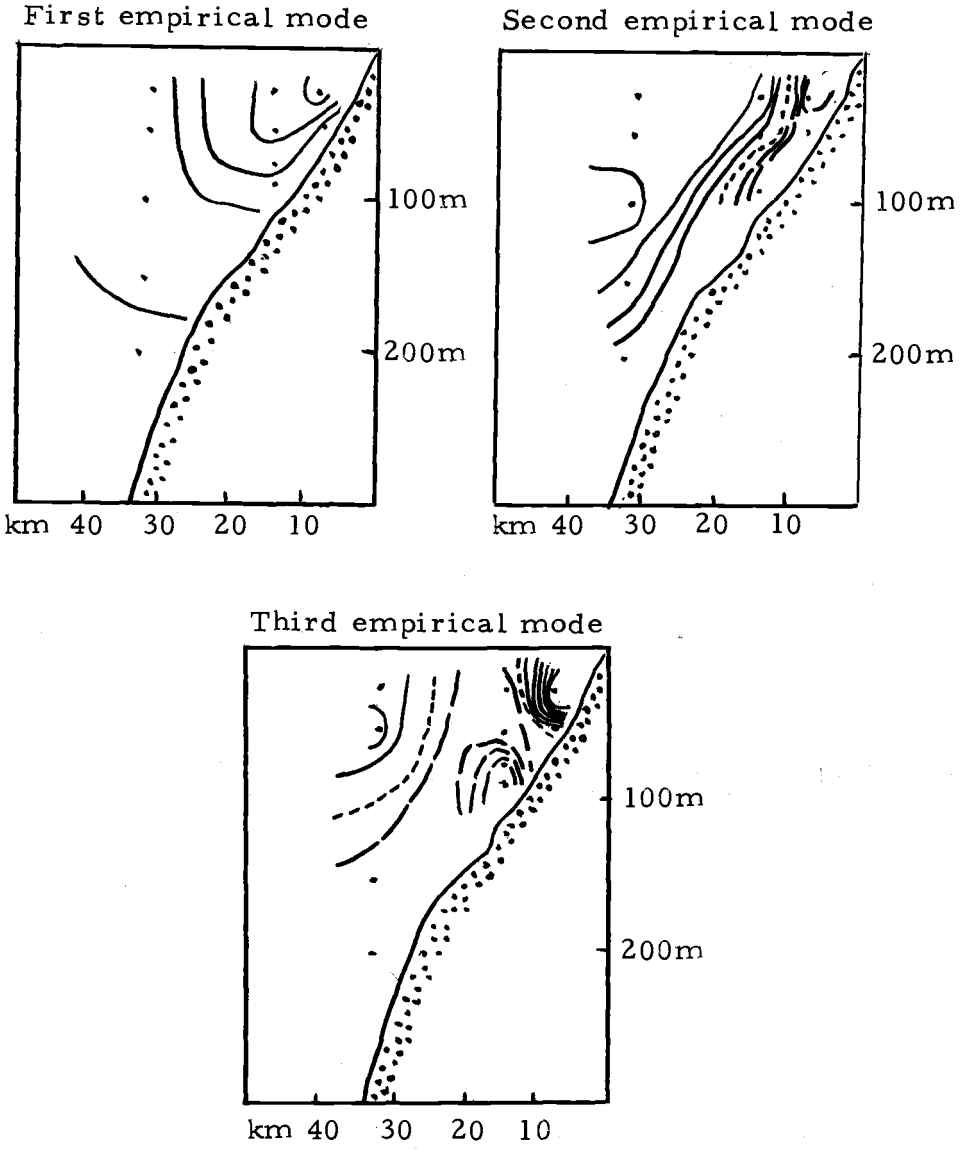

Figure 23. The characteristic patterns for the first three eigenvectors of the two dimensional empirical orthogonal decomposition of the WISP alongshore currents. These patterns correspond to the time series given in Figure 22. Dashed lines represent negative values of eigenvector components; solid lines represent positive values; and dotted lines represent zero values. The iso-lines are drawn every 0.10.

systems (Fofonoff, 1969). The condition which defines such a system is

$$\overline{u' v'} = 0$$

The angles of rotation (from a North-South, East-West reference system) for the WISP data are given in Tables 3 and 4. A fairly consistent picture appears when comparing the angles before and after the transition (between segments 2 and 3 in Table 3 and between segments 1 and 2 in Table 4). Except for Pikake 50 m, the principal axis rotates counterclockwise.

Seasonal Comparison of Fluctuating Flow Patterns

To see the temporal evolution of the modal structure, the WISP data set was again subdivided. Three equal length segments (26.25 days each) for the alongshore current modes are shown in Figure 24. Also shown in this figure is the two dimensional dominant mode for the data set taken during CUE-II in the summer of 1973. This data set was also rotated into its principal axis system. (Kundu and Allen [1976] calculated the two dimensional modes for these data in the unrotated coordinate system. The present, independent calculations agree with those presented by these authors.)

The characteristic patterns for the WISP alongshore data (Figure 24) change with time in three ways. First, there seems to be

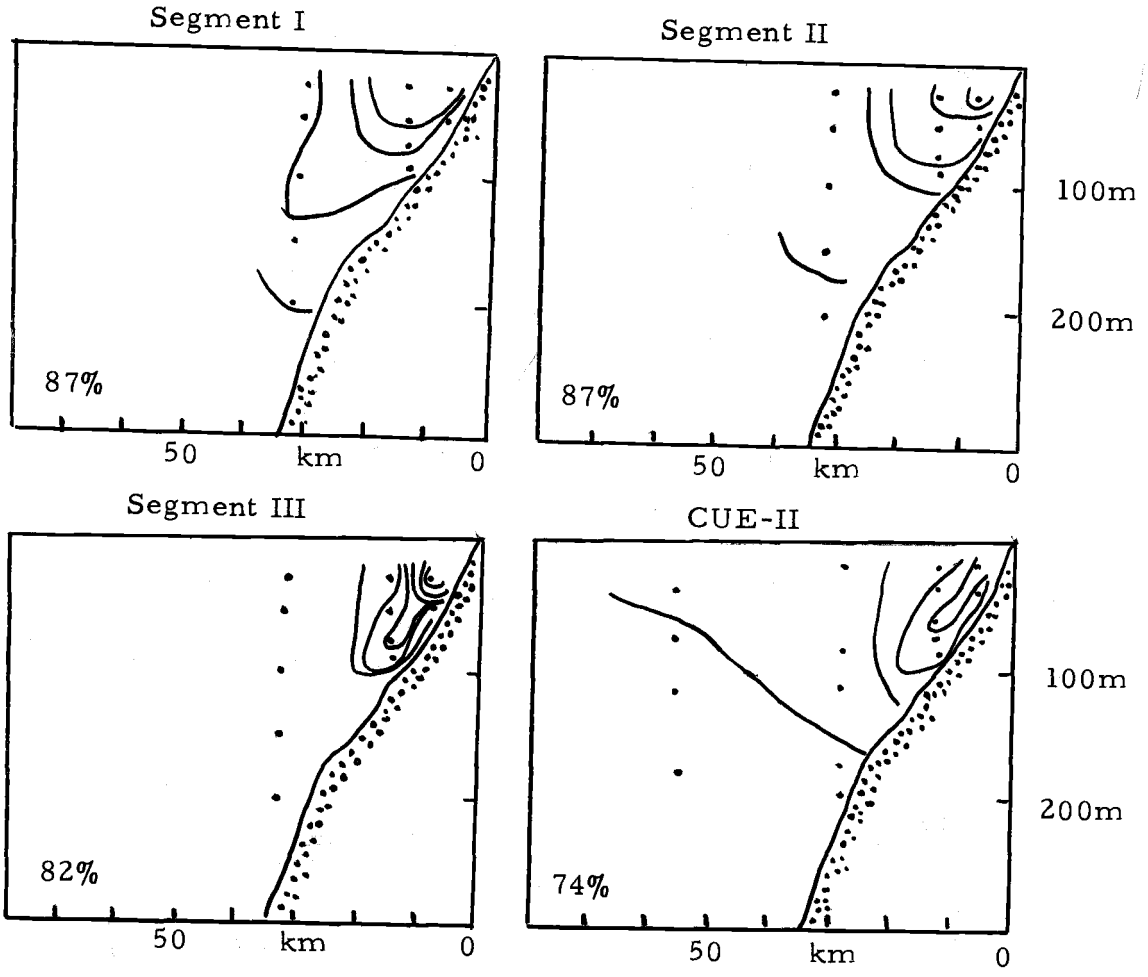

Figure 24. The two dimensional characteristic patterns of alongshore currents for three segments of the WISP array and one segment from the CUE-II array. The percentage of the total energy that is accounted for by the eigenvector is in the lower left corner of each frame.

Table 3. Principal axis rotations for equal length data segments (105 data points) of the WISP array. A gap has been inserted between the second and third segments so that the transition event is not included.

Array	Depth (m)	Segment 1	Segment 2	Segment 3
Pikake	25	- 9.90	- 8.87	-9.43
	50	- 6.75	- 5.89	1.00
Sunflower	25	-14.06	-14.79	-2.15
	50	- 7.34	- 8.92	-4.51
	75	- 6.32	- 5.90	-3.63
	90	- 1.41	0.17	3.31
Wisteria	25	-35.73	-33.53	9.29
	50	-28.80	-13.82	-6.31
	100	-16.44	-17.95	-0.45
	150	-17.64	-10.27	-0.43
	200	-17.03	-12.93	-3.41

Table 4. Principal axis rotations for four equal length segments (215 data points) for the Sunflower array. Between the first and second segments is a 15 data point gap at the time of the transition.

Depth (m)	Segment 1	Segment 2	Segment 3	Segment 4
25	-14.09	-6.16	-6.69	-5.24
50	- 8.27	-6.55	-6.58	-
75	- 6.34	-5.61	-7.40	-5.15
90	- 0.83	2.64	2.72	-0.98

an increasing concentration of the variance at the shallow, inshore current meter. Across the transition (the second to the third segments) the relative energy content of the dominant mode drops from 87% to 82% and the absolute energy content drops to a third of its pre-transition value. There is also an energy drop in the other modes. The third change is the shift at Sunflower from a quasi-barotropic state to a summer-like barotropic state.

The characteristic patterns of the third WISP segment and the CUE-II data are quite similar. The highest plateau in the contours parallels the shelf contours. At the mid-depth moorings, the structure is essentially barotropic, with a mid-depth maximum in the eigenvector components. Farther offshore and onshore the magnitude of the eigenvector components decreases with depth. The summer dominant mode accounts for slightly less of the total energy field than does the corresponding mode in the third WISP segment, and it contains only about one-half of the absolute energy of the third segment.

The first two largest onshore modes for the three WISP segments undergo an interesting change. The first mode of the first segment is similar to the second mode of the later segments. Conversely, the second mode in the initial segment becomes the dominant mode in the subsequent segments. To quantitatively test this idea, the inner products of the eigenvectors were taken and are shown below.

First segment Mode	Second segment Mode 1	Second segment Mode 2	Third segment Mode 1	Third segment Mode 2
1	0.34	0.73	0.37	0.81
2	0.93	-0.21	0.76	-0.29

Similar characteristic patterns should yield inner products greater than 0.7.[4] Thus there does seem to be a reversal of the dominance between these two modes.

Between the second and third segments, the onshore modal shapes undergo some changes, but they maintain their order of dominance. The area with maximum values of eigenvector components in the first mode moves onshore and takes on an appearance similar to that of the alongshore modes. Also the mid-shelf structure goes from a quasi-barotropic to more of a barotropic state. The second mode orients itself in a vertical position. Both the first and second modes in the third segment have the same pattern as those in the CUE-II data.

Between the first and second segments there is a large increase in the energy in all of the modes. A dramatic decrease is seen between the second and the third segments. A further decline in the energy content is seen in a comparison of the last segment with CUE-II modes.

---

[4] The inner product of two eigenvectors is an index of analogy. Values greater than 0.9 indicate identical eigenvectors and values of 0.7 or greater indicate a high degree of similarity (Grimmer, 1963).

Because the Sunflower array (the combination of three installations at the same location) is so much longer than the other current meter records (225 days as compared to 86 days), a separate modal analysis on Sunflower was performed. The record was subdivided into four segments as before. The data in each segment were rotated into their principal axis system by the angles listed in Table 4.

Figure 25 shows the dominant alongshore eigenvector and the two most dominant onshore eigenvectors. The dominant modes' eigenvectors become more barotropic with time (except for the last segment of onshore modes). Other than this change, the characteristic patterns and their associated relative energy content change very little (see Table 5).

Between the first and second segments, the first alongshore eigenvalue decreased by about 50% while the second eigenvalue remained unchanged. At the next segment the first eigenvalue decreased again by 50% and the second mode was cut almost to a fourth. Between the third and fourth segments, the dominant eigenvalue was essentially unchanged, while the second one was again cut in half. The eigenvalues of the fourth segment are in close agreement with those given by Kundu and Allen (1976) for the summer season.

The onshore dominant modes show a similar loss of energy as the season progresses. The final segment's eigenvalues are smaller

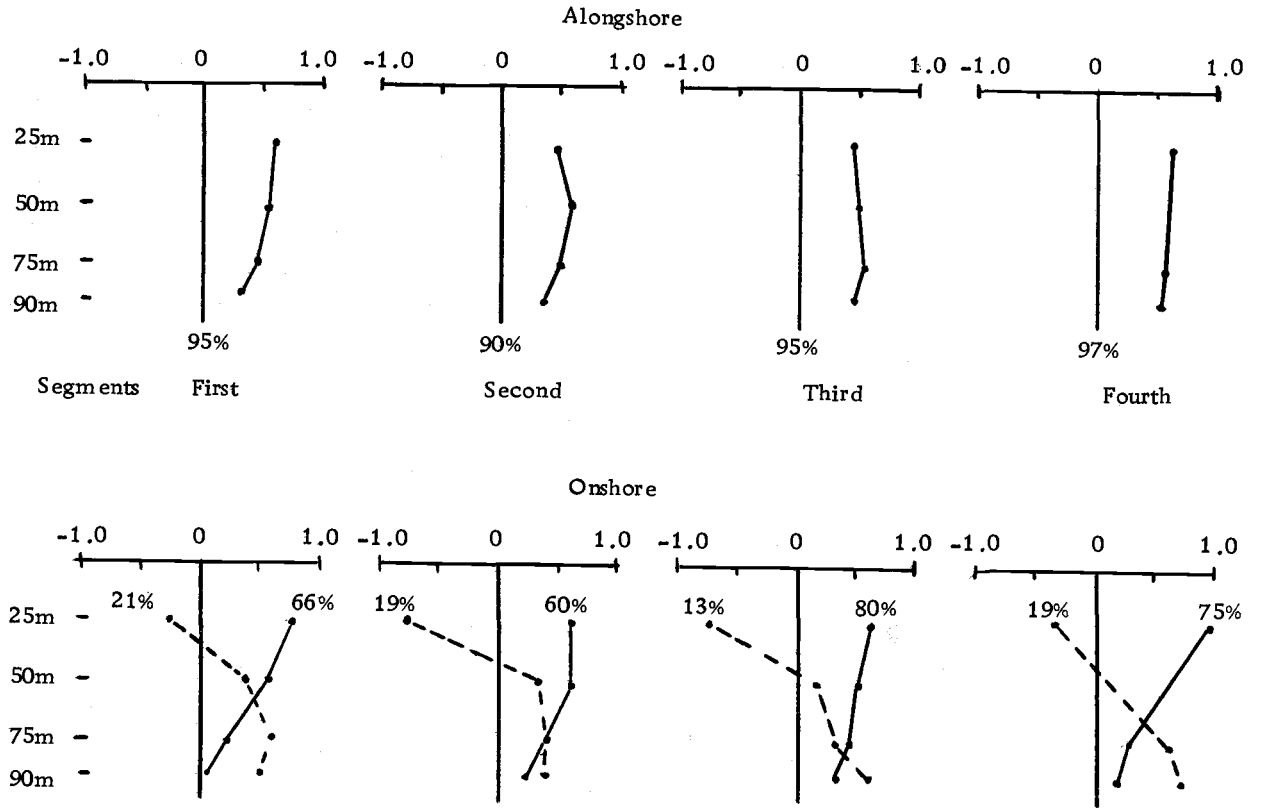

Figure 25. The characteristic patterns of the alongshore and onshore currents at Sunflower for four equal length segments. In the upper four frames are the first modes of the alongshore currents. The first and second (dashed lines) modes of the onshore currents are shown in the lower four frames. The percentages indicate how much of the variance can be accounted for by that particular mode.

Table 5. The inner product analysis of the first two eigenvectors of Sunflower alongshore and onshore components. The eigenvectors for the second and third segments are compared to those of the (pre-transition) first segment.

Mode	Segment	
	2nd	3rd
	Alongshore	
1	0.99	0.97
2	0.98	0.97
	Onshore	
1	0.96	0.93
2	0.93	0.92

than those given by Kundu and Allen, but they are in reasonable agreement.

Thus it appears that the Sunflower record spans the transition period from the winter season to the summer season. In this period there is a loss of energy from all modes. The seasonal loss of energy does not occur in the same proportions for each mode for each time increment. However, the relative amount of energy in each mode does not undergo any large changes. The eigenvectors (or characteristic patterns) also are nearly constant.

PROPAGATION AND FORCING OF OCEANOGRAPHIC EVENTS

Recent theoretical studies have indicated that changes in the current and density fields on continental shelves could be caused by propagating waves that are generated by distant sources (e.g., Gill and Clarke, 1974; Hurlburt et al., 1976). In order to evaluate the importance of long coastal trapped waves to the transition event, we will investigate the propagation and forcing of oceanographic events.

Continental shelf waves have already been found to be an important feature of the continental shelf dynamics off Oregon. Continental shelf waves are low frequency (less than the inertial frequency), long waves (wavelengths of hundreds of kilometers) that are trapped on the continental shelf by the change in bathymetry there. Their amplitudes are quite small: a few centimeters. Winds provide the generating mechanism (Buckwald and Adams, 1968). Because of the effect of the earth's rotation, free waves travel in a preferred direction. In the Northern Hemisphere they propagate with the coastline on their right. However, forced waves may travel in either direction (Mooers and Smith, 1968; Gill and Schumann, 1974). When the forcing function travels in the same direction and at the same speed as a free wave, a resonance condition can occur. Off the Oregon coast there has been evidence for resonant forcing (at approximately 0.15 cpd) in the summer (Huyer et al., 1975; Kundu

et al., 1975), and for direct forcing of waves in winter (Mooers and Smith, 1968) at approximately 0.10 cpd. The summer studies have found only northward traveling waves (in agreement with theory) while in the only winter study (Mooers and Smith, 1968) waves were found to travel in both directions. At 0.10 cpd there was a forced propagation going southward, while at 0.35 cpd a free wave was propagating northward.

To determine if free continental shelf waves are present during the winter the propagation speed and direction and the wavelength of fluctuations in sea level and currents (that are coherent along the coast) are computed and compared to the expected values. Spectral and cross spectral comparisons of winds and sea level and of winds and currents are carried out to determine the importance of local wind forcing on sea level and current fluctuations. The relationships between fluctuations in sea level, in currents and in density are investigated in the third section of this chapter. In this last section a model of directly wind forced sea level fluctuations is tested.

Alongshore and Onshore Propagation

Tide Gauge Data

Sea level observations from four locations (Tofino, Toke Point, South Beach, and Charleston) are shown in Figures 12 and 26).

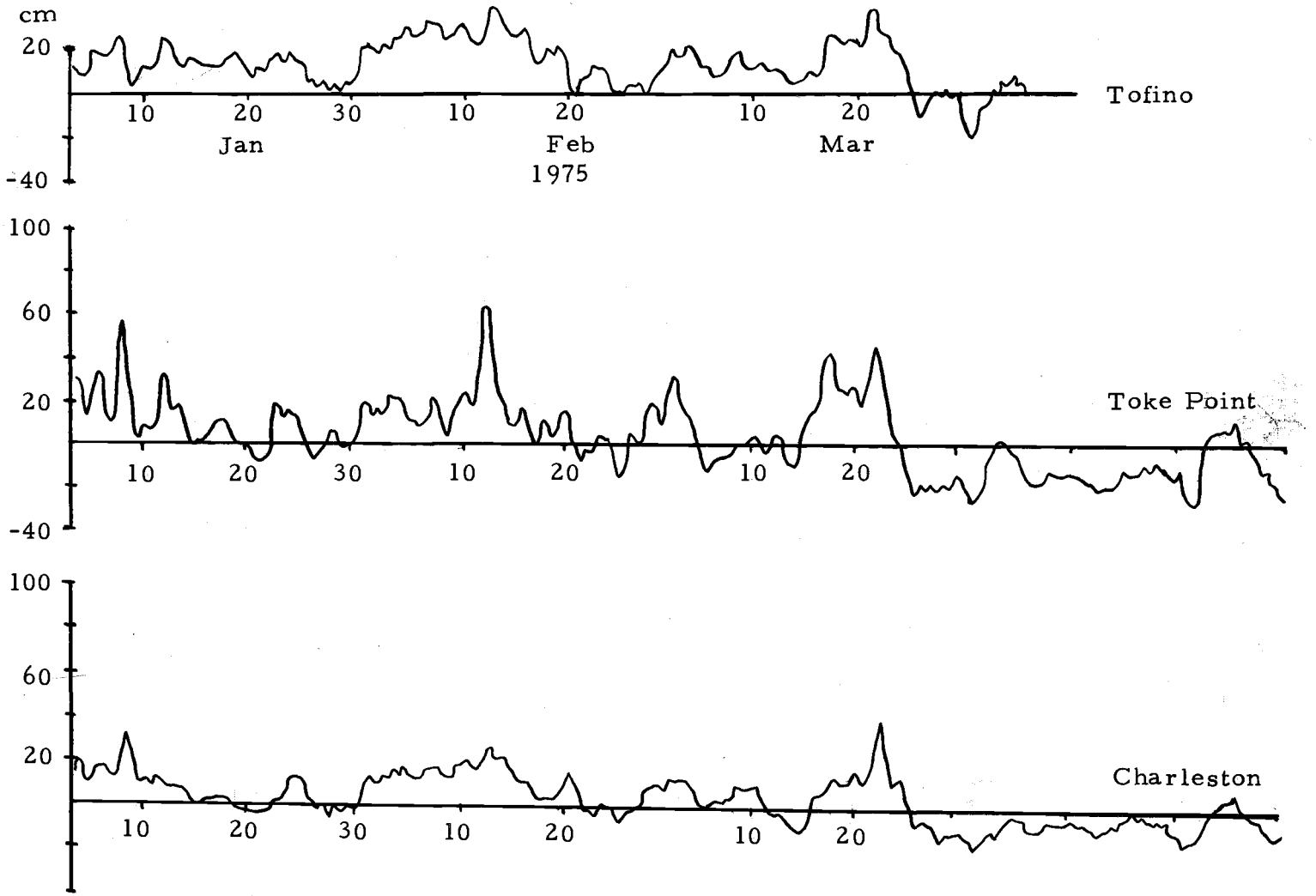

Figure 26. Sea level records of Tofino, British Columbia; Toke Point, Washington; and Charleston, Oregon for January through April, 1975.

Although there are differences between each of these time series, clearly there are similarities in the major events. Visually it is difficult to ascertain if there is a propagation of events along the coast, and , if there is, in which direction it is. It does appear that the transition event occurs earlier at the Tofino tide gauge than at the other gauges.

Cross correlations between the various pairs of records were calculated. In each case the cross correlation is maximized either at a small lag with the northern pair member leading, or at the zero lag. The pair with the largest spatial separation (Tofino and Charleston) also have the largest lag separation (two lags or 12 hours). Since cross correlations are averages across the entire frequency domain, there can be a danger in relying too heavily on them for phase speed calculations. With that warning we proceed anyway to calculate the phase speeds. Using the Tofino-Charleston pair, a speed of 1300 km/day southward is found.[4]

Coherence and phase calculations were made between all pairs of the four sea level data. Only one frequency band had phase relations between the various pairings that were self consistent: at

---

[4] In this analysis the following spatial separations are used:

Tofino	
	280 km
Toke Point	
	230 km
South Beach	
	140 km
Charleston	

0.16 cpd. Regression analysis was employed on the six phase estimates at this frequency against station separations. The calculated wavelength was 5500 km; and the phase speed was 880 km/day, southward. The correlation coefficient for this regression was 0.92.

At 0.113 cpd the phase angles indicate a northward propagation north of Toke Point, and a southward propagation south of Toke Point. At three frequencies (0.263, 0.425, and 0.525) all of the phase angles show a southward propagation except between South Beach and Toke Point, where they are northward.

A zero phase angle exists between all pairs of sea level observations at 0.025 cpd. Numerous other frequency bands with significant coherence have phase angles that are consistent between two or more pairs of stations. All of these other phase angles imply a southward propagation, except between Toke Point and South Beach where a northward propagation is often found. (Exceptions to this generalization could be found only at two frequencies.)

Alongshore Currents

The alongshore coherences between alongshore components of the Tofino and WISP arrays were also calculated. Coherence and phase angles for dominant frequencies are listed in Table 6.

At 0.16 cpd the alongshore coherence of currents yields a wavelength of 7200 km and a phase speed of 1200 km/day. Thus the

Table 6. Coherence squared and phase for the dominant frequencies of the alongshore velocities between WISP and Tofino arrays.

Current meter pairs	Coherence squared	Phase (°)	Phase error (°)	Direction
	Frequency 0.06 cpd			
Pikake-Tofino 50 m	0.89	7	6	northward
Sunflower-Tofino 50 m	0.89	15	6	southward
Sunflower-Tofino 90 m	0.78	11	15	southward
Wisteria-Tofino 50 m	0.45	27	25	southward
	Frequency 0.16 cpd			
Pikake-Tofino 50 m	0.77	10	16	southward
Sunflower-Tofino 50 m	0.77	43	16	southward
Sunflower-Tofino 90 m	0.81	30	15	southward
Wisteria-Tofino 50 m	0.75	20	20	southward
	Frequency 0.24-0.26 cpd			
Pikake-Tofino 50 m	0.60	10	23	southward
Sunflower-Tofino 50 m	0.77	4	16	southward
Sunflower-Tofino 90 m	0.75	35	17	southward
Wisteria-Tofino 50 m	0.58	25	24	southward
	Frequency 0.38-0.42 cpd			
Pikake-Tofino 50 m	0.60	36	23	southward
Sunflower-Tofino 50 m	0.59	15	23	southward
Wisteria-Tofino 50 m	0.75	28	17	southward

The frequencies included in this table were chosen on the basis of their having relative coherence maximum (which were significant) between two or more current pairings, or on the basis of their having spectral peaks.

sea level cross correlation, and the sea level and the current phase spectra (near 0.16 cpd) all have the same characteristics: a fluctuation propagating southward at 900-1300 km/day with a wavelength of 5500-7000 km.

Other significant values of coherence squared between the pairs of current meters do exist. At 0.24-0.26 cpd the alongshore current coherences indicated a northward traveling phenomena. Using a representative value for the phase, a wavelength of 8700 km and a phase speed of 1400 km/day were found. The sea level coherences at this frequency could not be unambiguously interpreted in regards to the phase angles or even the direction of propagation.

In the range 0.38-0.42 cpd, both sea level and current coherences indicated a southward propagation. The alongshore currents yield the following: wavelength, 8700 km; and a phase speed of 3500 km/day. The sea level coherences given smaller values: 4000 km for the wavelength; and 1600 km/day for the phase speed.

Onshore-Offshore Propagation

The values for wavelength and phase speed obtained above are larger than those commonly mentioned in the literature. By examining only the alongshore phase difference, one is neglecting the possibility that waves are propagating onshore or offshore. If such a condition existed, then anomalously large values for wavelength and

phase speed could be found. In this case wave crests would be nearly parallel to the long axis of the current meter arrays. Such is the case here.

Table 7 lists the coherence squared and phase between alongshore current records at 50 m in the WISP array. The phases are in general as large for this very small separation as they are for the much larger separation between the Tofino and WISP arrays. Of the four chosen frequency bands in Tables 6 and 7, two have phase relations that are consistent in both the alongshore and onshore sense. Plots of the two dimensional phase relations are given in Figure 27. The lines of constant phase are drawn every 10^{o} of phase and the arrows indicate the direction of propagation.

At 0.06 cpd, which is in the low frequency region that so dominates the spectra of the current meters (p. 92), the waves move offshore and southward. The crests, in general, are aligned with the bathymetry. At 0.16 cpd a unique phase diagram is shown. The propagation direction is southward. However, elements are propagating onshore and offshore. It appears that either we are seeing an incident and reflected wave (the reflected part quickly being dissipated) or we are seeing a southward moving wave propagating slowest at mid-shelf. The phase angles at 0.24-0.26 cpd are ambiguous. Those at 0.40 cpd are not consistent in magnitude but are consistent in direction. They show a southward and onshore propagation.

Table 7. Coherence squared and phase between the alongshore currents at the WISP array at 50 m depth. The frequency bands are the same ones used in Table 6.

Current meter pairs	Coherence squared	Phase (°)	Phase error (°)	Direction
	Frequency 0.06 cpd			
Pikake-Sunflower	0.93	18	4	offshore
Pikake-Wisteria	0.62	35	23	offshore
Sunflower-Wisteria	0.68	5	20	offshore
	Frequency 0.16 cpd			
Pikake-Sunflower	0.90	20	5	offshore
Pikake-Wisteria	0.85	5	9	offshore
Sunflower-Wisteria	0.81	25	14	onshore
	Frequency 0.24-0.26 cpd			
Pikake-Sunflower	0.82	25	13	offshore
Pikake-Wisteria	0.83	36	11	offshore
Sunflower-Wisteria	0.64	10	22	onshore
	Frequency 0.40 cpd			
Pikake-Sunflower	0.91	1	5	onshore
Pikake-Wisteria	0.80	13	15	onshore
Sunflower-Wisteria	0.83	50	11	onshore

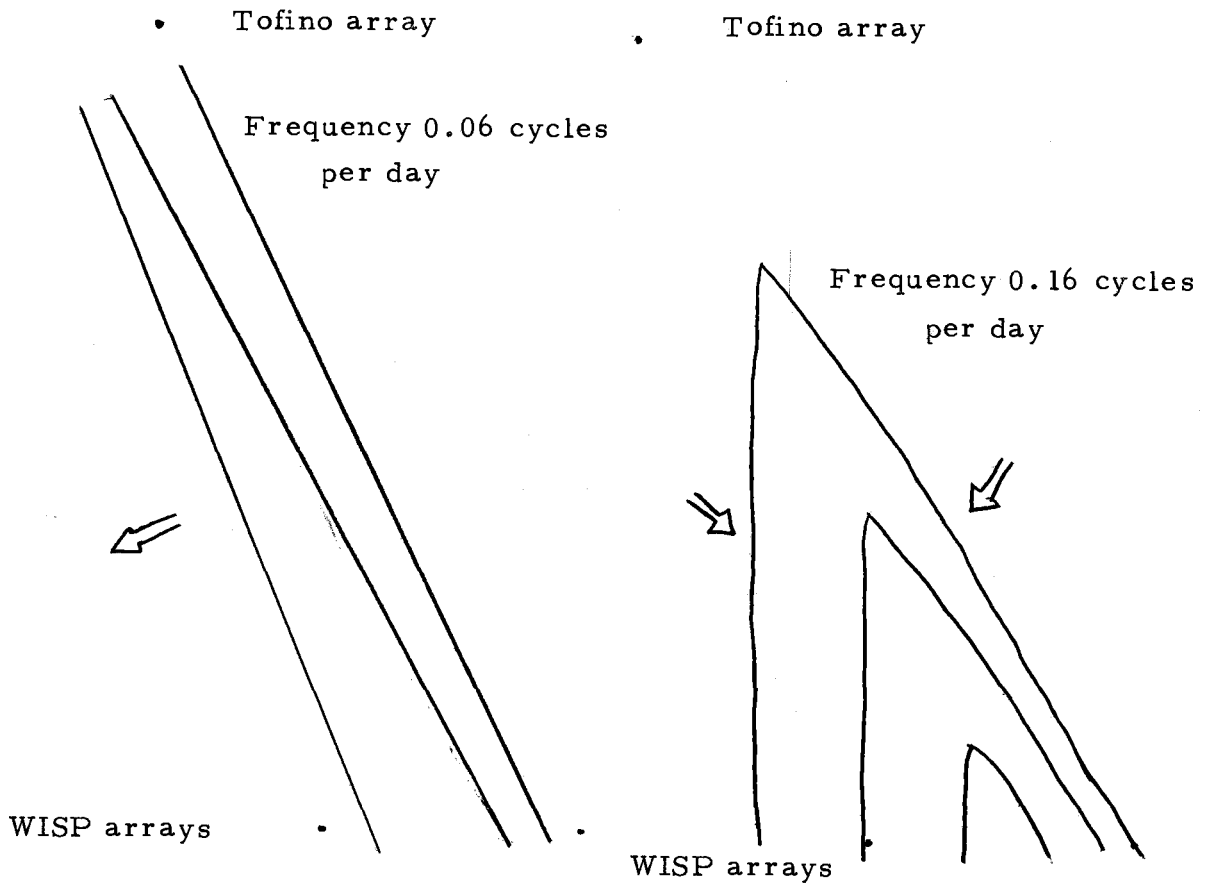

Figure 27. The two dimensional phase diagrams for fluctuations in alongshore currents at the Tofino and WISP arrays. The diagrams are for frequencies 0.06 cpd and 0.16 cpd. Arrows indicate the direction of propagation and the lines of constant phase are drawn every 10^{o}.

Thus rather than a series of waves at various frequencies confined to the (continental shelf) waveguide and moving either northward or southward, there exists a more complicated spectrum of onshore and offshore as well as alongshore propagating fluctuations. Onshore (and southward) propagating waves could be driven by storms in the predominant storm track. Fluctuations moving offshore might be indicative of a generating mechanism that operates preferentially on the continental shelf.

Conclusions

Although the presence of northward propagating waves cannot be ruled out, the dominant direction of alongshore propagation is southward. In the only previous research conducted in winter, Mooers and Smith (1968) found free waves propagating northward and forced waves propagating southward. All other studies have been conducted in summer and have found only northward propagation. Thus the southward propagation may be a feature of winter conditions.

Since northward propagating waves are not a dominant feature in winter, it is unlikely that the dynamics of Oregon's continental shelf are greatly influenced by disturbances that are generated by distant sources and propagate onto the shelf as free waves. It is then also unlikely that the transition event is the result of such a free wave. However since spectral techniques cannot describe singular

events, we will undertake further analysis of the forcing of the transition event.

Wind Forcing of Oceanographic Fluctuations

The cross correlations between north components of wind at several latitudes were shown in the preceding chapter (Figure 18). That analysis showed that wind events propagated rapidly southward along the Oregon coast. The cross coherence between the wind at 47^{o}N and 43^{o}N showed a southward propagation throughout most of the frequency range as did the cross coherence between currents. The wavelengths and phase speeds computed from the wind phase spectra are in reasonable agreement with those computed for the alongshore propagation of currents (see Tables 2 and 6). These are conditions that we might expect if there were wind forcing of oceanographic fluctuations. We now employ spectral techniques to investigate the possibility of wind forcing of sea level and current fluctuations.

Spectral Techniques

In the following spectral comparison of winds with currents both rotary and orthogonal component spectral techniques will be used. In the latter the scalar components of a time series are analyzed separately while in the former they are analyzed together. Current spectra will be presented in the rotary format because in that format

spectral values are independent of the axis of orientation. Although the scalar component series were rotated to be aligned with the local bathymetry, different frequencies could have different scales of motion and thus it is difficult to achieve an optimum rotation. In scalar series' spectral representations, a rotation away from the natural coordinate system may cause energy from the dominant component to be represented as if it were in the subdominant component. Even a small, incorrect rotation could mask the much weaker component. In rotary analysis this problem is avoided.

In rotary component analysis, the vector series are represented by a pair of counter rotating vectors. If the motion of the time series were purely circular, then its rotary representation would consist of only one of the rotating vectors; the length of the vector would correspond to the magnitude of the motion, and the direction of the rotating component would be the same as in the data. Rectilinear oscillating flows correspond to equal and opposite rotations of the two vectors. An imbalance in the length of the rotors causes one side to dominate and the represented motion is that of an ellipse. Gonella (1972) defines the rotary spectra and discusses its use.

The rotary coherence is also used here and is defined by Gonella (1972). The value of the rotary coherence is 1.00 if there is a linear relationship at that frequency between the two (similarly rotating) rotary components. The rotary coherence, like the rotary

spectrum, is, in general, not symmetric about the zero frequency axis.

Spectral Comparison of Winds to Sea Level

The winter (January-April, 1975) spectrum of the north component of Newport winds and of the South Beach sea level are presented in Figure 28. There is a faster decline with increasing frequency in the spectral levels of sea level than in those of wind. However, there is a general alignment of spectral peaks throughout the range of frequencies, but especially at low frequencies (0.0-0.12 cpd). We note that there is a plateau in the sea level spectrum from 0.32-0.48 cpd. There is also a (less distinct) plateau in the wind spectrum in the same frequency band.

The coherence squared between sea level and the north component of winds is shown in Figure 29. When the values of the coherence squared are significantly greater than zero (we use the 5% level of significance in this study), there is a linear relationship between the variables being tested. Such a relationship exists between the winds and sea level at low frequencies (0.0-0.13 cpd). This is the same band where the spectra of winds and sea level were quite similar in shape. There are several other frequency bands in which the coherence squared is significant, including the region of the spectral plateau, 0.31-0.36 cpd. Another band with significant coherence is

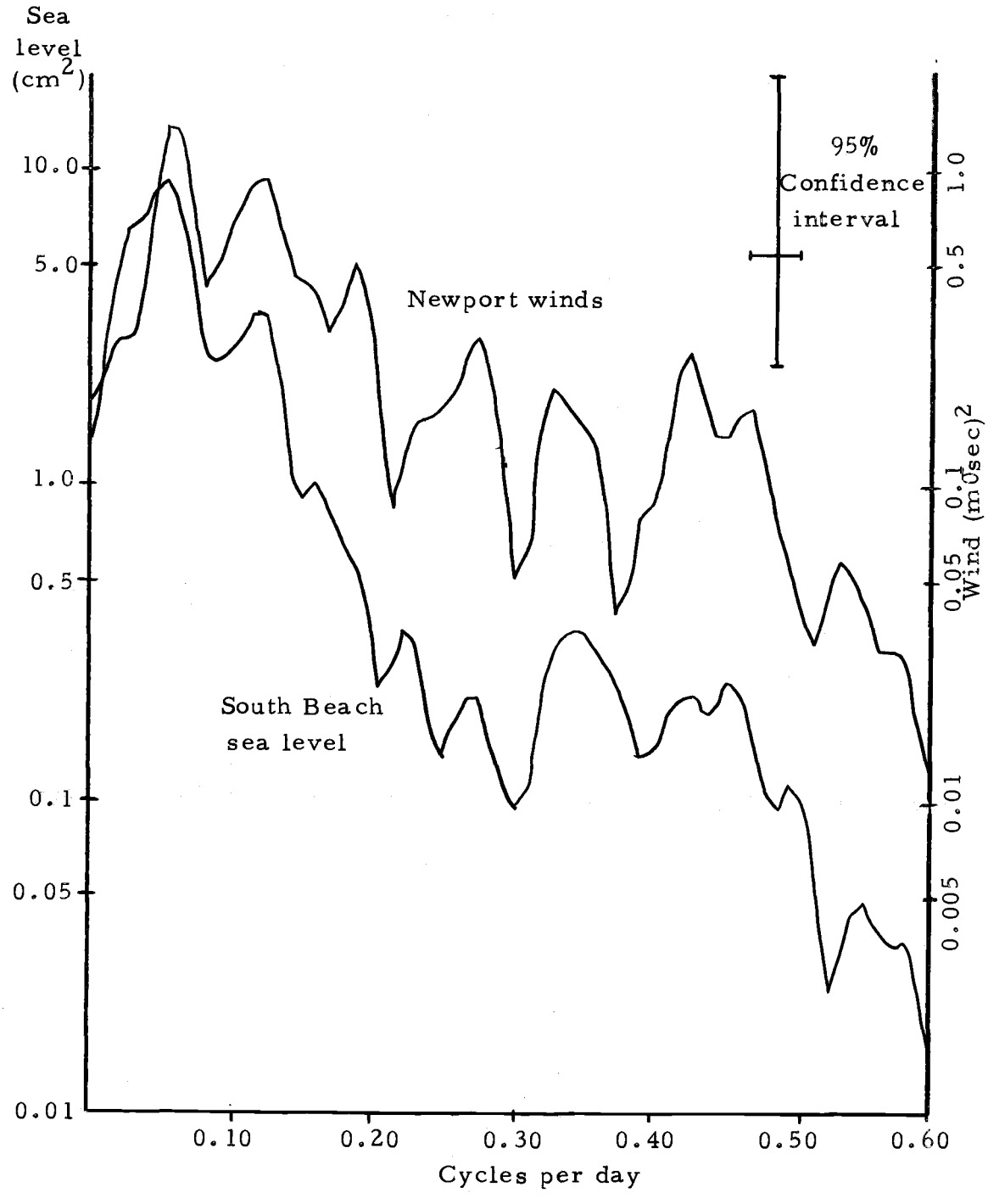

Figure 28. Spectrum of the Newport winds (north component) and of the South Beach sea level (January to April, 1975).

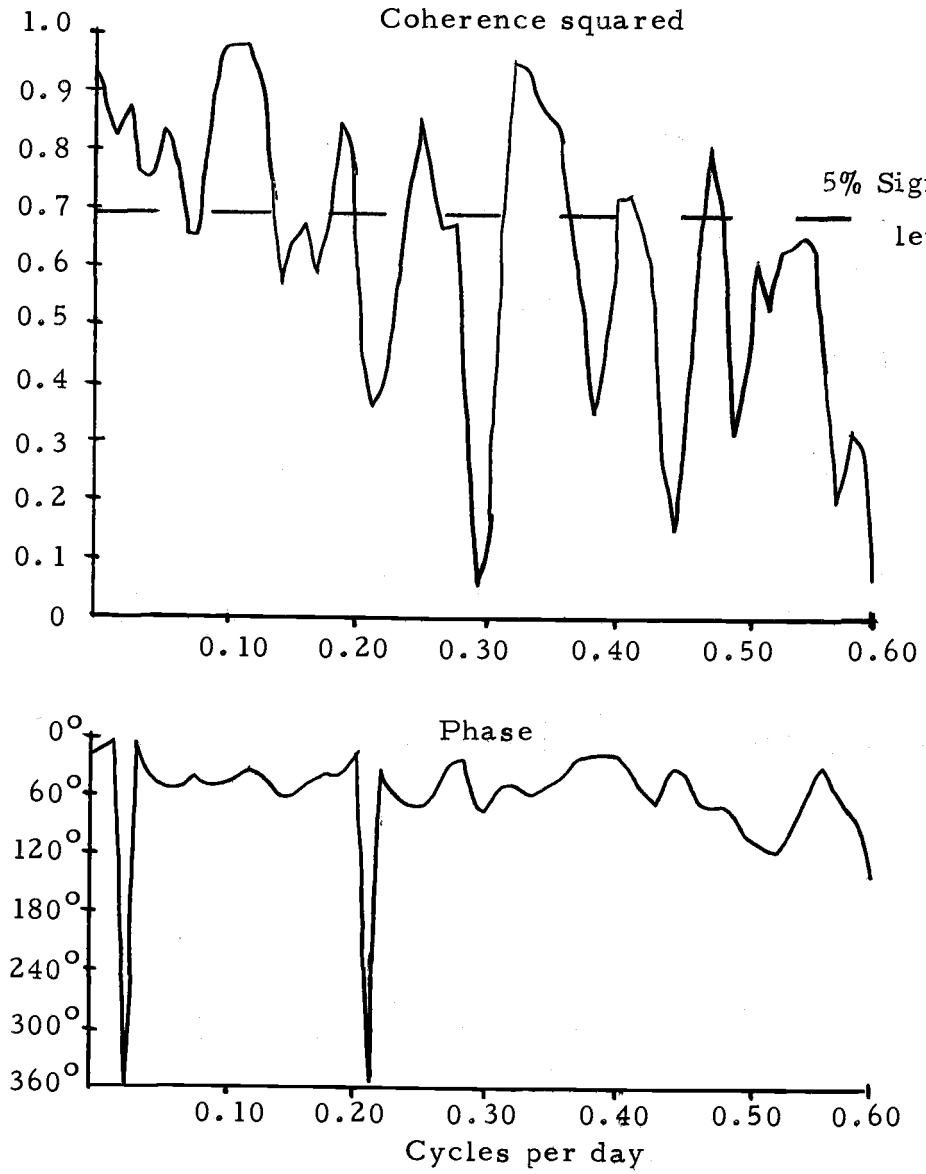

Figure 29. Coherence squared and phase between the north component of Newport winds and the South Beach sea level. Phase angles are plotted with the winds leading the sea level.

from 0.18-0.20 cpd, which is near the frequency of the southward propagating waves found in the alongshore coherence between sea level records.

The phase spectrum between winds and sea level is shown in the bottom half of Figure 29. Wind leads sea level throughout the spectrum, except at two frequencies. Since the errors in phase angles at these two frequencies are greater than their numerical value, no significance can be attached to the interpretation that sea level leads winds there. The phase angles generally range from 15^{o} to 40^{o}.

Thus in the low frequency band, where most of the energy in sea level is concentrated, there is a strong spectral similarity; there is a large and significant value for the coherence squared, and a small phase angle (with wind leading) between wind and sea level. There are several higher frequency bands with the same properties. Thus this analysis indicates that there is a linear relationship (and possibly a forcing) between fluctuations in local winds and in sea level.

Spectral Comparison of Winds to Currents

Both the 25 m and 50 m Pikake rotary current spectra are quite similar in shape to the rotary spectrum of the Newport winds (Figure 30; Pikake 50 m spectrum is not shown). There are broad bands of frequency in which the rotary coherence is significant. In these regions the wind leads the currents by up to 60^{o}. The coherence

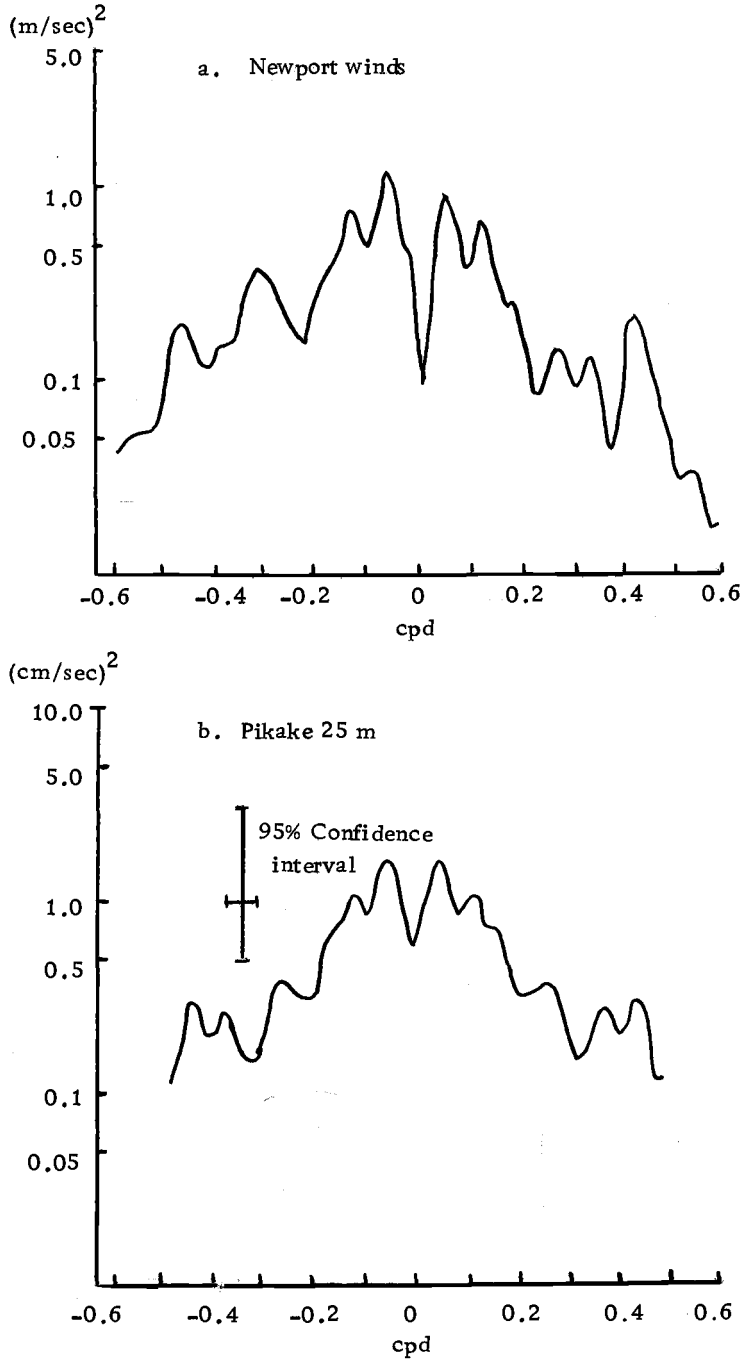

Figure 30. Rotary spectra of the Newport winds and of three of the 11 current records of the first WISP installation. a. Winds. b. Pikake 25 m. c. Sunflower 90 m. d. Wisteria 25 m.

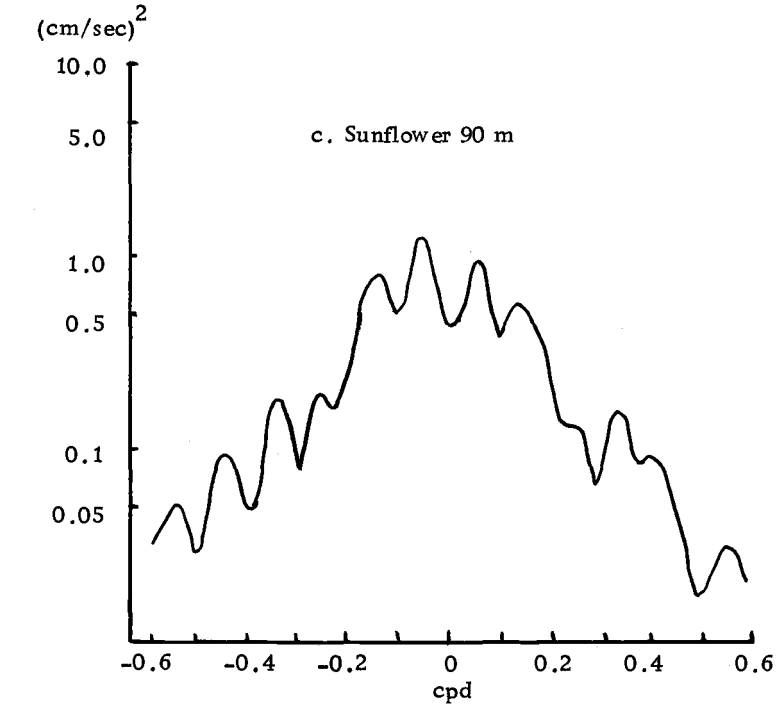

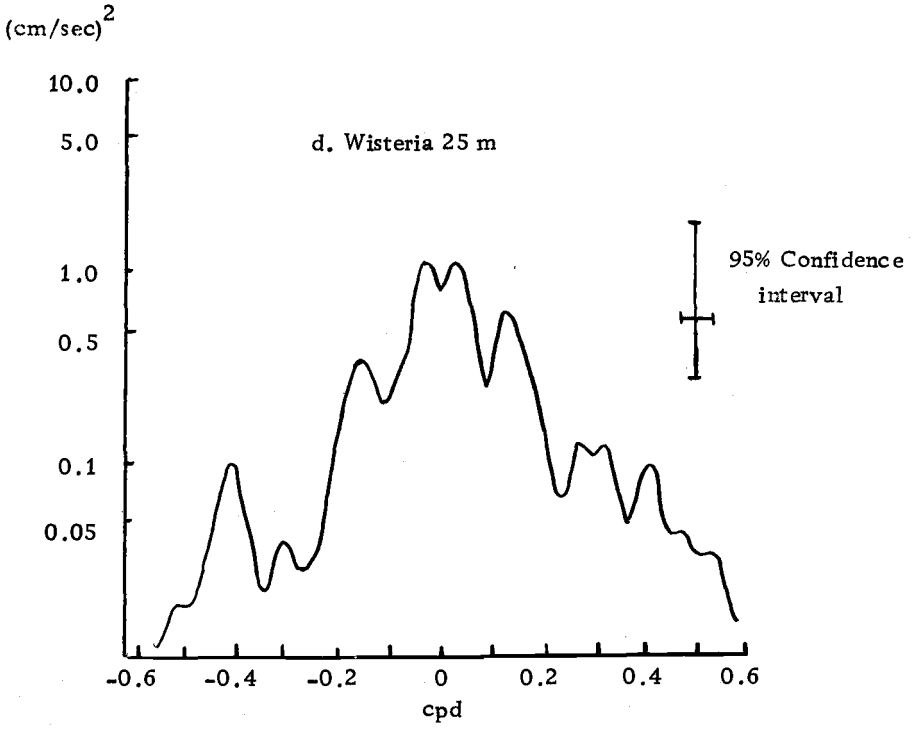

Figure 30. (Continued)

between the east wind component and the onshore current component is not significant except between 0.18 and 0.20 cpd. Here the wind leads by 180°. There are three bands with significant coherence between the north component of winds and the alongshore current component. The phase angle is approximately 30° for these bands; the winds lead.

At Sunflower the rotary spectra of winds and currents (Figure 30; only the spectrum of Sunflower 90 m is shown) also have nearly the same shape. Only four scattered frequencies are significantly coherent for the east-west to onshore-offshore comparison. In the comparison of the other orthogonal components, four bands (three of which were represented in the analysis at Pikake) have significance. The significant bands are 0.0-0.17, 0.24-0.27, and 0.32-0.34 cpd. The additional band present at Sunflower is 0.53-0.59 cpd. The phase angles for these bands range from 0.0° to 70°, with the winds leading.

Whereas at Pikake and Sunflower there is close spectral agreement between currents and Newport winds (especially between the more energetic north and alongshore components), at Wisteria there is not. The frequency of the lowest frequency spectral peak at Wisteria is lower than those at the inshore arrays. The rotary coherence between the 25 m currents and the winds is small and there are no significant coherences between east winds and onshore

currents. Five frequency bands (subsets of those listed for Sunflower) have significant coherence between alongshore currents and north winds. Their phases vary from -15° to 40°, where a positive phase indicates that winds are leading.

Empirical Current Modes

The two major empirical orthogonal modes at the Sunflower array were compared to the Newport winds. In a cross correlation between the north wind component and the alongshore modes, the quasi-barotropic mode had the maximum correlation (0.7) and it occurred with that mode lagging the winds by 12-18 hours. Two correlation peaks occurred in the comparison of winds with the second empirical mode. Both of these peaks were weak, although significant: correlation coefficients of 0.27 at 12 hours lag, and -0.39 at a lag of five and one-quarter days. Winds lead in both cases. Thus there is a much stronger relationship between winds and the first empirical orthogonal mode than with the second mode.

While the coherence was high between the north wind component and the first mode of the alongshore currents, it was low for the wind and the second mode. In the former only a few nonsignificant peaks occurred. At low frequencies the phase angles were smaller (about 30°) than at higher frequencies (lag of about $60-90^{\circ}$). Wind led throughout the spectral plane. For the north wind-first baroclinic

mode comparison, there were only a few isolated frequencies that had significant coherence. Typically in these regions the winds led by 30-90°.

Comparing the wind field to the onshore Sunflower modes, low coherences were found. In the few frequency regions that had significant coherence, the east winds led the barotropic currents by 140-180°. Using these winds and the second empirical mode, the analysis gave a low overall coherence and a large variation in phase where there was a significant coherence. The north component of windstress gave several significant peaks in coherence with the first mode and fewer with the second. In both cases the windstress led by 120-180°.

For direct forcing of currents by the windstress, the phase angle between the northward windstress and the barotropic alongshore current mode should be approximately 90°. The onshore component should lag this windstress by 180°. These differ from the expected values for resonant response conditions: small phase angles for the alongshore component, and 90° phase angles for the onshore component (Kundu et al., 1975). The model for resonant response is that wind fluctuations travel in the alongshore direction with wavelength and phase speeds that are similar to those found in continental shelf trapped, long waves. As the atmospheric and oceanic fluctuations move along the coast they remain in phase and energy is

efficiently transferred to the oceanic fluctuations. In Table 8 are the coherences and phases for frequency bands that have significant coherence (and that are pertinent to this discussion). From this table it appears that resonant response is unlikely and that direct forcing seems to predominate at all four of the frequency bands. Resonant response has been found during summer by Kundu et al. (1975) and thus the mechanism by which energy is transferred from the atmosphere to the ocean currents may be seasonally altered.

Table 8. Coherence squared and phase between northward windstress and the first empirical orthogonal modes of alongshore and onshore currents at Sunflower. Windstress leads in the phases.

Frequency (cpd)	Component	Coherence squared	Phase (degrees)	Phase error (degrees)
0.06	onshore	0.68	165	20
	alongshore	0.77	35	15
0.16	onshore	0.73	200	18
	alongshore	0.72	70	19
0.26	onshore	0.63	180	23
	alongshore	0.59	40	24
0.42	onshore	0.62	210	23
	alongshore	0.92	60	4

As discussed above all 11 currents were grouped and analyzed by the method of orthogonal decomposition. The dominant mode contained 86% of the total energy of the current field while the second mode had only 6%. The first alongshore mode was cross correlated with the north component of the windstress. The maximum

correlation (76%) occurred at a lag of between zero and six hours, the windstress leading. This indicates the time lag between the windstress variations and the corresponding response of the entire shelf waters. The coherence was also calculated between these variables. Almost all frequencies up to 0.5 cpd winds and the first alongshore empirical mode were significantly coherent. The east wind component and onshore first mode yield a significant coherence only at two frequencies: 0.12 and 0.56 cpd.

Summary

In the only previous winter study off Oregon, Mooers and Smith (1968) concluded that the southward propagating fluctuations (that they found in winter tide gauge data) were directly forced by the wind. The above analysis found that throughout almost the entire spectrum considered here (0.0-0.6 cpd), current and sea level fluctuations propagate southward (in the direction of propagation of wind fluctuations) and are directly forced by the wind. This direct forcing of waves by the energetic winter winds may mask any (much less energetic) free continental shelf waves that may be present.

The Relationship between Fluctuations of Density, Currents and Sea Level

We have seen large fluctuations on the time scale of a few days in density, currents and sea level. Are these fluctuations independent?

If not, what is the relationship between them? The mid-depth current fluctuations are quasi-barotropic and since the mid-shelf density fluctuations are largest near the bottom in winter, the 90 m records at Sunflower are used in the following analysis.

Fluctuations of Currents and Density at Sunflower 90 m

To evaluate the dynamic importance of density fluctuations, we compare the energies of fluctuations of density and alongshore currents at Sunflower 90 m. In order to make a direct comparison of the spectra, the density time series were multiplied by a constant. This constant was obtained from an energy equation for fluctuations in the horizontal velocity field and in the density field. A derivation is presented here.

$$\frac{\partial v'}{\partial t} + fu' = -\left(\frac{\partial p'}{\partial y} + \frac{\partial \tau^{y}}{\partial z} \right) \frac{1}{\rho_o} \tag{1}$$

$$\frac{\partial u'}{\partial t} - fv' = -\frac{\partial p'}{\partial x} \frac{1}{\rho_o} \tag{2}$$

These are the linearized equations of motion assuming that the wind-stress is aligned with the y axis. We have already done a Reynold's decomposition so that we are using only the fluctuating components. Equation (3) is the hydrostatic equation for fluctuating components.

$$\frac{g\rho'}{\rho_o} = -\frac{\partial p'}{\partial z} \frac{1}{\rho_o} \tag{3}$$

$$\frac{\partial \rho'}{\partial t} = w' \left| \frac{\partial \rho_o}{\partial z} \right| \tag{4}$$

Equation (4) describes the density fluctuations at a position in the water column in the presence of a vertical density gradient. The continuity equation for fluctuating components is given in equation (5).

$$\frac{\partial u'}{\partial x} + \frac{\partial v'}{\partial y} + \frac{\partial w'}{\partial z} = 0 \tag{5}$$

We now multiply equation (1) by v', and equation (2) by u'. These two new equations are added to give us a first energy equation.

$$1/2 \frac{\partial}{\partial t}(u'^2 + v'^2) = -\frac{v'}{\rho_o}\frac{\partial p'}{\partial y} - \frac{u'}{\rho_o}\frac{\partial p'}{\partial x} + \frac{v'}{\rho_o}\frac{\partial \tau^y}{\partial z}$$

$$= -\frac{1}{\rho_o}\frac{\partial}{\partial y}(v'p') - \frac{1}{\rho_o}\frac{\partial}{\partial x}(u'p') + \frac{v'}{\rho_o}\frac{\partial \tau^y}{\partial z}$$

$$+\left[-\frac{1}{\rho_o}\frac{\partial}{\partial z}(w'p') + \frac{w'}{\rho_o}\frac{\partial p'}{\partial z}\right.$$

$$\left. + \frac{p'}{\rho_o}\left(\frac{w'}{z} + \frac{u'}{x} + \frac{v'}{y}\right)\right]$$

We use the continuity equation (5) to remove the last term.

$$1/2 \frac{\partial}{\partial t}(u'^2 + v'^2) = -\frac{1}{\rho_o}\frac{\partial}{\partial y}(v'p') - \frac{1}{\rho_o}\frac{\partial}{\partial x}(u'p') - \frac{1}{\rho_o}\frac{\partial}{\partial z}(w'p')$$

$$+ \frac{1}{\rho_o} w' \frac{\partial p'}{\partial z} + \frac{v'}{\rho_o}\frac{\partial \tau^y}{\partial z}$$

Now we combine equations (3) and (4) to give equation (6); this we can substitute into the above energy equation.

$$\frac{w'}{\rho_o}\frac{\partial p'}{\partial z} = -w' g \frac{\rho'}{\rho_o}$$

$$w' = \frac{\partial \rho'}{\partial t}\left(\left|\frac{\partial \rho_o}{\partial z}\right|\right)^{-1}$$

$$\frac{w'}{\rho_o}\frac{\partial p'}{\partial z} = -\frac{1}{2}\frac{g}{\rho_o}\frac{1}{\left|\frac{\partial \rho_o}{\partial z}\right|}\frac{\partial}{\partial t}\rho'^2 \qquad (6)$$

$$\frac{\partial}{\partial t}\left[\frac{u'^2}{2} + \frac{v'^2}{2} + \frac{g}{2\rho_o}\left(\left|\frac{\partial \rho_o}{\partial z}\right|\right)^{-1}\rho'^2\right] =$$

$$\frac{v'}{\rho_o}\frac{\partial \tau^y}{\partial z} - \frac{1}{\rho_o}\frac{\partial}{\partial y}(v'p') - \frac{1}{\rho_o}\frac{\partial}{\partial x}(u'p')$$

$$-\frac{1}{\rho_o}\frac{\partial}{\partial z}(w'p') \qquad (7)$$

Equation (7) is a description of the kinetic and potential energy balance. In order for the two energies to be comparable in dynamics, the second and third terms on the left side must be of the same order (the first term is much smaller than the second and so we can neglect it here). Thus in a comparison of the potential and kinetic energies we must multiply the density fluctuations by the term

$$\sqrt{\frac{g}{\rho_o}\left(\left|\frac{\partial \rho_o}{\partial z}\right|\right)^{-1}}$$

With this transformation, the units for the density and velocity spectra will be the same: $(cm/sec)^2$. The magnitude of the coefficient was estimated from hydrography. The resulting density spectrum for

Sunflower 90 m along with the velocity spectrum at that location are shown in Figure 31. It can be seen that the spectral estimates of the density and velocity fields are the same order of magnitude throughout most of the frequency range. The spectral peaks are not aligned and the density spectrum falls off at a faster rate with increasing frequency than do those of either sea level or currents. The important feature here is that the density and the current spectra are comparable in magnitude and thus the pycnocline fluctuations are energetic and dynamically important.

The current and density fields are coherent only at very low frequencies (0.0-0.07 cpd) and at 0.17 and 0.53 cpd (Figure 32). The phase angles are ambiguous. As drawn in this figure the density fluctuations lead the current fluctuations by approximately 120^{o} (however they could be interpreted as the currents leading by 240^{o}). Since we expect that northward current fluctuations accompany (downwelling and) warmer temperature (see Figures 5 and 9), and southward currents accompany cooler temperatures, the two fields should be approximately in phase. In that case, density fluctuations lead current fluctuations throughout the phase spectrum.

We have already noted the strong alongshore coherence in records of wind, sea level and alongshore currents at 0.06 cpd and at 0.16 cpd. The rotary spectra of currents at these frequencies showed a large decay in energy in going from above the permanent pycnocline

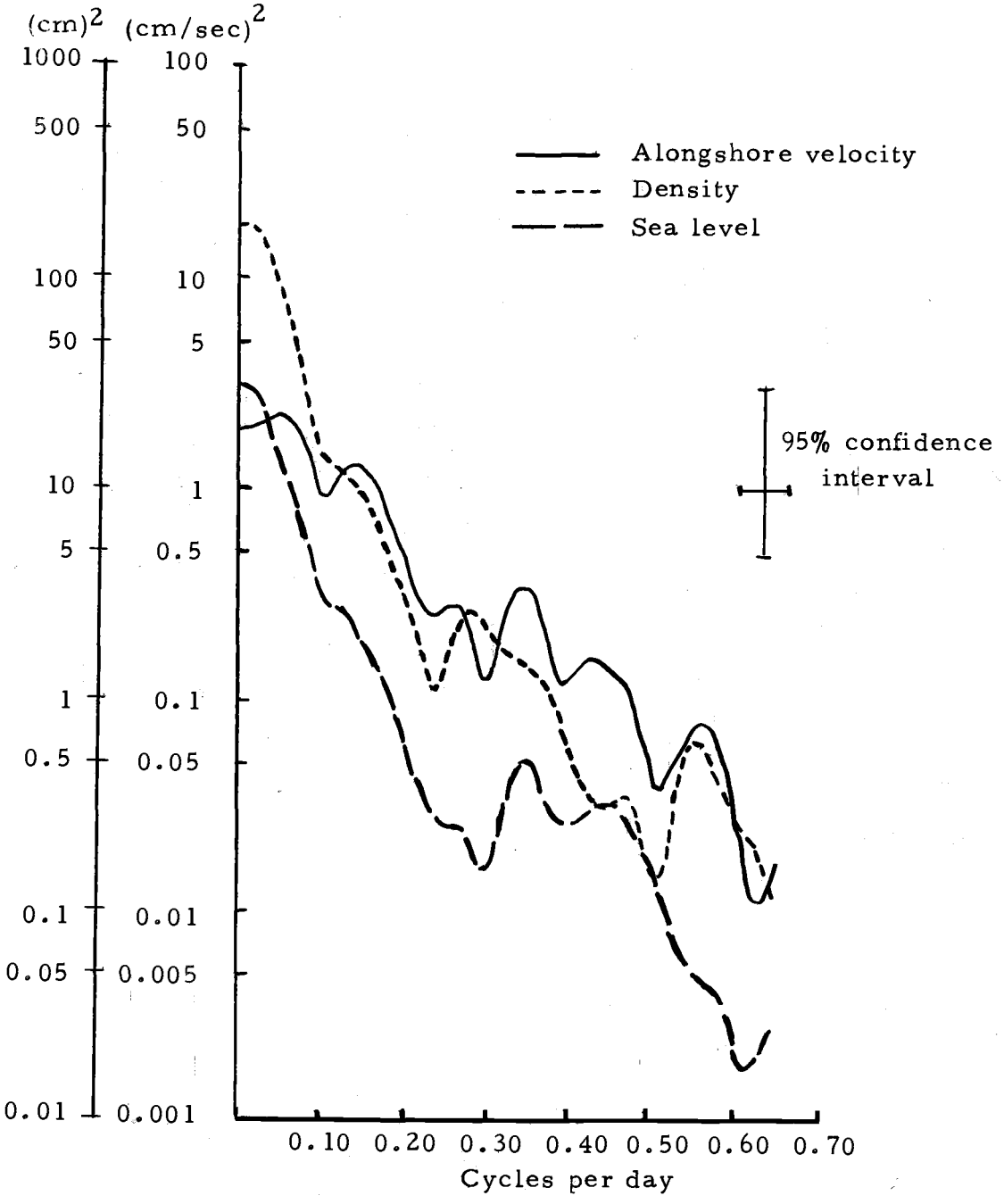

Figure 31. Spectra of South Beach sea level, alongshore currents and density at Sunflower 90 m. The density time series have been multiplied by a constant factor so their energy levels are in units of $(cm/sec)^2$ and can be directly compared to the velocity spectrum. The sea level spectrum is in units of $(cm)^2$.

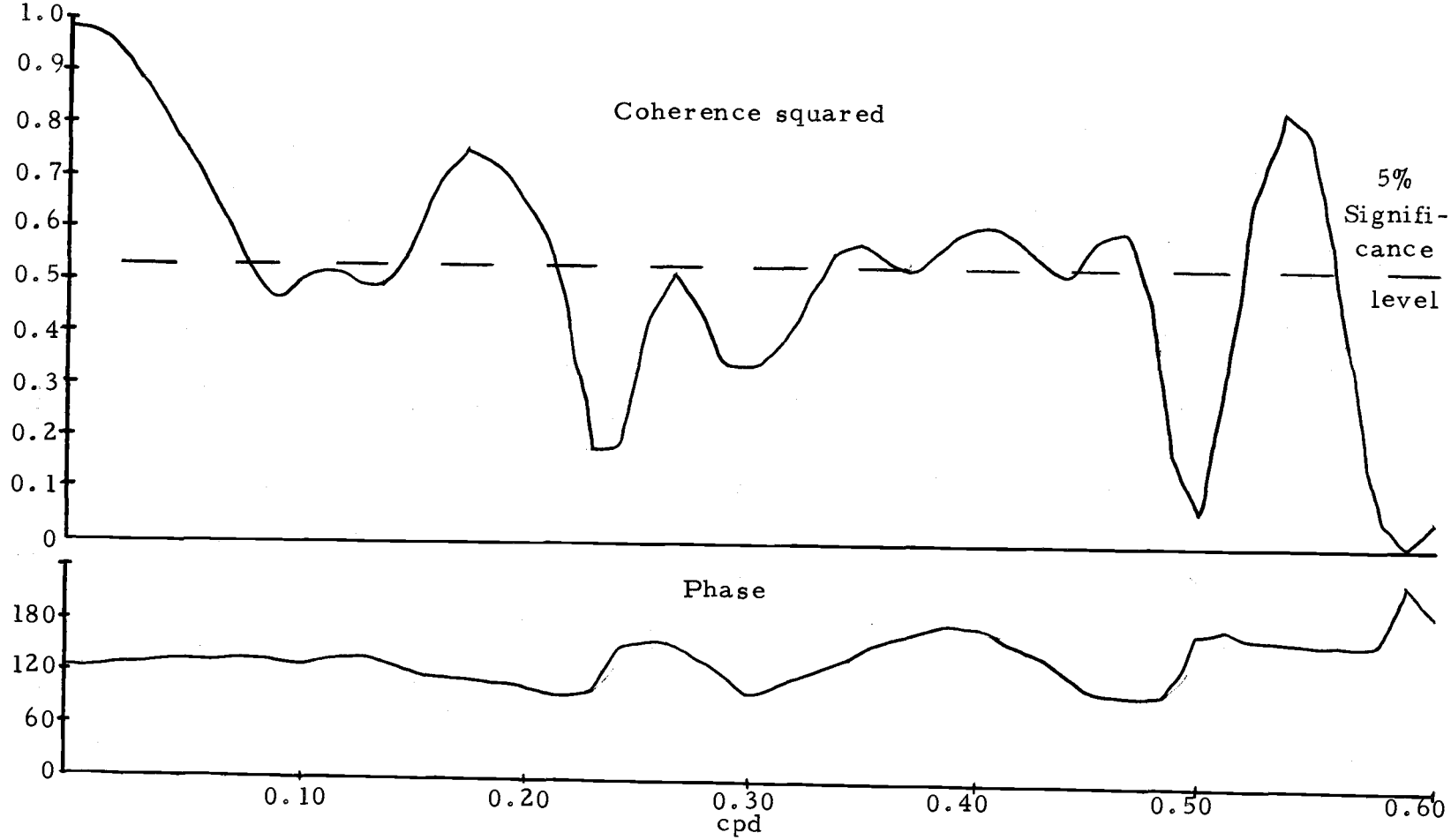

Figure 32. Coherence squared and phase between the alongshore velocity component and the density at Sunflower 90 m. In the phase spectrum density fluctuations lead current fluctuations.

(the 26.0 sigma-t isopycnal) to below it. In the present analysis we find a significant linear relationship between the alongshore current and the density at 90 m at these frequencies. We conclude that the fluctuations near 0.06 and 0.16 cpd represent waves (or wave-like phenomena) that are baroclinic.

Isostatic Adjustment

The coherence squared and phase between sea level and the Sunflower 90 m density are shown in Figure 33. In general the coherence squared decreases with increasing frequency. There are several bands in which the coherence is significant. The highest coherence is located at the lowest frequencies (0.0-0.10 cpd). It is also significant near 0.17 cpd where there appears to be baroclinic wave activity, and from 0.31-0.47 cpd where there is a plateau in the sea level spectrum.

Phase angles are plotted so that positive phase indicates that sea level is leading. The phase angles are generally slightly greater than 180^{o}, and lead density fluctuations. As sea level rises, the density decreases and thus an isostatic adjustment is maintained.

The fluctuations in sea level are probably driven by winds. Since density fluctuations lag those in sea level, it appears that they are in response to the sea level and indirectly to the wind fluctuations.

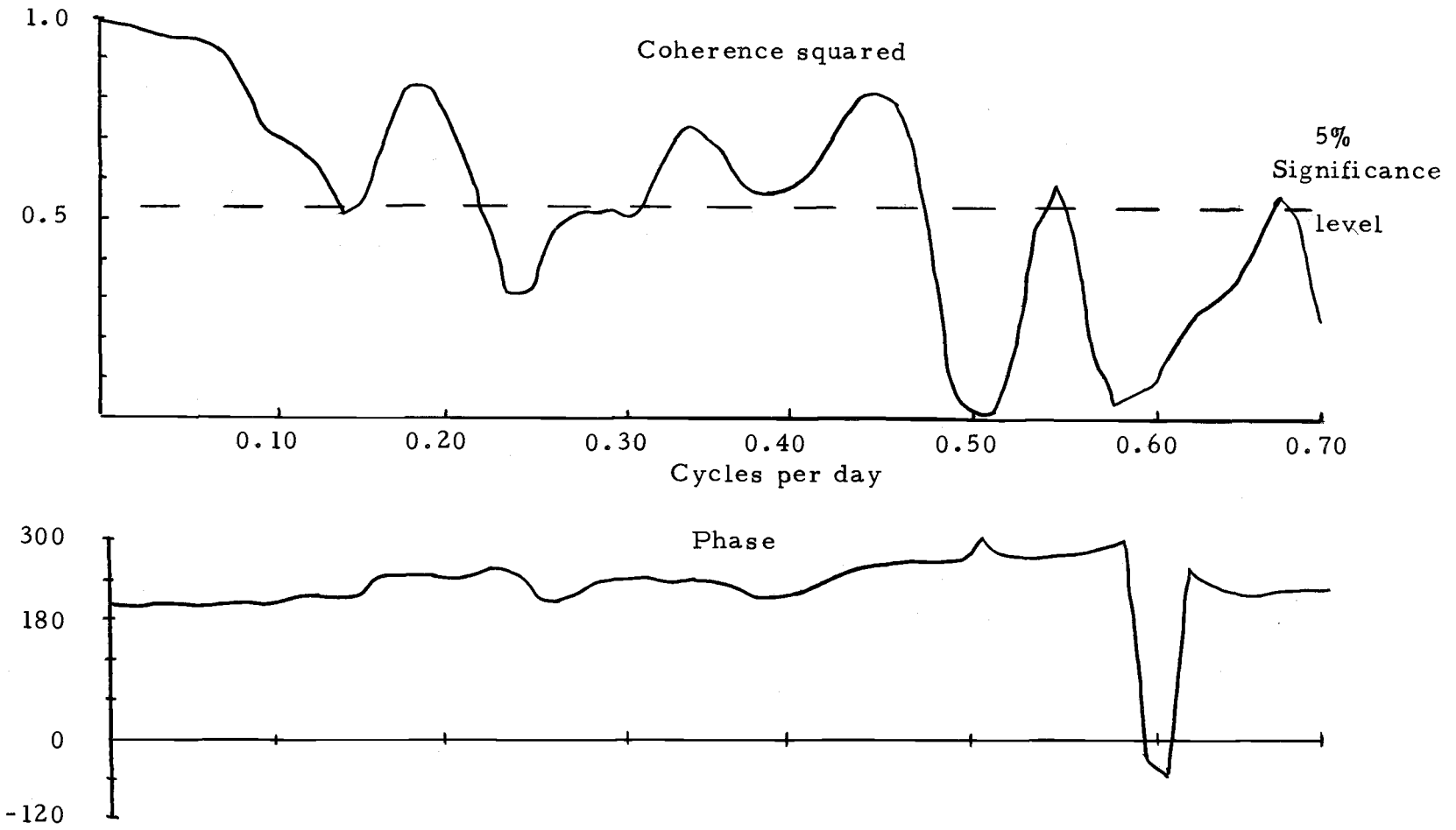

Figure 33. Coherence squared and phase between South Beach sea level and the density at Sunflower 90 m. Positive phase angles indicate that sea level leads. The 5% significance level is shown.

Barotropic Geostrophy

The coherence squared between the 90 m Sunflower alongshore currents and the South Beach sea level (Figure 34) is significant almost throughout the entire spectrum. The phase angles are small throughout, which indicates that northward fluctuations in the currents are associated with raised sea level. Thus there appears to be a geostrophic balance at nearly all frequencies between sea level and the mid-shelf currents.

The regression of sea level and velocity fluctuations to obtain an estimate of the width of the barotropic alongshore current was first suggested by Collins (1968). A geostrophic balance for the fluctuating flow is assumed[5]

$$\Delta v = \frac{g}{fL} \Delta S$$

The regression analysis gives a value for the coefficient, $\frac{g}{fL}$, and thus L can be calculated. Calculations for the summer have given values for the width of 56-72 km (Smith, 1974). For the WISP data we find a width of the barotropic alongshore current of about 50 km.

[5] The coherence analysis indicates that the assumption of barotropic geostrophy is valid for these data.

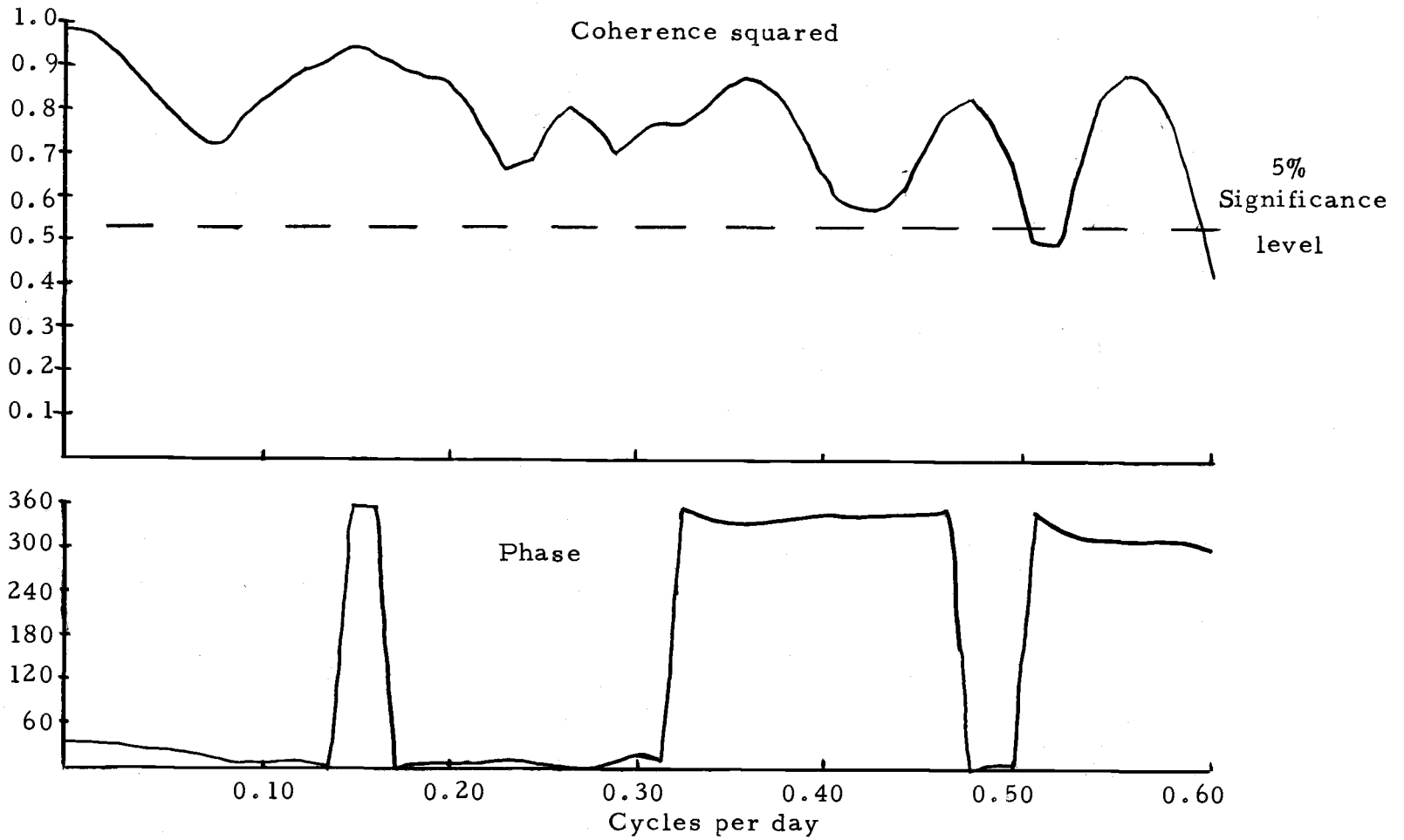

Figure 34. Coherence squared and phase between the South Beach sea level and the Sunflower 90 m alongshore currents. The phase angles have been plotted with currents leading sea level.

Modelling Sea Level Fluctuations

Because of the significant coherence between wind and sea level fluctuations, an attempt was made to model the latter using wind data. The model chosen was that of Gill and Schumann (1974).

Three questions are addressed in this section:

1. Can the transition be modelled?
2. Is the model applicable to both winter and summer?
3. Are there seasonal differences in the fit of the model?

Gill and Schumann's model assumes wind generation of continental shelf waves. As the atmospheric events propagate along the coast, they excite wave activity at the frequency of the forcing element, w, and at the free wave frequency, mc. Here c is the free wave phase speed determined by the shelf geometry and the mode of the wave, and m is the free wave number. If the forcing wind propagates at the same speed as the local free shelf wave speed, a resonant condition is established and the wave amplitude increases rapidly with time. If this condition is not met, two wave responses are generated: the free wave response traveling with its right side toward shore (in the Northern Hemisphere) and the forced wave traveling in the direction of the propagation of the forcing function.

Shelf waves are generated when an alongshore wind component produces a surface Ekman flux. The coastal boundary ensures that

continuity is met with an opposing and balancing flux of deeper water (Gill and Schumann, 1974). Potential vorticity is conserved in the vertical columns advected into deeper or shallower regions: the depth induced changes in potential vorticity are balanced by increases or decreases in relative vorticity. Continental shelf waves are the resulting propagation of the rotating columns (Longuet-Higgins, 1968).

Since these waves can travel long distances with little dissipation, they can be generated by the wind at large distances from the place where sea level is being observed. Thus the South Beach sea level could be determined to a large degree by wind fluctuations that are not observed at the Newport anemometer. A regression mode of sea level based on local winds at Newport gave a correlation coefficient of 0.57. Only about one-third of sea level fluctuations can thus be accounted for by local wind fluctuations. By using more wind observations, from distant stations, this correlation might be improved.

The Gill and Schumann model describes shelf wave behavior by solutions to first order wave equations. The total solution involves the combinations of an infinite number of solutions, one for each mode. However, the authors are able to show that the coefficients of higher modes decay as n^{-3} (where n is the mode number) and thus only the lowest order modes need to be considered. In this study only

the first mode behavior will be analyzed.

The model employed in this study is

$$F(t) = K_1 \sum_{i=1}^{n} (\tau(\chi_i,\ t-T)\ e^{-r\chi_i}\ \Delta\chi_i)$$

from Gill and Schumann (1974) with the following definitions:

K_1 = a coefficient depending on shelf geometry

n = number of data sets used in this model

τ = windstress time series at location χ_i, at time t-T

T = time lag appropriate for a given location having the phase speed specified

t = time

r = frictional damping factor

$\Delta\chi_i = 1/2(\chi_{i+1} - \chi_{i-1})$; i = (2, 3, . . ., n-1)

$= \chi_1 + 1/2(\chi_2 - \chi_1)$; i = 1

$= 1/2\ (\chi_n - \chi_{n-1})$; i = n

F(t) = predicted sea level time series (assuming that the shelf wave amplitude goes to zero at the seaward edge of the shelf)

Time series of alongshore windstress at five coastal locations were used in this analysis. The locations were two degrees of latitude apart, from 37°N to 45°N, along the United States west coast. For a test of the model, a sea level time series from Newport was used. The data interval of this time series and of the simulations was six hours.

The windstress data were provided by Bakun (1976). Surface winds, from which the windstress values were calculated, were computed from synoptic surface atmospheric pressure charts. Frictional effects were accounted for by a 15° counterclockwise rotation and by a 30% reduction in magnitude (Bakun, 1973). Missing data were substituted for by linear interpolation of adjacent data.

A non-zero frictional factor ($r = 0.0006$/km) was used. This gives the data from 37°N (the farthest data location from the observed sea level station) a coefficient of 0.59. With this choice of r, the inclusion of more data from more distant locations would little influence the computations.

Three predictions of sea level were made each with a different phase speed. (For a chosen phase the five input data series were offset relative to one another to achieve the required time delay.) In the first attempt the phase speeds that were used were interpolated from the values given by Clarke (1976). He found the free wave speed (from an equation given by Gill and Schumann [1974]) for the shelf profile at three degree increments of latitude along the west coast. These values were not constant along the coast; they were, in general, slower than the values used in the subsequent schemes. A northward constant speed of 450 km/day was used in the second analysis. This value corresponds to the phase speed of shelf waves off Oregon (at 45°N) according to the form given by Gill and Schumann

(1974). For the third trial, propagation was simulated at 900 km/day, or twice that used in the second trial.

Winter Season

All three simulated sea level series visually correlate well with the observed sea level (see Figure 35). The magnitudes of all three are smaller than that of the observed, but strong events are shared between simulated and observed series and these are in phase. The relative magnitudes of adjacent peaks do not always agree well with the observed (e.g., on 13 February; and on 23 March). All show a transition on or about 25 March from a period of predominately positive sea level to one of negative (below the time series mean value) sea level.

What is lacking in the models is a persistence: only in the observed sea level are strong events surrounded by other peaks and plateaus of the same sign. This observed persistence is probably due to factors besides the windstress field. The geostropic adjustment of currents with sea level fluctuations may account for it.

The simulation run at 900 km/day phase speed seems to be a better model than the slower ones. The magnitudes of that series are closer to the observed and it does not have the high frequency variations that are present in the other two simulations. These variations are not in the observed sea level.

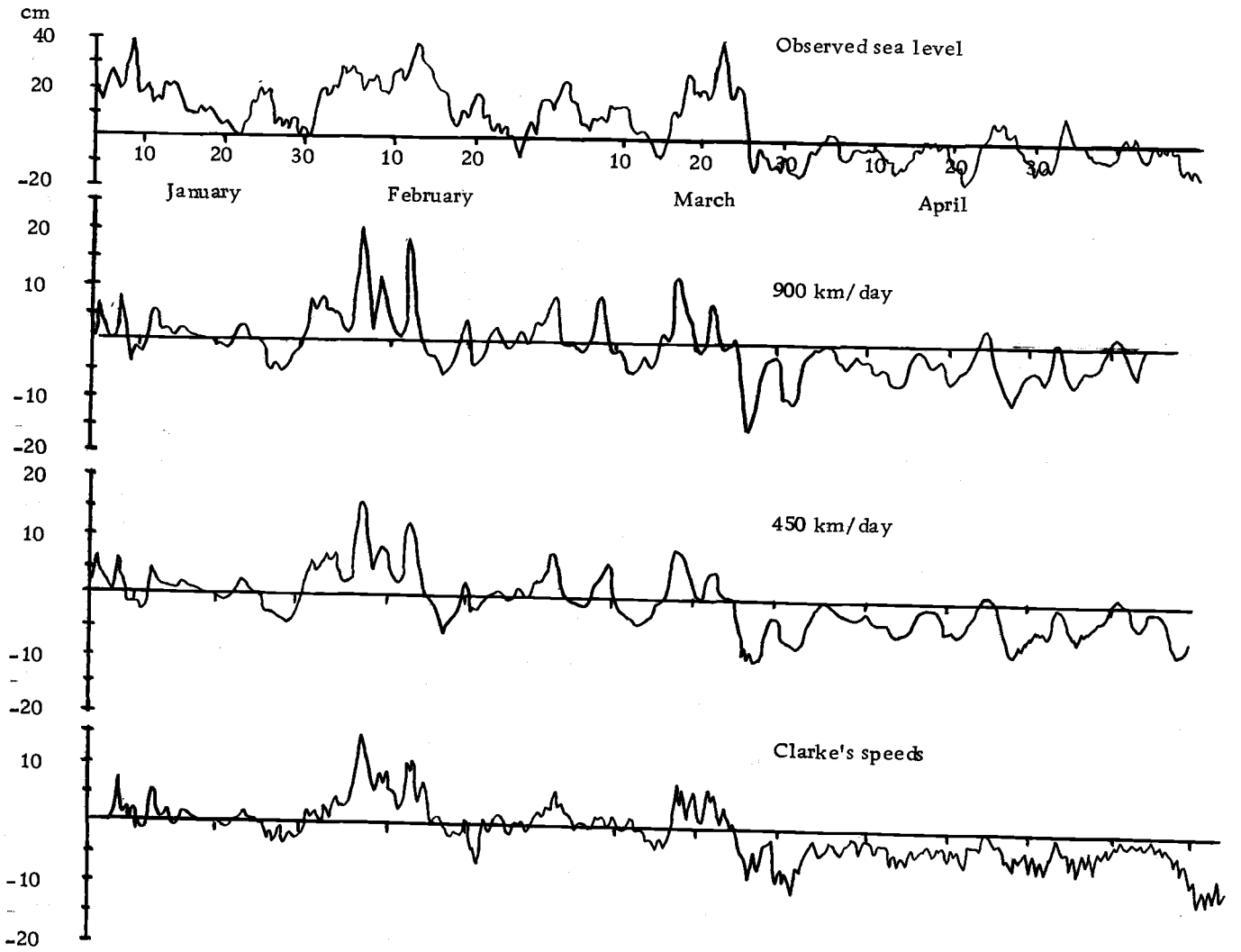

Figure 35. Simulations of South Beach sea level using the Gill and Schumann (1974) model at three propagation speeds for January to May, 1975. Also shown are the sea levels observed at South Beach.

An additional simulation was carried out (Figure 36). In that experiment only the local windstress was input into the model. As with the other trials, major events correlated in parity and phase with the measured sea level. However, the fit was not as good as with the worst of the above simulations.

Spectra of sea level and of the three prediction series are given in Figure 37. Except at spectral valleys in the sea level (at 0.23 and 0.53 cpd), it has a larger energy level than any of the simulations at all frequencies. Especially at the high frequency end of the spectra the variance of the predictions increases (and thus more closely approximates measured sea level) with increasing phase speed. The simulations' spectra all have the same general shape, and this is not very dissimilar to that of the sea level. However, there are no shared peaks which are significant. (Mutually shared peaks could be an indication of a resonance phenomena.)

Cross correlations of sea level versus the simulations at lags from zero to 180 hours are given in Figure 38. Each lag corresponds to a time delay of six hours. The correlations are maximized at their respective zero lags, and all are significant there. The highest zero lag correlation coefficient is 0.81. This was achieved in the slowest model. The lowest correlation value is for the scheme using the fastest speed, and is 0.74. Thus the simulation schemes account for at least 54% of the variance in the measured sea level. This is an

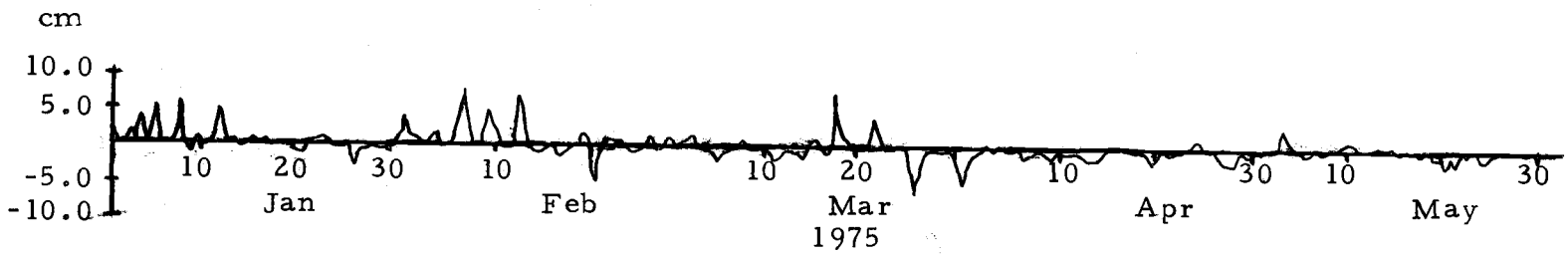

Figure 36. The simulation of South Beach sea level using Bakun's wind data only from 45°N.

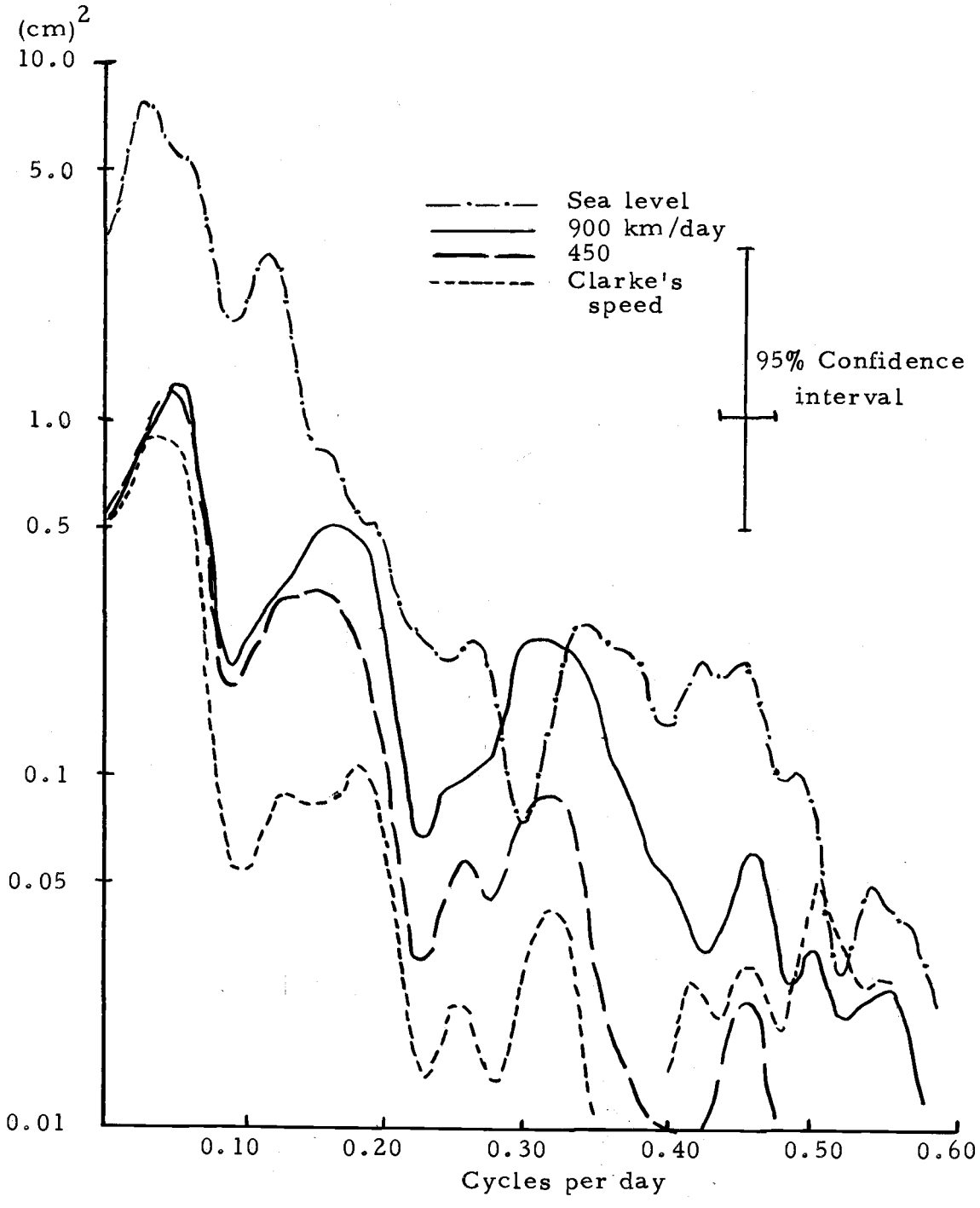

Figure 37. Spectra of the winter sea level observations and simulations.

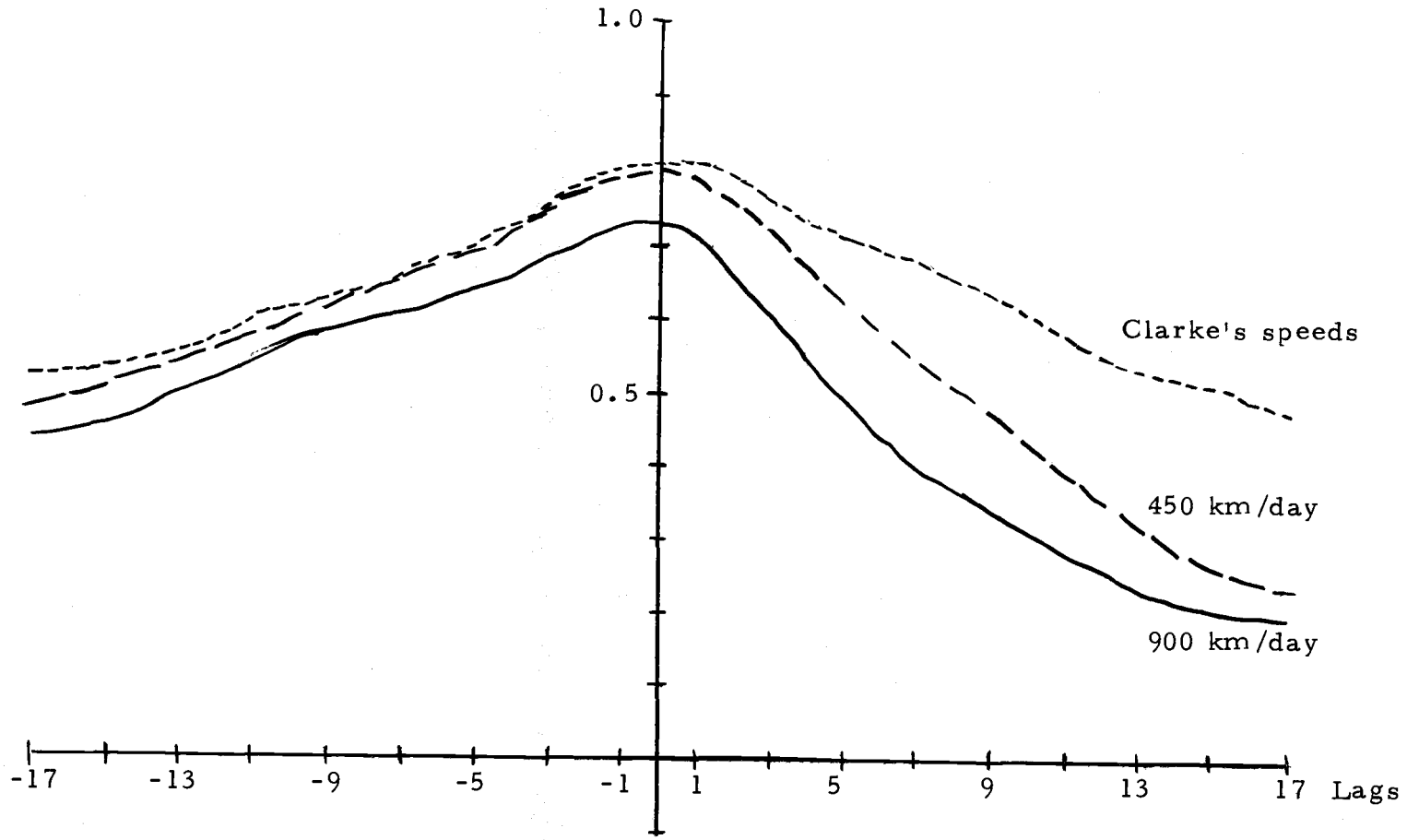

Figure 38. Cross correlations of the South Beach sea level and the sea level simulations for the winter of 1975. Each lag corresponds to six hours, and positive lags mean that the observed sea level leads.

improvement over the sea level regression model using only local winds.

The squared coherence between the three simulations and the measured sea level are shown in Figure 39. At low frequencies (0.0-0.061 cpd) all three pairings are coherent; the two schemes with faster propagation speeds are coherent to a higher frequency (0.168 cpd). Throughout most of this range (0.0-0.137 cpd), sea level lags by up to 40^{o}.

There are several frequency ranges in which one or more of the three simulations are significantly coherent with sea level. Cutchin and Smith (1973) found evidence for continental shelf waves between 0.2 and 0.3 cpd. In this band one can see two particular frequencies at which significant coherence is achieved: at 0.244 and at 0.321 cpd. Near both of these frequencies the phase angle passes through zero degrees and the spectra at these frequencies have peaks (although not all are significant). Also at 0.15 cpd there is a spectral peak and a zero phase angle. Northward propagating events in sea level and in currents were seen only at 0.24 cpd. Thus this frequency could be a region for resonant continental shelf waves. The other frequencies could be regions of forced continental shelf wave activity.

The model adequately predicts sea level fluctuations from a knowledge of the windstress field. All three simulations yield

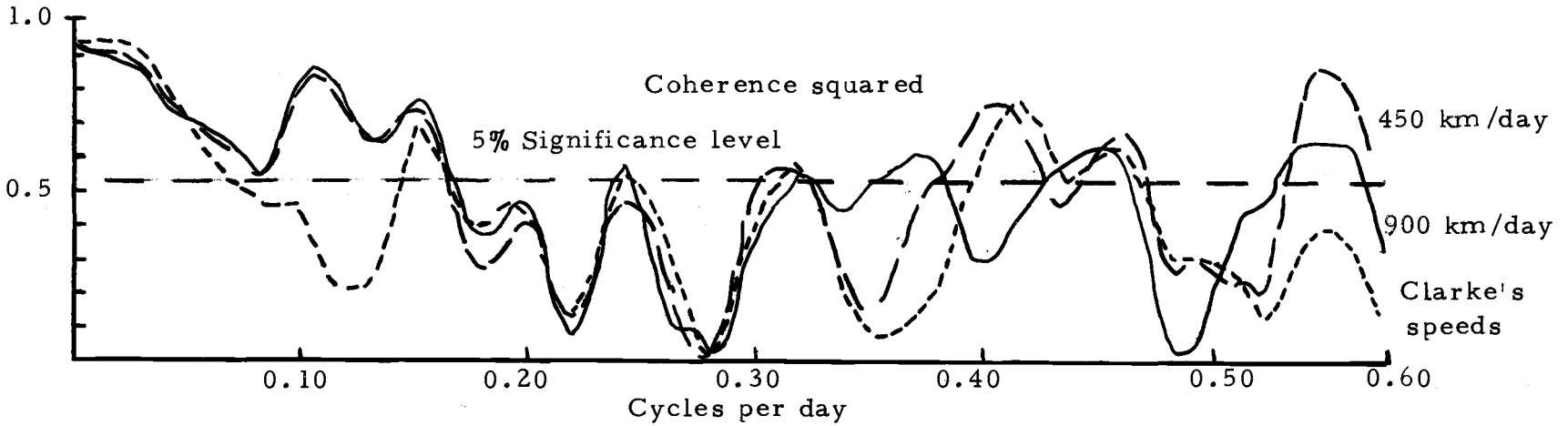

Figure 39. Coherence squared of the South Beach sea level and the sea level simulations for the 1975 winter.

satisfactory fits to the observations and all show the transition event. The good fit of the model, which assumed northward propagation, could indicate the presence of northward travelling waves whose magnitude was much smaller than the forced response of the ocean to the winds so that they could not be seen in the spectral calculations.

Summer Season

A nearly identical set of simulations was carried out for the summer of 1975. Three months of Bakun's winds were used: June through August. The same phase speeds were employed. However, only four input data series were used (from locations at 39^{o}, 41^{o}, 43^{o}, and 45^{o}N).

In Figure 40 are the time series for the three summer simulations. The fit is again remarkably good (especially when considering that only one mode is used in these simulations). As for the winter simulations the best visual fit appears to be at the fastest phase speed.

The cross correlation between each of the simulations and the Newport sea level is shown in Figure 41. Clearly the best of the three is that simulation using the slowest propagation speeds. The second best is the next fastest.

The maximum cross correlation coefficient, although significant, is less than that during the winter. Whereas in winter, the

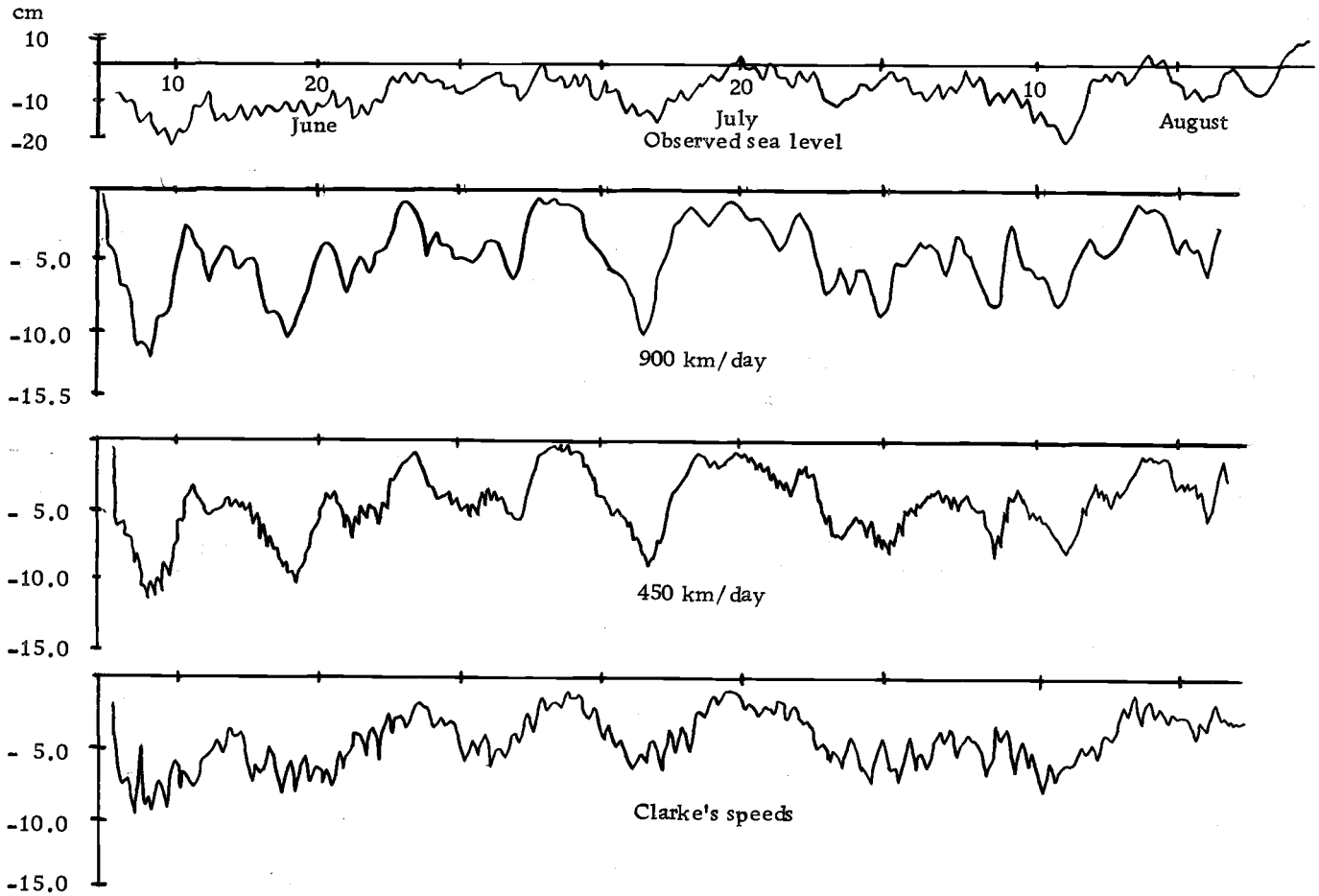

Figure 40. Simulations of South Beach sea level using the Gill and Schumann (1974) model at three propagation speeds for June through August, 1975. Also shown are the sea levels observed at South Beach.

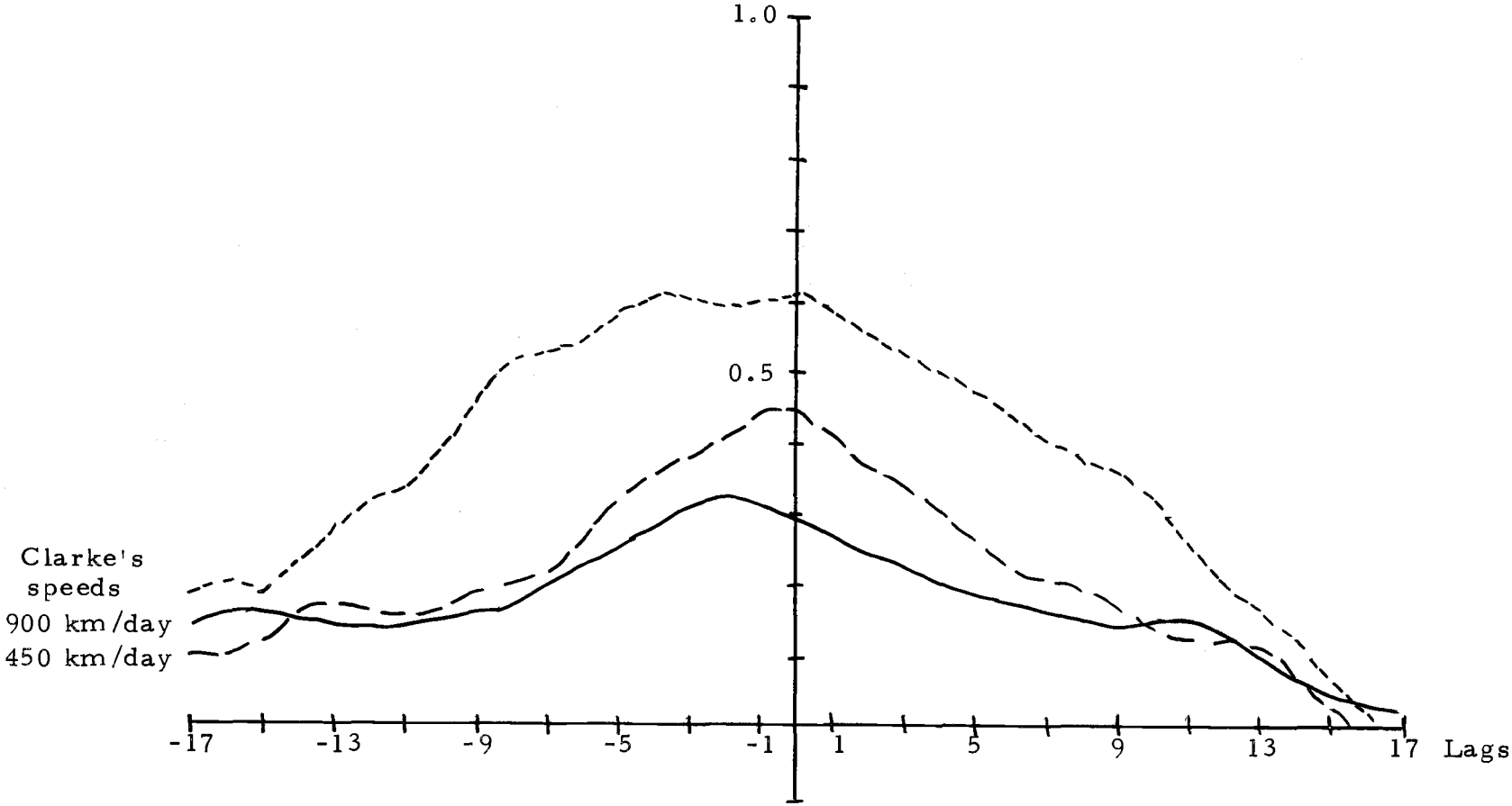

Figure 41. Cross correlation between the observed sea level and the sea level simulations for the summer of 1975. Each lag corresponds to a period of six hours and positive lags indicate that the observed sea level leads.

simulation at the slowest speeds can account for about 65% of the variation in the observed sea level, in summer it can account for less than 40%. All three simulations have cross correlation coefficients greater than 0.73 in winter, while in summer the largest is 0.60. There is also a clearer difference between the three correlations in summer than in winter.

The spectra of sea level and the three summer simulations are shown in Figure 42. From 0.0 to about 0.4 cpd, the spectral values of the simulations increase with increasing phase speed. All three are smaller than the sea level spectrum. The shapes of the four spectra are nearly the same in this region. At higher frequencies, these properties do not exist.

The same properties can be seen in the winter spectra (Figure 37). One of the few differences between the winter and summer spectra is the absence of the spectral plateau from 0.34-0.46 cpd in summer.

The final comparison of sea level and simulations is shown in Figure 43. This figure contains plots of coherence squared and phase. At low frequency (0.0-0.09 cpd) the coherence is high and the phase is small for all three simulations. At higher frequencies, there are isolated frequency bands that have significant coherence for one or more of the simulations. The phase angles at these bands increase with increasing frequency.

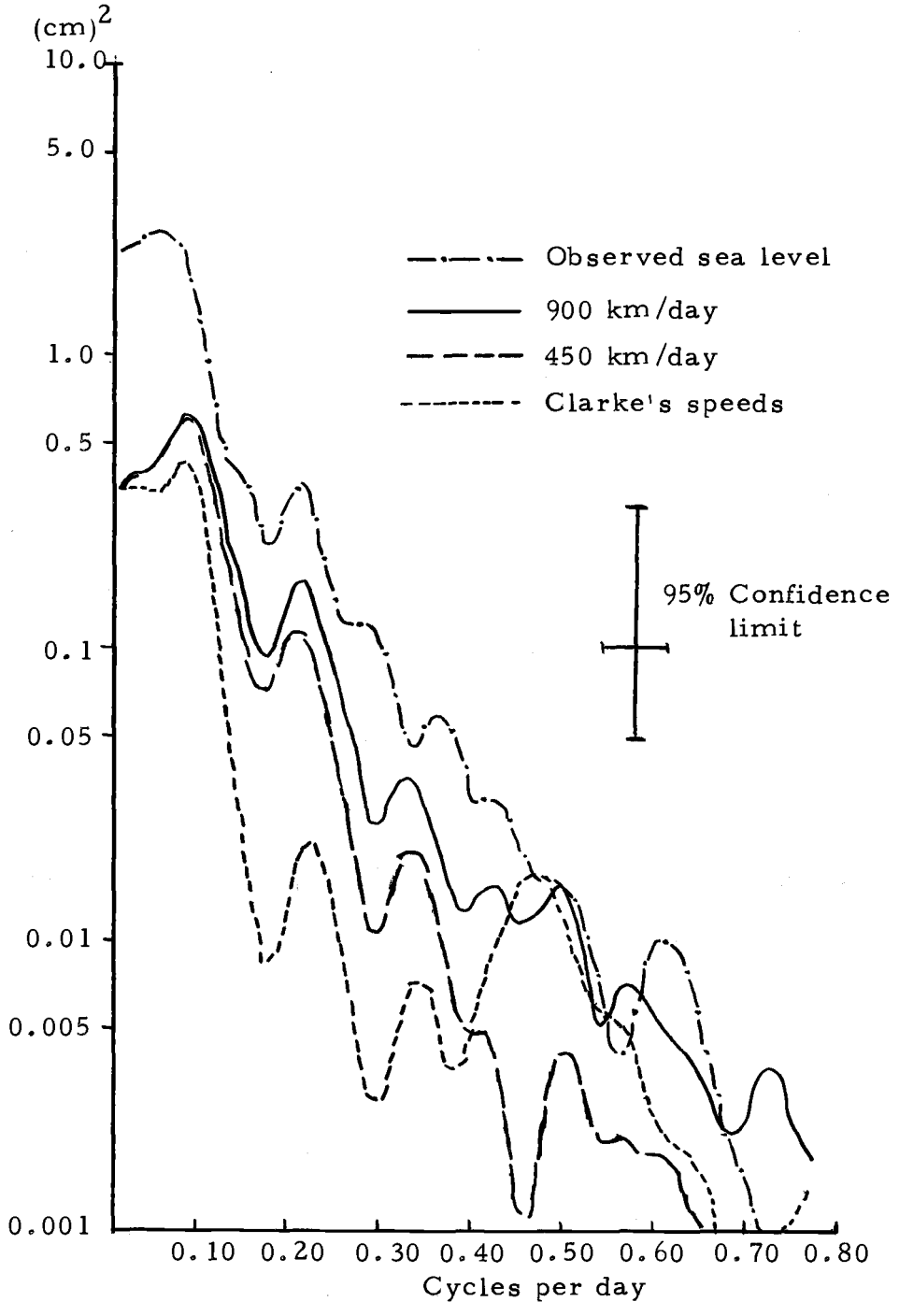

Figure 42. Spectra of the observed and simulated summer sea level at South Beach.

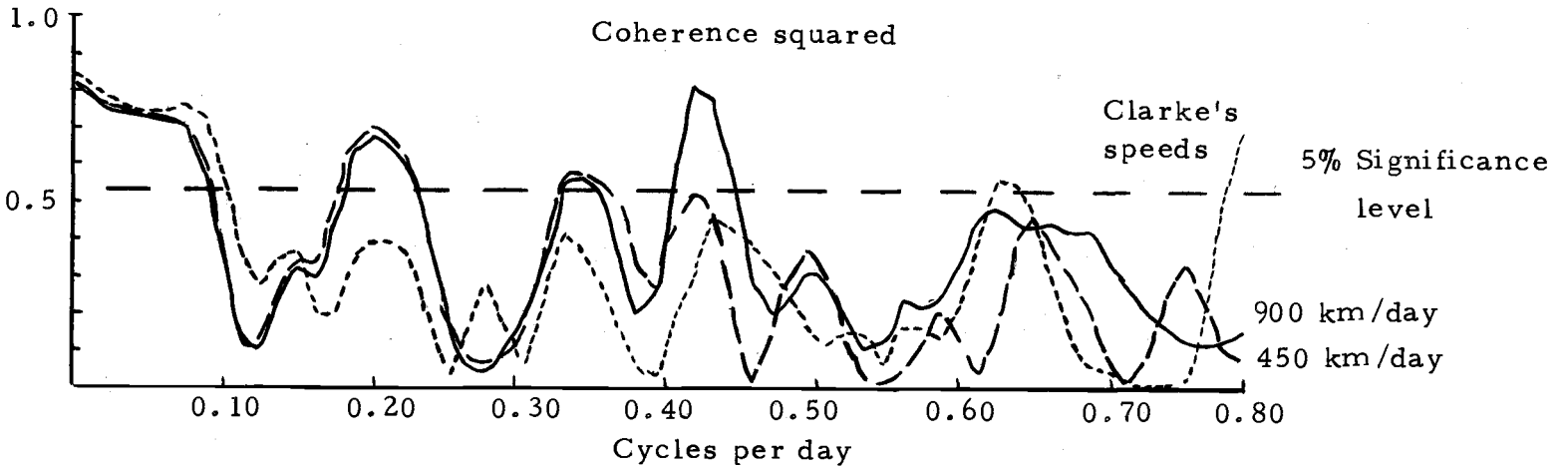

Figure 43. Coherence squared between the observed and simulated South Beach sea level for the summer of 1975.

The coherence and phase diagrams are not unlike those of Clarke (1976). The most striking difference is that the very high coherence at low frequency which dominates the plots shown here is not seen in Clarke's coherences.

In previous simulations using the Gill and Schumann model (Hamon and Clarke, 1975; Clarke, 1976), authors have relied solely upon coherence calculations to test the applicability of the model. The test has been found to be useless here for differentiating between models run at different phase speeds. The cross correlation offers a more definitive test. This is especially true in this study where we were more interested in the response of the sea level at all frequencies. In the other studies, the investigators were looking for responses at discreet frequencies that might represent wave activity.

Using this test of cross correlation, an evaluation of the model in the two seasons can be made. In winter, all three phase speeds yielded similar and high correlations at the zero lag. All three provided good sea level predictions. In summer the best predictor was clearly that model run at the slowest speeds. However it was a less adequate description of sea level fluctuations. Possibly a slower phase speed would have yielded a more accurate model in summer.

It appears that the Gill and Schumann model can fairly accurately predict sea level fluctuations, with an appropriate choice of phase speeds. However, more experiments should be carried out with

a larger range of variables. The reporting of results should show time series of the simulations and the observed sea level, their cross correlations, their spectra, and their coherence and phase.

THE TRANSITION EVENT

The change in seasons, from winter to summer, on the Oregon continental shelf takes place over a period of approximately three to four months. The initiation of this seasonal change occurs in a short duration barotropic event which we have called the transition event. It will be shown here that the oceanic transition is directly forced by the wind field. The wind event, which is associated with the transition event in the ocean, is not fundamentally different than the many other (non-transition causing) winter storms that pass over the continental shelf.

Our definition of the transition event is based on changes in observed parameters. These changes have been examined in Chapter III.

1. Sea level. The sea level changes from predominately positive values (above the sample mean) to predominately negative values (below the sample mean). This change occurs in about a day's time.

2. Currents. The change in currents, which occurs simultaneously with the change in sea level, is from strong northward to strong southward flow. In winter the mean current is weakly northward, as large events alternate in both northward and southward directions. Immediately after the transition the currents at mid shelf are strongly southward with only rare and weak reversals of

northward events. The currents change from their weakest monthly mean (northward) to their strongest monthly mean (which is southward) at the transition event. The currents over the shelf in winter are barotropic in the mean; after the transition the mean currents are quasi-barotropic and evolve into a baroclinic flow in summer.

The 1975 Transition Event

Based on the preceding characteristics, the 1975 transition occurred on 25 March. During the week before this event the winds at Newport were strongly northward. At the time of the transition they shifted to a southward direction.

This shift in the local winds was caused by the movement onshore of a storm center. Low pressure systems, during winter, pass from over the Pacific Ocean to over the North American Continent along the coasts of British Columbia, Washington, and Oregon. As each storm approaches the coast the local winds become northward. The wind direction shifts as the storm moved inland: the coastal winds become southward. Each low pressure center that intersects the coastline of the Pacific Northwest induces the same local wind conditions.

What is different after the 25 March 1975 shift in wind direction is the subsequent presence of a high pressure center off the coast. This causes strong southward winds to persist along the coast. After

other winter storms in 1975 new low pressure centers quickly replaced storms that had moved onshore, thus interrupting the persistence of the southward winds.

Does this continuity of the southward winds mark a seasonal transition in the atmosphere? Meteorological, seasonal transitions have been described by Bryson and Lahey (1955). The authors predict that the third week in March is the winter to spring transition period. That date agrees surprisingly well with these data. The cause of the transition is the shifting of centers of atmospheric pressure systems. During winter a high pressure center is statistically located off Baja, California. In spring this high migrates northward to become the North Pacific High (Lahey et al., 1958). This movement of the dominant high pressure center may be the atmospheric transition.

The oceanic transition can be seen most clearly in sea level records. It occurs not only at South Beach (Figure 14) but also at all of the other three sea level stations (Figure 26). All four records show that the transition occurred almost simultaneous along the coast from southern Oregon to Vancouver Island.

Shelf currents also undergo a shift in direction from northward to southward on 25 March. The shift takes place in about 12 hours.[6]

[6] The rapid reversal of currents with local winds is similar to the monsoon transition reported by Leetmaa (1972). There the Somali current reversed directions under the influence of local winds.

Of the three current meter arrays, Sunflower's currents show the transition most strikingly. Here all four meters were recording strong northward currents before and strong southward currents afterward. The largest currents and the largest current changes occurred at the shallowest Sunflower current meter. However the transition event is essentially barotropic. Time series of two dimensional empirical orthogonal components (Figure 22) show the transition is manifested almost entirely in the lowest mode. This mode is quasi-barotropic.

The transition can also be seen at Pikake. However, subsequent northward reversals make the transition event less striking. At Wisteria it can be seen down to 100 m. Below that depth very little or no change can be associated with the transition. The currents at Wisteria are smaller and their transition changes are smaller than those at corresponding depths at Sunflower.

The transition event was also observed at current meters located off Vancouver Island (Huyer et al., 1976). There the rapid northward to southward shift in current direction occurred on 23-24 March. The current shear at this northern array also changed sign at the transition as it did at the WISP arrays. The transition thus occurred off Vancouver Island before it occurred off Oregon.

As discussed previously, northward winds cause onshore flow and induce some downwelling along the coast and southward winds

induce upwelling. During the period that preceded the transition (starting on 17 March), winds were strongly northward and the shelf waters became isothermal, isohaline, and isopycnic (see Figures 9, 10, and 11). The density at the shallowest Pikake and Sunflower current meters was essentially unchanged. At greater depths at these arrays, a decrease in density occurred until the entire water column was homogeneous (having the temperature, salinity and density values of the 25 m records). On 25 March, stratification was restored, apparently in response to the southward, upwelling favorable local winds.

The transition event is a barotropic event. The barotropicity may be accounted for by the lack of stratification in the water column prior to the transition. However the highly stratified waters during the summer also respond barotropically to wind events, so the lack of vertical stratification just prior to the transition event may not be a necessary condition. The water immediately begins to stratify with the transition event and tends quickly toward geostrophic balance. There is good correlation (0.71) between the terms of the thermal wind equation: the current shear at 50 m at Sunflower is correlated with the horizontal density gradient there, even shortly after the time of the transition (Figure 44).

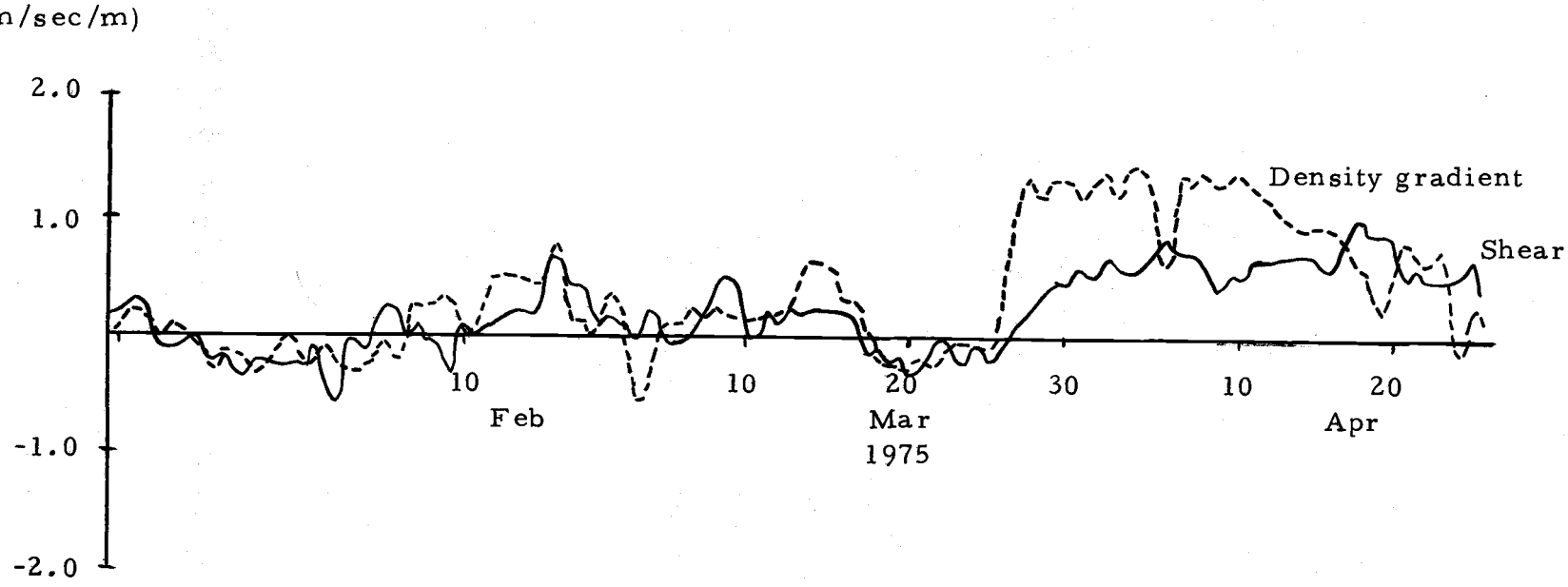

Figure 44. Time series of the vertical current shear and the horizontal density gradients (along 45°N) at 50 m, Sunflower. The equality of these time series demonstrates geostrophy through the thermal wind equation: $\partial v/\partial z = g/f\,\rho \cdot \partial \rho/\partial x$.

The Transition in Other Years

Current meter time series spanning 16 months (December 1972 to April 1974) were shown in Figure 1. This period includes two winter-summer transitions. In 1973 the current reversal occurred on 22 March. The following year the date of the transition event was 12 April. The sea level and wind time series included in Figure 1 show that the transition in these variables occurs at the same time as in the currents.

The coastal upwelling indices for 1973-1975 are shown in Figure 45. These were calculated from surface winds which were calculated from surface atmospheric pressure (Bakun, 1975). The onshore-offshore component of the Ekman transport is called the upwelling index. Offshore Ekman transport implies a replacement of near surface waters by deeper waters because of continuity. Here the upwelling index would be positive.

For 1973 the change from a predominately negative (downwelling) to a predominately positive (upwelling) index occurs on 22 March. A strong negative index preceded a long period of positive indices; this transition was abrupt. In 1974 the transition is less well defined. It occurs on 11 April. The transition is abrupt in 1975 and it occurs on 24 March. For all three years examined, the seasonal change in the upwelling indices coincides with the seasonal changes in sea level and currents (see Figure 1).

a. 1973 Upwelling indices 45°N

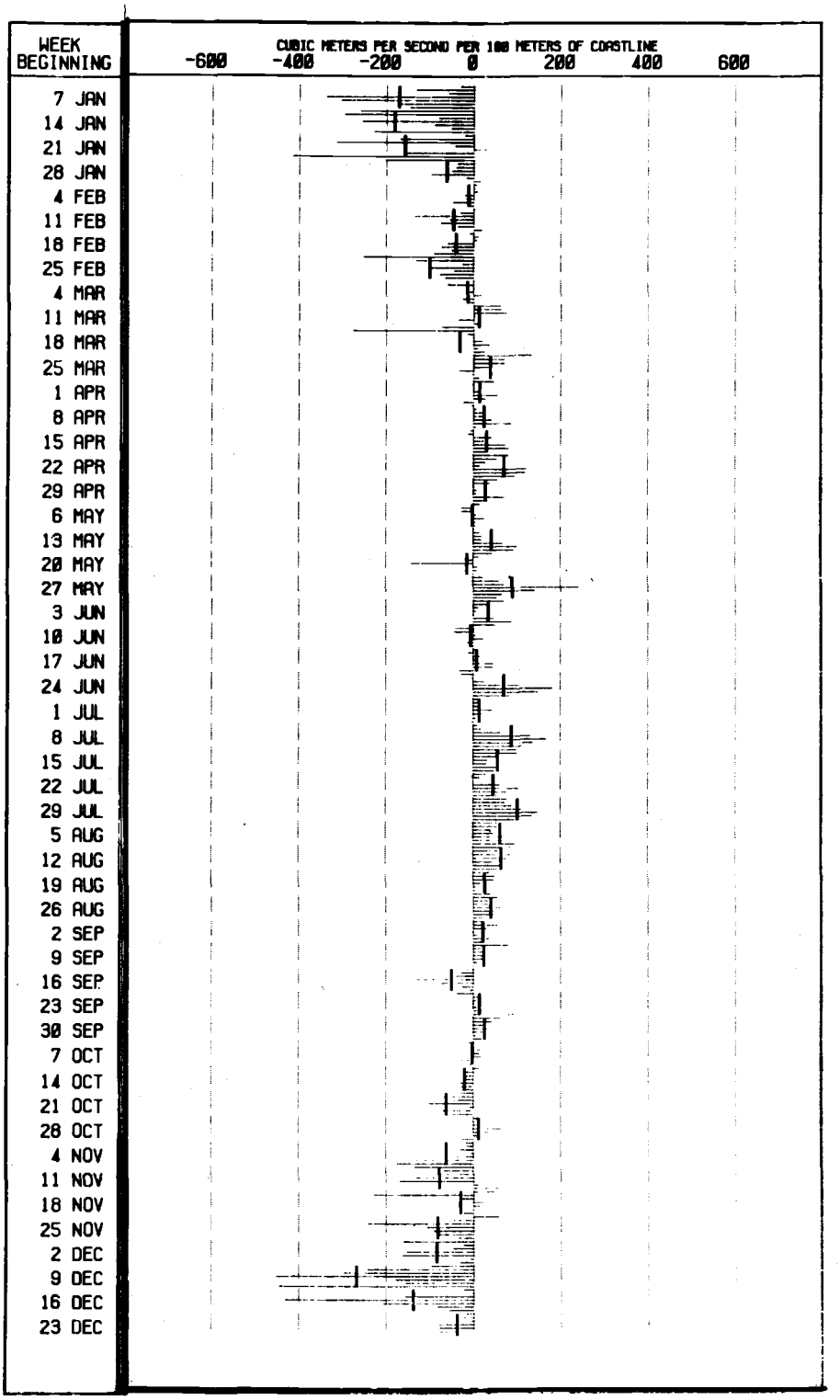

Figure 45. Upwelling indices for 45°N for 1973-1975 (Bakun, 1976). Units are cubic meters per second per 100 meters of coastline.

b. 1974 Upwelling indices 45°N

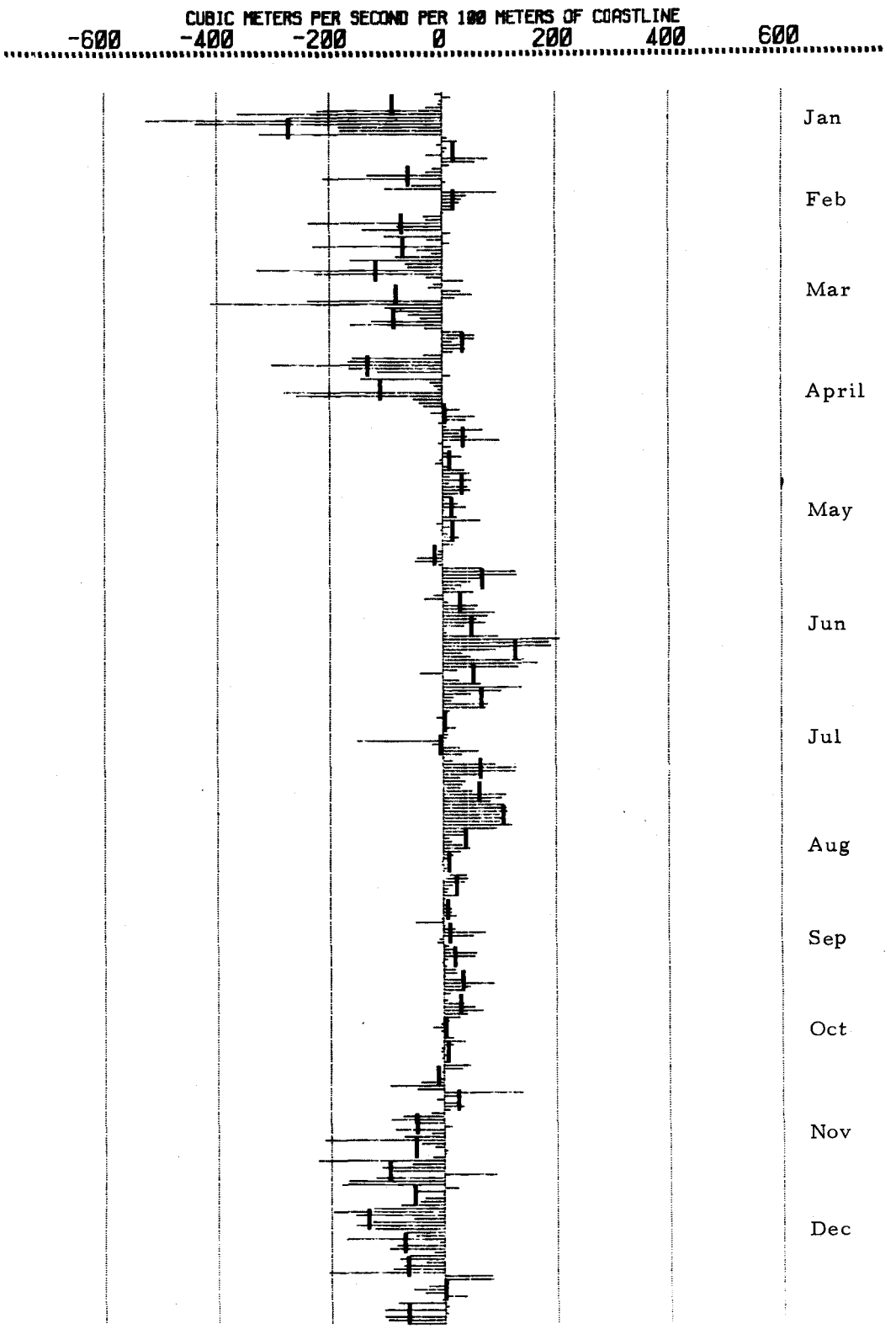

Figure 45. (Continued)

c. 1975 Upwelling indices 45°N

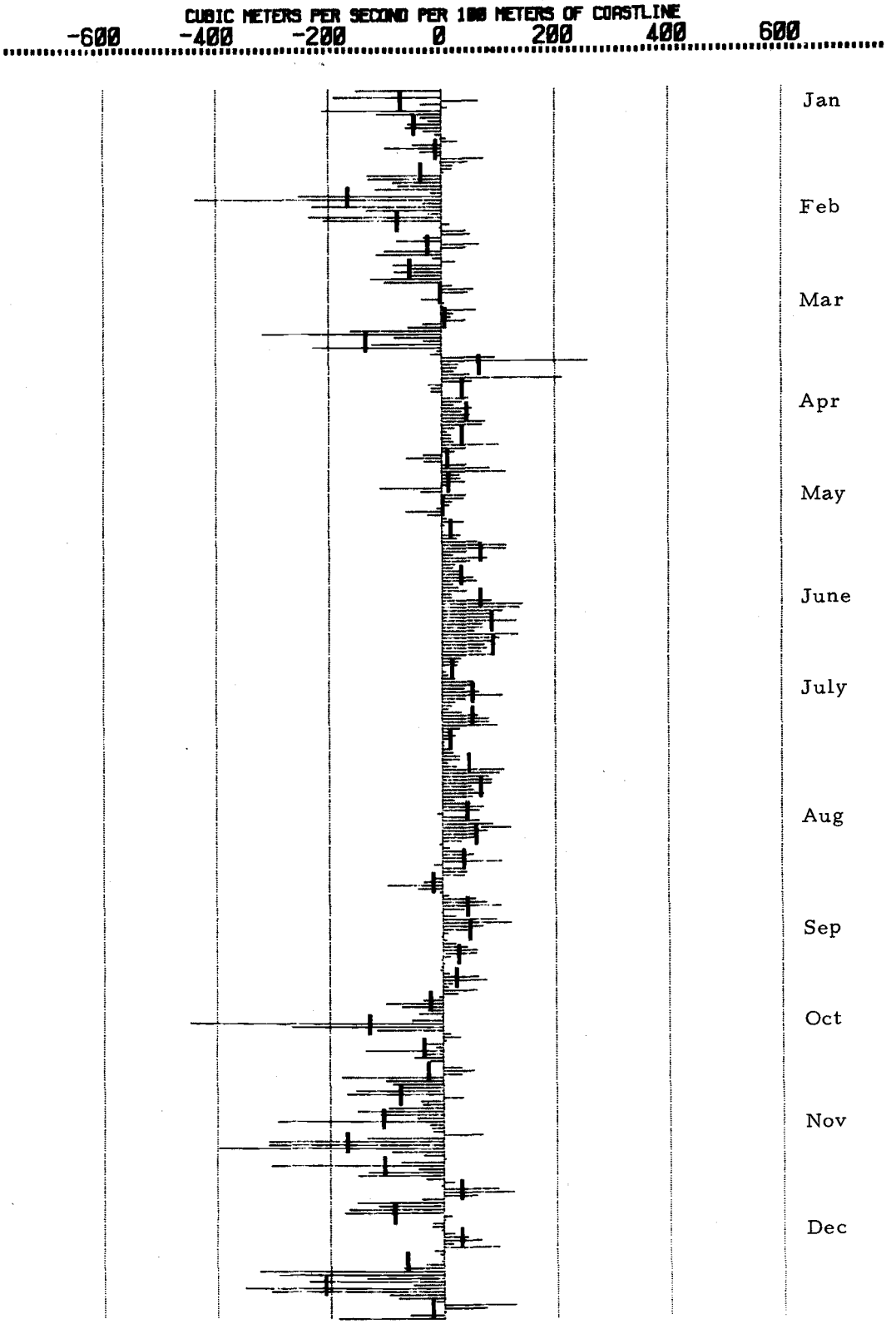

Figure 45. (Continued)

In all three years the observed transition occurred as a low pressure center moved onshore. In 1975, when the transition was more pronounced than in the other years, the low pressure system was immediately followed by the establishment of a strong, stationary high. Although no strong high was established in 1973 or in 1974, local winds along the coast were southward for a period of at least one week. The weekly averages of the offshore Ekman transport remained positive for several months, as no strong low pressure systems moved into the region.

The Transport of Mass

Steric heights of sea level relative to the 600 db surface were computed from hydrographic data collected during the WISP experiment. The techniques of the calculation follow those of Reid and Mantyla (1976). Huyer (1977) presents several plots of ten year averages of the steric heights of sea level from these data. The steric height anomalies relative to 600 db, for the WISP hydrographic cruises are plotted in Figure 46.

Seaward of 124° 40'W the seasonal change in the steric height in 1975 is smaller than the changes from one month to another. However, inshore of that point, seasonal changes are more prominent. Cruises for January, February, and March (two cruises) show inshore levels greater than 880 dynamic cms. The four subsequent

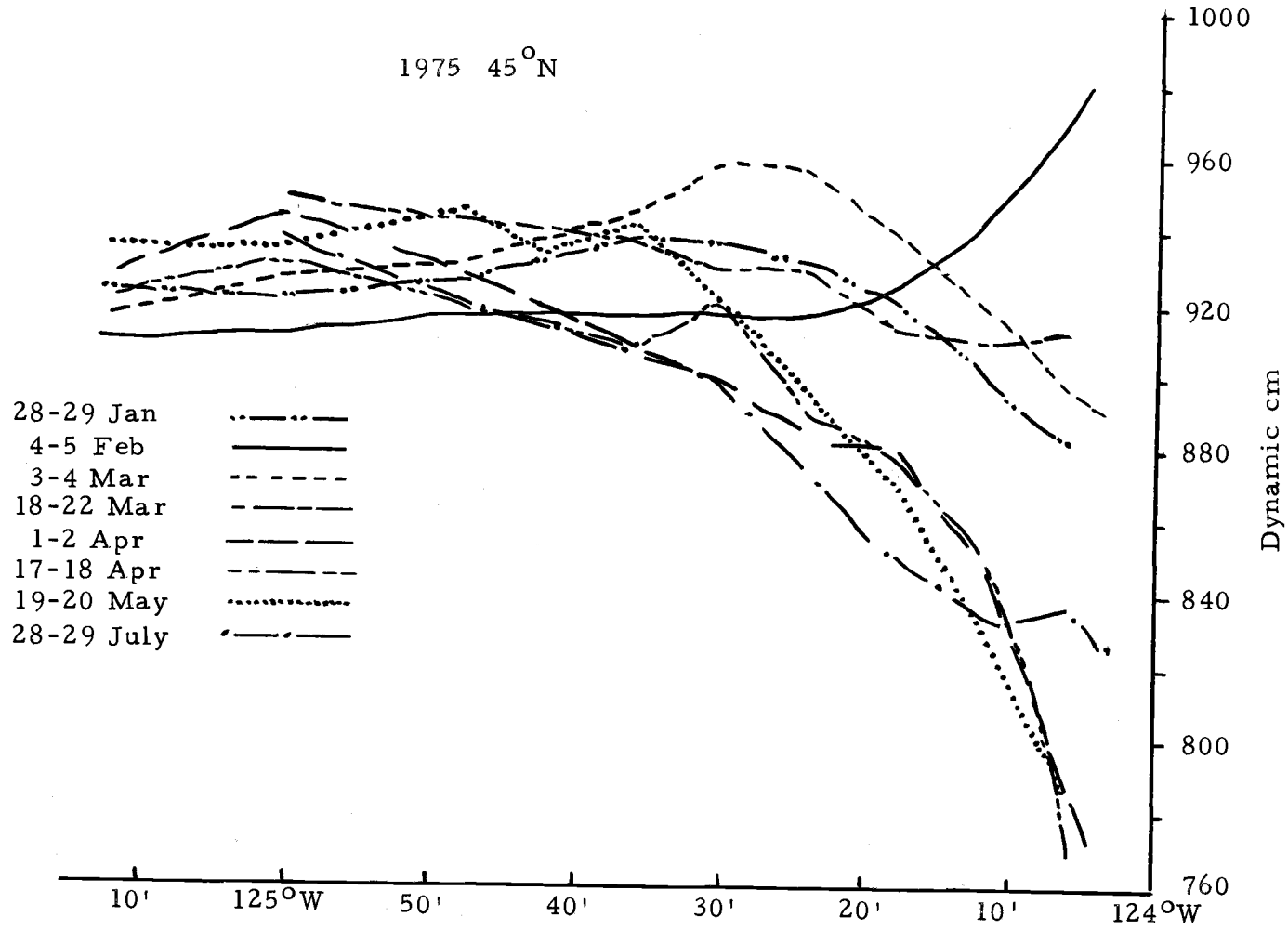

Figure 46. Steric height anomalies at the sea surface relative to 600 db over the continental shelf along 45°N, 1975.

cruises (two in April, May; and July) show much lower levels. These observations are in agreement with those of the Newport tide gauge. A similar plot for ten year averages (by month of observation) of hydrographic data was made. Again winter months (October-March) had high nearshore sea levels and summer months (April-September) had lower values.

The steric height curves are a measure of the volume of sea-water above the 600 db surface and thus changes in steric heights between hydrographic cruises are measures of the change in volume. The offshore Ekman transport is a measure of the transport of mass. Here we compare these two independent measurements.

The change in volume was found by manually integrating the area between two steric height curves. The resulting units are volume per unit length of coastline (cm^3/cm).

An Ekman transport results in a movement of water onshore or offshore. Continuity requires that this mass of water be replaced. With the presence of the coastline this replacement must come from deeper waters for offshore Ekman transports. Although there is no net change of mass, therecan be a net change in the volume. With offshore Ekman transport less dense, near surface waters are replaced by more dense, deeper waters and hence there is a net volume decrease. This change in volume is directly proportional to the Ekman transport (and hence windstress) and to the difference in

the densities of the replacing and the replaced waters. The volume offshore (V_1) and the volume onshore (V_2) are

$$V_1 = \left(\frac{\tau}{f}\right) \frac{1}{\rho_1}$$

$$V_2 = \left(\frac{\tau}{f}\right) \frac{1}{\rho_2}$$

Then the change in volume due to an Ekman transport is

$$\Delta V = \left(\frac{\tau}{f}\right) \left(\frac{\rho_2 - \rho_1}{\rho_1 \rho_2}\right)$$

$$\approx \frac{\tau}{f} \Delta\rho$$

This change in volume was compared to the change in volume calculated by the steric height measurements. There was a hydrographic cruise immediately before the transition (on 18-22 March) and soon after it (on 1-2 April). The volume change induced by the Ekman transport during this period was 6.2×10^7 cm^3/cm. The change in volume calculated from steric height data was 2.2×10^7 cm^3/cm. Thus the offshore Ekman transport can fully account for the steric height change. Also these estimates are in reasonable numerical agreement. Better agreement would occur with the choice of a smaller value for $\Delta\rho$. A value of 1 sigma-t unit was used. (In this calculation it was assumed that near surface waters would be replaced by near shelf bottom waters. The chosen value for $\Delta\rho$ was based on this assumption and on the hydrographic data from WISP.

The smaller than expected size of the steric height calculation might indicate that the near surface waters were replaced, at least in part, by mid-depth waters.)

A similar calculation was made using the first and last hydrographic cruises' data. The comparison of the Ekman transport was not good. The change in volume calculated from the wind field was much larger than the change actually observed. In downwelling situations the onshore Ekman transport probably gives an overestimation of the increase in volume. As the pycnocline gets depressed to lower depths, the exchange of onshore and offshore waters occurs above the pycnocline, and thus the density difference between the onshore and offshore moving waters is small.

Summary

After the transition there was a change in the density field over the continental shelf. This change caused a lowering of the steric sea level which was consistent with the changes in the observed sea level at South Beach. The change in steric height can be accounted for by local winds through a simple Ekman type model. Thus we have strong evidence that the transition event is the result of local wind forcing.

SUMMARY AND CONCLUSIONS

The winds, currents and sea level differ significantly with season. In this thesis it has been shown that the change from winter to spring is marked by a barotropic event, which can be readily seen in the sea level and current records in all years for which data were available. The data from 1975, which is the most extensive data set of any year yet, and with which this thesis is primarily concerned, are used to establish the significance of the transition event, to determine what significant differences occur in oceanographic parameters before and after the event, and to show that the changes are the result of the local wind field rather than effects propagating into the region from afar.

Sea level and winds change at the time of the transition. Sea level goes from values above its annual mean to values below it. The monthly averaged Newport winds go from northward to southward and the Ekman transport changes direction from onshore to offshore (upwelling favorable). From the wind record the transition event itself appears to be no different from any other winter storm impinging upon the coast. However only after the transition event do the weekly average Ekman transports remain offshore. This subsequent behavior distinguishes the transition event from other events.

In winter, the monthly mean currents are barotropic and northward, but small in magnitude because of the many reversals on the time scale of a few days. They become southward and quasi-barotropic in the spring, with the strongest flow near the surface. The flow field becomes baroclinic, with a southward near surface current and a northward undercurrent, in summer.

Current fluctuations on the time scale of a few days have a variable shear in winter: the sign of the shear changes with each northward and southward phase of an event, but the near surface currents are always larger in magnitude regardless of the direction of flow. Thus the mean shear in winter is small. At the transition event a large shear is established with the near surface currents always southward relative to the deeper currents. The layer of maximum shear moves upward after the transition event and in summer it is located in the near surface region. The current fluctuations in winter are quasi-barotropic; in spring and summer they are more barotropic but have a slight maximum at mid-depth as can be seen in the empirical orthogonal eigenvector components.

Large variations in the shelf waters' stratification occur in winter. Strong northward coastal winds cause an apparent downwelling and a decrease in, or even a destruction of, stratification; southward winds restore the stratification. Fluctuations in the density field are seen simultaneously at all depths in winter, with the

magnitude of the fluctuations increasing with depth. After the transtion the isopycnals on the shelf rise in response to the mean southward winds and the offshore Ekman transport. The magnitude of the fluctuations in density is now largest at the shallowest current meter. By summer, fluctuations in the density field, which were observed at all depths in winter, do not occur at depth. In summer they occur only above 20 m depth.

Fluctuations in sea level and shelf currents are coherent throughout the spectrum (0.0-0.6 cpd) and the phase angles are consistent with geostrophic balance: raised sea level accompanies northward currents. Fluctuations of sea level and density are coherent throughout most of the band from 0.0-0.5 cpd and show the expected isostatic relationship that as sea level rises, the isopycnals deepen. There is also a baroclinic geostrophic balance between the current shear and the horizontal density gradient.

Fluctuations in sea level, currents and winds have alongshore phase speeds and wavelengths that are reasonably similar. Coherence and phase calculations indicate that current fluctuations are directly forced by wind fluctuations. These fluctuations propagate southward and thus cannot be interpreted as continental shelf waves. This is a fundamental difference with the conditions encountered in summer when free continental shelf waves, which can only propagate northward, are found.

Two unusual features in current fluctuations were found. Fluctuations in alongshore currents have significant cross shelf phase lags. Also the two most energetic fluctuations (at 0.06 and at 0.16 cpd) appear to be of a baroclinic nature.

Fluctuations in sea level can be predicted by local winds but the prediction improves through the use of more data in the Gill and Schumann (1974) model. The applicability of the model might indicate the presence of northward free propagating waves which are too weak to be seen in the spectral analysis in comparison to much more energetic, southward propagating forced fluctuations. The Gill and Schumann model predicts a marked drop in sea level at the time of the transition event.

The strong southward flow, after the transition, on the continental shelf is consistent with the geostrophic adjustment to reduced sea level. The Gill and Schumann model cannot predict the persistence in the depressed sea level that results from the adjustment of the density field after the transition event. However, local winds can also account for the redistribution of mass over the continental shelf after the transition event by a simple Ekman model. The mass redistribution, seen in the plots of steric height relative to 600 db, is consistent with the changes seen in the local sea level.

The coastal winds can thus account for the seasonal change in sea level at the transition event and local winds can account for the

adjustment of the density field after the transition event. We conclude that the transition event is wind forced and that the seasonal transition can be explained in terms of the wind.

BIBLIOGRAPHY

Bakun, A. 1973. Coastal upwelling indices, west coast of North America, 1946-1971. NOAA Technical Report NMFS, SSRF-671.

Bakun, A. 1975. Daily and weekly upwelling indices, west coast of North America, 1967-73. NOAA Technical Report NMFS, SSRF-693.

Bakun, A. 1976. Personal communication.

Bakun, A., D.R. McLain and F.V. Mayo. 1974. The mean annual cycle of coastal upwelling off western North America as observed from surface measurements. Fisheries Bulletin 72(3):815-826.

Barnes, C.A., A.C. Duxbury and B.A. Morse. 1972. Circulation and selected properties of the Columbia River effluent at sea. The Columbia River Estuary and Adjacent Ocean Waters, edited by A.T. Pruter and D.L. Alverson, pp. 41-80.

Bryson, R.A. and J.F. Lahey. 1955. The march of the seasons. Factors in Wisconsin Rainfall, edited by R.A. Bryson and J.F. Lahey, U.S. Air Force contract AF 19(604)-992.

Bryson, R.A. and K. Hare. 1974. The climates of North America. World survey of climatology, 11, R.A. Bryson, editor. American Elsevier Publishing Co.

Buckwald, V.T. and J.K. Adams. 1968. The propagation of continental shelf waves. Proceedings of the Royal Society of London: 235-250.

Burt, W.V. and B. Wyatt. 1964. Drift bottle observations of the Davison Current off Oregon. Studies on oceanography: 156-165.

Clarke, A.J. 1976. Observational and numerical evidence for wind-forced coastal trapped long waves. In preparation.

Collins, C.A. 1968. Description of measurements of current velocity and temperature over the Oregon continental shelf, July 1965-February 1966. Ph.D. thesis, Oregon State University. 154 pp.

Cutchin, D.L. and R.L. Smith. 1973. Continental shelf waves: low-frequency variations in sea level and currents over the Oregon continental shelf. Journal of Physical Oceanography 3(1):73-82.

Fofonoff, N.P. 1962. Dynamics of ocean currents. The Sea, edited by M.N. Hill. Interscience: 323-380.

Fofonoff, N.P. 1969. Spectral characteristics of internal waves in the ocean. Deep-Sea Research, Supplement to Volume 16: 58-71.

Gilbert, W.E., A. Huyer, E.D. Barton and R.L. Smith. 1976. Physical oceanographic observations off the Oregon coast, 1975: WISP and UP-75. School of Oceanography, Oregon State University Reference 76-4, 189 pp.

Gill, A.E. and A.J. Clarke. 1974. Wind-induced upwelling, coastal currents and sea level changes. Deep Sea Research 21(5):325-345.

Gill, A.E. and E.H. Schumann. 1974. The generation of long shelf waves by the wind. Journal of Physical Oceanography 4(1):83-90.

Gonella, J.A. 1972. A rotary-component method for analyzing meteorological and oceanographic vector time series. Deep-Sea Research 19:833-846.

Grimmer, M. 1963. The space-filtering of monthly surface temperature anomaly data in terms of pattern, using empirical orthogonal functions. Quarterly Journal of the Royal Meteorological Society 89:395-408.

Hamon, B.V. and D.J. Clarke. 1975. Generation of shelf waves on the east Australian coast by wind stress. Proceedings of the 1975 Liege Colloquium in Hydrodynamics.

Hurlburt, H.E., J.C. Kindle and J.J. O'Brien. 1976. A numerical simulation of the onset of El Nino. Journal of Physical Oceanography 6(5):621-631.

Huyer, A. 1974. Observations of the coastal upwelling region off Oregon during 1972. Ph.D. thesis. Oregon State University. 149 pp.

Huyer, A. 1977. Seasonal variation in temperature, salinity and density over the continental shelf off Oregon. Limnology and Oceanography 20(1):90-95.

Huyer, A., J. Bottero, J.G. Pattullo and R.L. Smith. 1971. A compilation of observations from moored current meters and thermographs. Volume V: Oregon Continental Shelf, 31 July-21 Sept. 1969. School of Oceanography, Oregon State University Reference 71-1.

Huyer, A., R.D. Pillsbury and R.L. Smith. 1975a. Seasonal variation of the alongshore velocity field over the continental shelf off Oregon. Limnology and Oceanography 20(1):90-95.

Huyer, A., B.M. Hickey, J.D. Smith, R.L. Smith and R.D. Pillsbury. 1975b. Alongshore coherence at low frequencies in currents observed over the continental shelf off Oregon and Washington. Journal of Geophysical Research 80(24):3495-3505.

Huyer, A., J. Gagnon and S. Huggett. 1976. Observations from current meters moored over the continental shelf off Vancouver Island, 28 November 1974 to 8 April 1975 and related oceanographic and meteorological data. Ocean and Aquatic Affairs, Environment Canada, MED's Technical Report, no. 4.

Kundu, P.K., J.S. Allen and R.L. Smith. 1975. Modal decomposition of the velocity field near the Oregon coast. Journal of Physical Oceanography 5(4):683-704.

Kundu, P.K. and J.S. Allen. 1976. Some three-dimensional characteristics of low-frequency current fluctuations near the Oregon coast. Journal of Physical Oceanography 6(2):181-199.

Lahey, J.F., R.A. Bryson and E.W. Wahl. 1958. Atlas of five-day normal sea-level pressure charts for the Northern Hemisphere. University of Wisconsin Press.

Leetmaa, A. 1972. The response of the Somali Current to the southwest monsoon of 1970. Deep-Sea Research 19:319-325.

Longuet-Higgins, M.S. 1968. Double Kelvin waves with continuous depth profiles. Journal of Fluid Mechanics 34:49-80.

Lighthill, M.J. 1971. Time-varying currents. Philosophical Transactions of the Royal Society of London, A270:371-390.

Mesecar, R. and D. Barstow. 1975. Suggested method for modifying and calibrating the conductivity range on an RCM-4 current meter. EXPOSURE 3(2):4-7.

Mooers, C.N.K. and R.L. Smith. 1968. Continental shelf waves off Oregon. Journal of Geophysical Research 73(2):549-557.

Niiler, P.P. 1975. A report on the continental shelf circulation and coastal upwelling. Reviews of Geophysics and Space Physics 13(3):609-659.

Perkin, R.G. and E.R. Walker. 1972. Salinity calculations from in situ measurements. Journal of Geophysical Research 77(33):6618-6621.

Peterson, R.G. 1973. Exercises in statistical inference. Oregon State University Book Stores, Corvallis, Oregon, 259 pp.

Pillsbury, D., R.L. Smith and R.C. Tipper. 1969. A reliable low-cost mooring system for oceanographic instrumentation. Limnology and Oceanography 14(2):307-311.

Pillsbury, R.D., J.S. Bottero, R.E. Still and W.E. Gilbert. 1974a. A compilation of observations from moored current meters. Volume VI, Oregon Continental Shelf, April-October, 1972. School of Oceanography, Oregon State University, Reference 74-2, 230 pp.

Pillsbury, R.D., J.S. Bottero, R.E. Still and W.E. Gilbert. 1974b. A compilation of observations from moored current meters. Volume VII, Oregon Continental Shelf, July-August, 1973. School of Oceanography, Oregon State University, Reference 74-7, 87 pp.

Ramsey, F.L. 1976. Personal communication.

Reid, J.L. and A.W. Mantyla. 1977. The effect of the geostrophic flow upon coastal sea elevations in the Northern Pacific Ocean. Journal of Geophysical Research (in press).

Schwartzlose, R.A. 1964. Nearshore currents off western U.S., Baja California, as measured by drift bottles. CALCOFI

Progress Report 1 July 1960-June 1962, California Department of Fish and Game, Sacramento, pp. 15-22.

Smith, R.L. 1974. A description of current, wind and sea level variations during coastal upwelling off the Oregon coast, July-August 1972. Journal of Geophysical Research 79(3):435-443.

Smith, R.L., A. Huyer and E.D. Barton. 1975. The transition from winter conditions to spring upwelling off Oregon. EOS, Volume 56(12), abstract only.

Wyatt, B., W.V. Burt and J.G. Pattullo. 1972. Surface currents off Oregon as determined from drift bottle returns. Journal of Physical Oceanography 2(3):286-293.